Direct Digital Control

of a

Synchronous Machine.

by

G.M. Tatlow.

Submitted to the University of Cape Town in fulfilment of the requirements for the degree of Master of Science in Engineering.

September, 1977.

SYNOPSIS

With the advancement of thyristor technology, variable speed alternating current drives are providing improved performance over conventional systems. The aim of this thesis is to investigate the possibilities of direct digital control of a thyristor converter and to determine the major parameters affecting the operation of a variable speed synchronous machine drive.

ACKNOWLEDGEMENTS

1. To Mr. S.G. McLaren, my supervisor, for his advice and encouragement.

2. To the Council for Scientific and Industrial Research for their financial support.

3. To the staff of the Electrical Engineering Department, U.C.T., for their assistance.

CONTENTS

NOMENCLATURE

V_{dc}	Average D.C. voltage
V_{ac}	Rectifier input phase voltage
I_{dc}	Average D.C. current
E	Motor phase emf. (fundamental component)
V	Motor terminal phase voltage (fundamental component)
I	Motor line current (fundamental component)
I_f	Motor field current
X	Motor synchronous reactance (per phase)
R	Motor armature resistance (per phase)
Z	Motor synchronous impedance (per phase)
L_{sr}	Motor stator to rotor inductance
X_q	Motor quadrature axis synchronous reactance
X_d	Motor direct axis synchronous reactance
X_l	Motor armature leakage reactance
N	Motor speed in r.p.m.
ω	Electrical angular frequency
T	Motor torque
p	Number of poles
α	Inverter advance angle
β	Inverter delay angle
γ	Rectifier delay angle
μ	Thyristor overlap angle
δ	Motor internal power angle
ϕ	Motor input power angle.

CHAPTER 1.

INTRODUCTION

To date, the majority of industrial variable speed motor drives have been based on D.C. machines with armature voltage or field current control. The most popular being the converter fed D.C. motor drive.

A.C. machines, however, are more versatile, robust and efficient, and require less maintenance than that of D.C. machines.

The main disadvantage of A.C. machines as variable speed drives is that they require a variable frequency supply, which requires more complex and costly control equipment than a D.C. drive. The drop in prices, together with increased power handling capability of thyristors, have made A.C. motor drives economically attractive.

Thus, although A.C. machines require more complex and costly control equipment than D.C. machines, they have the advantage of being simpler and cheaper and do not suffer from voltage, current and speed limitations of the mechanically commutated D.C. motor.

D.C. machines require more maintenance than A.C. machines and in conditions where service interruptions are costly or when motors are operated in inaccessible locations A.C. motors have

a definite advantage over D.C. machines. A.C. motors also have the advantage of a better power to weight ratio than D.C. motors.

Variable frequency inverters can be divided into forced and naturally commutated types.

Forced commutation inverters require expensive and bulky capacitors and inductors needed for thyristor commutation. The commutating energy ($\frac{1}{2}CV^2$ or $\frac{1}{2}LI^2$) becomes excessive at high speeds due to the square law relationship shown. This additional energy can cause inverter inefficiency and/or oscillation problems. Forced commutation inverters are limited, by commutation problems, to a few hundred kW. The advantage of this type of inverter is that frequency of operation is determined by the circuit conditions alone (Bowler, Chan, 1974; Alston, Hayden, 1972).

Naturally commutated inverters rely on the load or the supply (or a combination of both) to enable thyristor commutation. They have smaller and simpler main and control circuits and are economically feasible up to the MW range. Their main disadvantage lies in the frequency dependence of the system on the load or supply frequency.

There are two types of A.C. motors to be considered; induction and synchronous machines.

Induction motors are robust, simplest and cheapest but suffer

from the disadvantages of poor lagging power factor (requiring inverter upgrading), relatively large copper losses at low speed (about twice that of synchronous motors) and lower torque at low speed than synchronous motors (McLeod, Renfrew, Shepherd, 1974).

Synchronous machines have the disadvantage of requiring D.C. field excitation (except permanent magnet motors). This can be supplied via slip rings in smaller motors or by an asynchronous motor mounted on the same shaft with a diode rectifier supplying the poles. The field current, however, offers another control variable which may be advantagous (Fitzgerald, Kingsley, Kusko, 1961; Alston, Hayden, 1972). Synchronous motors suffer from the effects of armature reaction to a greater extent than D.C. motors.

Considering the above, it was decided to investigate a variable speed, naturally commutated synchronous machine drive. The drive envisaged would be adaptable to any motor rating, from kW's to MW's. Reversible and regenerative operation would be easily accomplished. Speed control from standstill to over rated speed would be possible.

A D.C. link converter with fully controlled rectifier and inverter bridges has the properties discussed and it was decided to investigate this type of converter. The inverter requires a D.C. input and this is derived from a 3-phase supply by using a controlled rectifier. The inverter acts as a static commutator replacing the mechanical commutator of D.C. motors.

This gives rise to a commutatorless D.C. machine and allows well established D.C. motor control principles to be used.

Thyristors are used as the main power control devices. These have definite on or off states and are therefore essentially digital devices. Digital control methods are thus an obvious choice, especially with the now cheaply available micro-processors. Direct digital control avoids the necessity of expensive analog-to-digital and digital-to-analog converters, reduces the susceptibility of the system to noise and also enables easy interfacing to a central control computer which many industrial plants now employ for process control.

The research comprises two sections :-

(a) Development of digital systems for controlling the rectifier and inverter thyristor bridges;

(b) Development of a digital feedback processor to enable the motor speed to be controlled.

CHAPTER 2.

SYSTEM DESCRIPTION

The basic system comprises a fully controlled bridge rectifier supplying direct current to an inverting bridge. The inverter is commutated by the motor induced electromotive force and synchronization of the inverter to this emf. is therefore necessary. This is accomplished by synchronizing the inverter to the rotor position by using a disc encoder mounted on the machine shaft.

Both rectifier and inverter are 3-phase, phase controlled, full-wave bridges. Fig. 2.1 shows the overall system. The essential elements of the drive are:

(a) Three-phase transformer to supply correct maximum motor voltage if required.

(b) Three-phase, 6 pulse, phase controlled thyristor rectifier and associated firing and control circuitry.

(c) Direct current link with a series inductor which smooths the input current to the inverter and hence smooths the motor current and torque. The inductance prevents the input current from rising during thyristor commutation and also carries the instantaneous potential difference between the rectifier output and the motor terminal voltage. In addition, the inductor limits the maximum rate of change of rectifier and motor current.

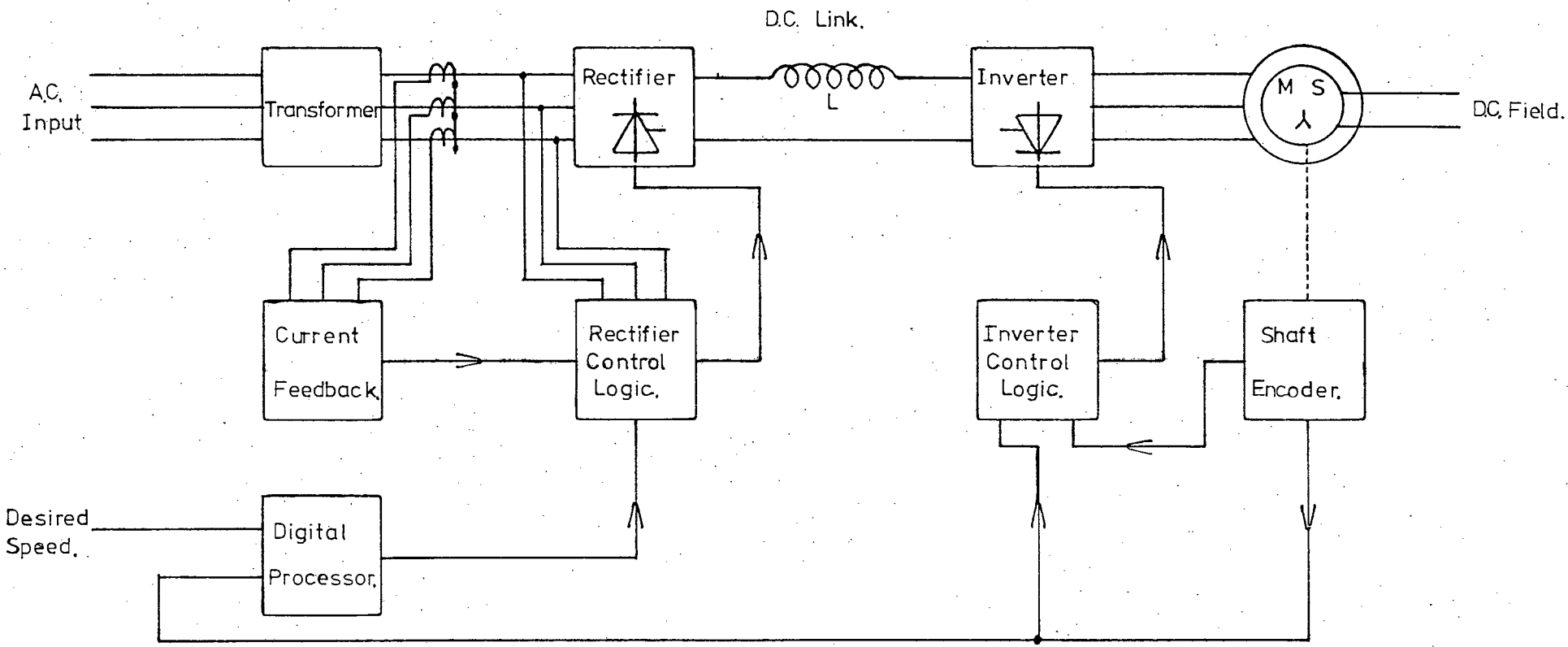

Figure 2.1

Block Diagram of System.

(d) Three-phase, 6 pulse thyristor inverter and associated firing and control circuitary. The latter being synchronized to the motor shaft position.

(e) A conventional unmodified synchronous motor.

(f) A slotted disc fitted to the motor shaft to enable determination of the shaft position and speed.

(g) A digital processor to control the thyristor bridges enabling motor speed control.

At this stage it is informative to look at some simplified equations relative to the rectifier, inverter and motor. The derivation of these is shown in Appendix A.

Rectifier output: $V_{dc} = a.V_{ac}.\cos(\gamma)$ 2.1

Inverter output: $V = \frac{V_{dc}}{b.\cos(\alpha)}$ 2.2

Motor: $E = c.I_f.N$ 2.3

These equations are based on very simple models and effects such as leakage inductances, resistance, saturation, armature reaction are not considered at this stage.

Thus

$$N = \frac{a.V_{ac}.\cos(\gamma)}{b.c.I_f.\cos(\alpha)} = \frac{k.V_{ac}.\cos(\gamma)}{I_f.\cos(\alpha)} \quad \ldots\ldots 2.4$$

This shows that to obtain variable speed there are 3 controllable variables, namely γ, α and I_f.

As the drive is to have full range speed control, from zero upwards, it is obvious that it is necessary to control γ . It was therefore decided to make γ (the rectifier delay angle) the main control variable for this project. Thus motor speed is obtained by varying the inverter input D.C. voltage.

The basic speed equation for a D.C. motor is:

$$N = \frac{k.V_{dc}}{I_f} \qquad \ldots\ldots\ldots\ldots\ 2.5$$

The similarity of equations 2.4 and 2.5 is the reason for the system being called a D.C. commutatorless motor. The system performance is thus similar to that of a D.C. machine with shunt or series operation possible. In the latter case the field coil could possibly replace the D.C. smoothing inductor. For this project a separately excited field is used giving a "shunt characteristic".

As there are 3 variables in equation 2.4, variation of any one of these would effect the motor performance. To optimize the operation of the whole system it would be necessary to control all three parameters. This, however, was considered to be beyond the scope of this project and only the effects of variation of I_f and α , with γ being the main controlled parameter, are considered.

At zero and very low speed there is insufficient motor emf. to commutate the inverter thyristors. Under these conditions it is necessary to use a different method of commutation. This

is relatively easily accomplished and is discussed in Chapter 4.

To obtain maximum motor acceleration the motor should be given maximum rated current. A current controller or limiter is therefore essential. This also helps to protect the rectifier, inverter and motor under adverse load or even fault conditions. This is discussed in Chapter 3.

The overall system therefore comprises the rectifier, inverter, motor with the major speed feedback loop controlling the rectifier and minor feedback or feedforward loops controlling the inverter commutation at low speeds, and the current.

CHAPTER 3.

THE RECTIFIER

The rectifier is a conventional 3 phase, 6 pulse, phase controlled thyristor rectifier which allows unidirectional current to be passed to the load.

Fig. 3.1 shows the power circuits, supply voltage waveforms and the range of valid thyristor firing pulses.

The maximum D.C. output voltage is obtained by firing the relevant thyristor at the earliest instant of the possible firing range shown in Fig. 3.1. The bridge is then fully advanced, or the firing delay is zero. By delaying the thyristor firing pulse the output voltage is progressively reduced.

For a purely resistive load the current becomes discontinuous for delay angles greater than 60° and the current is zero for a delay angle of 90° as at this delay angle only one thyristor is receiving a gate pulse at any one instant. It requires two thyristors to be conducting for current flow. The firing pulses could be modified to allow current flow into a resistive load for delay angles up to 120°. This was unnecessary as the smoothing choke presents a largely inductive load.

For a purely resistive load the output voltage is (see Appendix A):

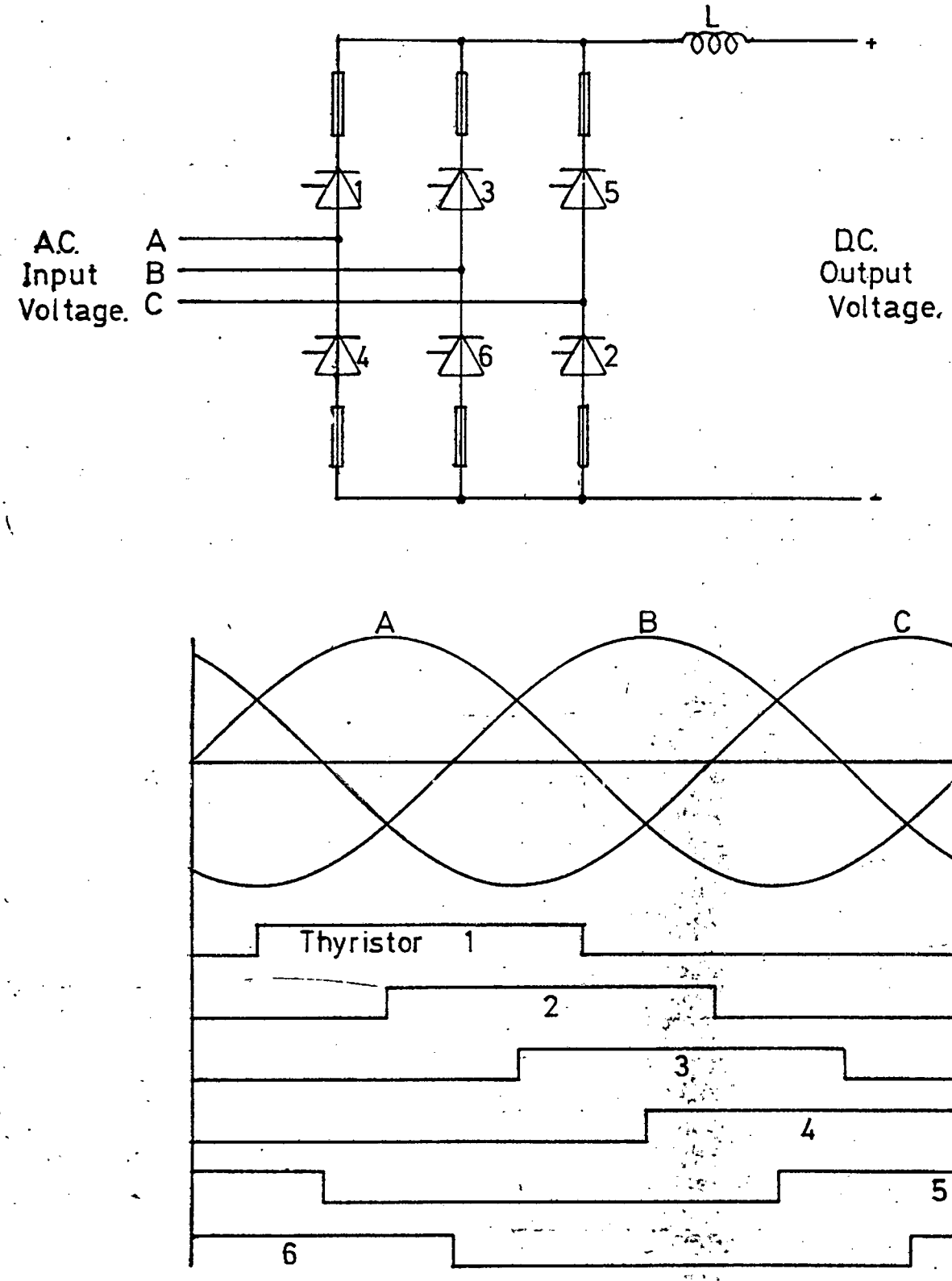

Rectifier Circuit Diagram and
Thyristor Firing Range.

Figure 3.1

$$V_{dc} = \frac{3\sqrt{6}}{\pi} \cdot V_{ac} \cdot \cos(\gamma) \quad \text{for } 0^\circ \leq \gamma \leq 60^\circ \qquad \ldots\ldots 3.1$$

$$V_{dc} = \frac{3\sqrt{6}}{\pi} \cdot V_{ac} \cdot (1 + \sin(\gamma - 30^\circ)) \quad \text{for } 60^\circ \leq \gamma \leq 120^\circ \qquad 3.2$$

If the load is inductive and resistive and providing that the current does not become discontinuous the output D.C. voltage is positive for a delay angle of less than 90° and negative for a delay angle greater than 90°. In the latter case it is still necessary for the current to be positive and continuous. Thus the voltage is negative and the current is positive and the power supplied to the D.C. system is negative. This is regeneration or inversion because power is now flowing from the D.C. system to the A.C. system.

For continuous current the D.C. output voltage (see Appendix A):

$$V_{dc} = \frac{3\sqrt{6}}{\pi} \cdot V_{ac} \cdot \cos(\gamma) \quad 0^\circ \leq \gamma \leq 120^\circ \qquad \ldots\ldots 3.3$$

Fig. 3.2 shows the effects of variation of the delay angle on the output D.C. voltage for continuous and discontinuous current cases.

Under steady state conditions each thyristor, after being fired, conducts for 120° and is commutated when the "parallel" thyristor connected to the lagging phase voltage is fired, thus reverse biasing the thyristor to be commutated. The D.C. current which is assumed to be constant, due to the D.C. smoothing inductor is then transferred from the one thyristor

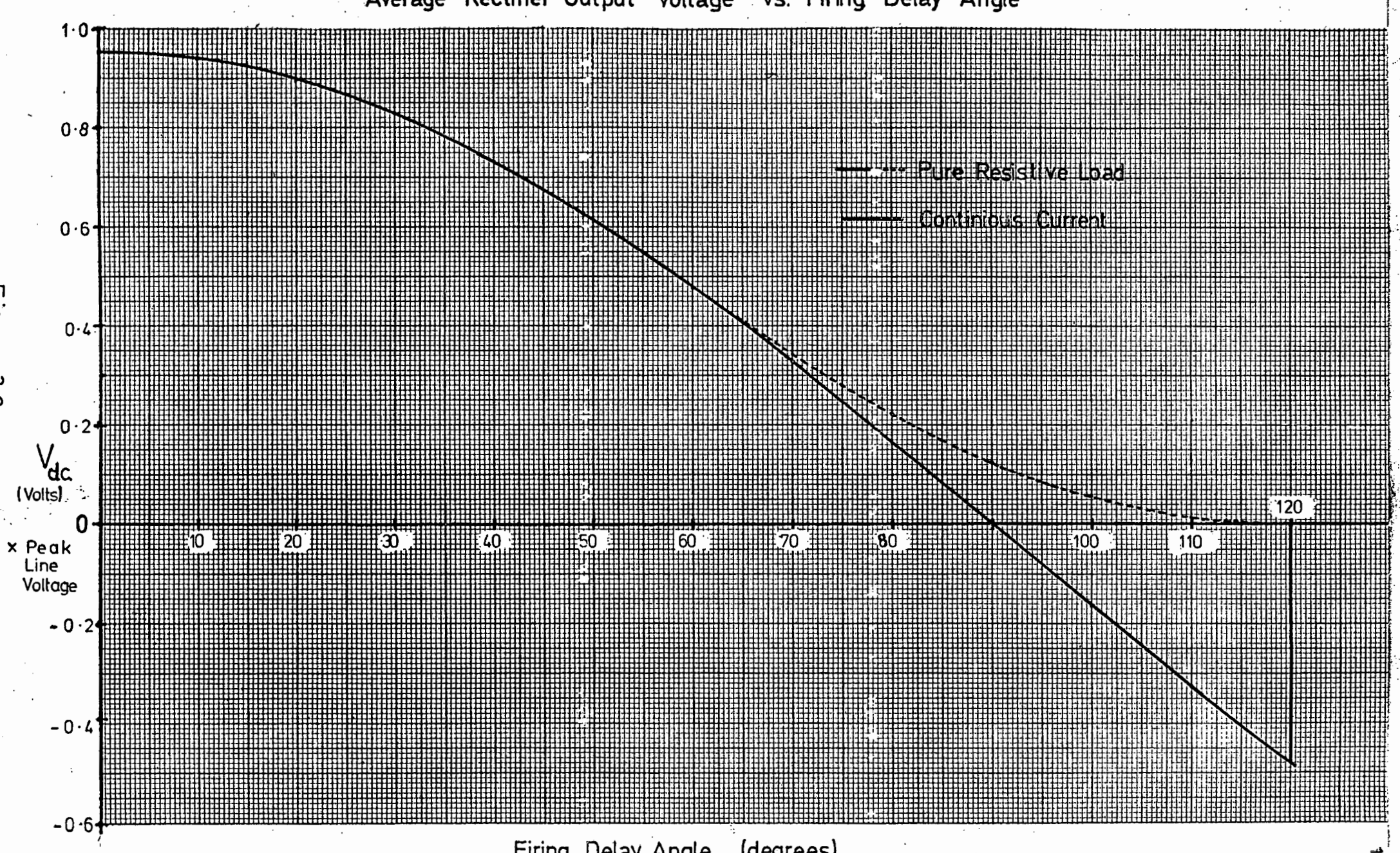
Average Rectifier Output Voltage vs. Firing Delay Angle
1·0
0·8
0·6
0·4
0·2
0
-0·2
-0·4
-0·6
V_{dc} (Volts)
x Peak Line Voltage
Pure Resistive Load
Continious Current
10
20
30
40
50
60
70
80
100
110
120
Firing Delay Angle (degrees)

Figure 3.2

to the next. The speed at which this transfer of current occurs, the commutating time, is dependent upon the commutating voltage and the total series inductance in the A.C. circuit. This finite commutating period causes a phase shift in the current waveform and alters the D.C. output voltage. During commutation two phases of the A.C. supply are effectively short-circuited. The effects of this overlap time are discussed in Chapter 5. In this project the effects of rectifier thyristor overlap have been disregarded as they are small. Fig. 3.3(a) is an exaggerated diagram showing thyristor overlap effects.

3.1 Rectifier Control Logic

Fig. 3.4 is a block diagram showing the main components of the control logic for the thyristor firing circuits. An eight bit binary number is loaded into the counters. These start counting up, at the clock frequency (starting from the input number), when the relevant control signal is received from the comparators. When the counters are full an output signal is given and this is gated with the comparator outputs to give a pulse to the relevant thyristor firing circuits. Each counter is only used for 150^{o} of a mains cycle and hence each counter is able to service two thyristors.

It is a simple matter to show that the delay time is given by:

$$\text{Delay time} = \frac{377_8 - (\text{input number})_8}{(\text{clock frequency})} \qquad \ldots\ldots\ldots 3.4$$

or for a 50 Hz supply:

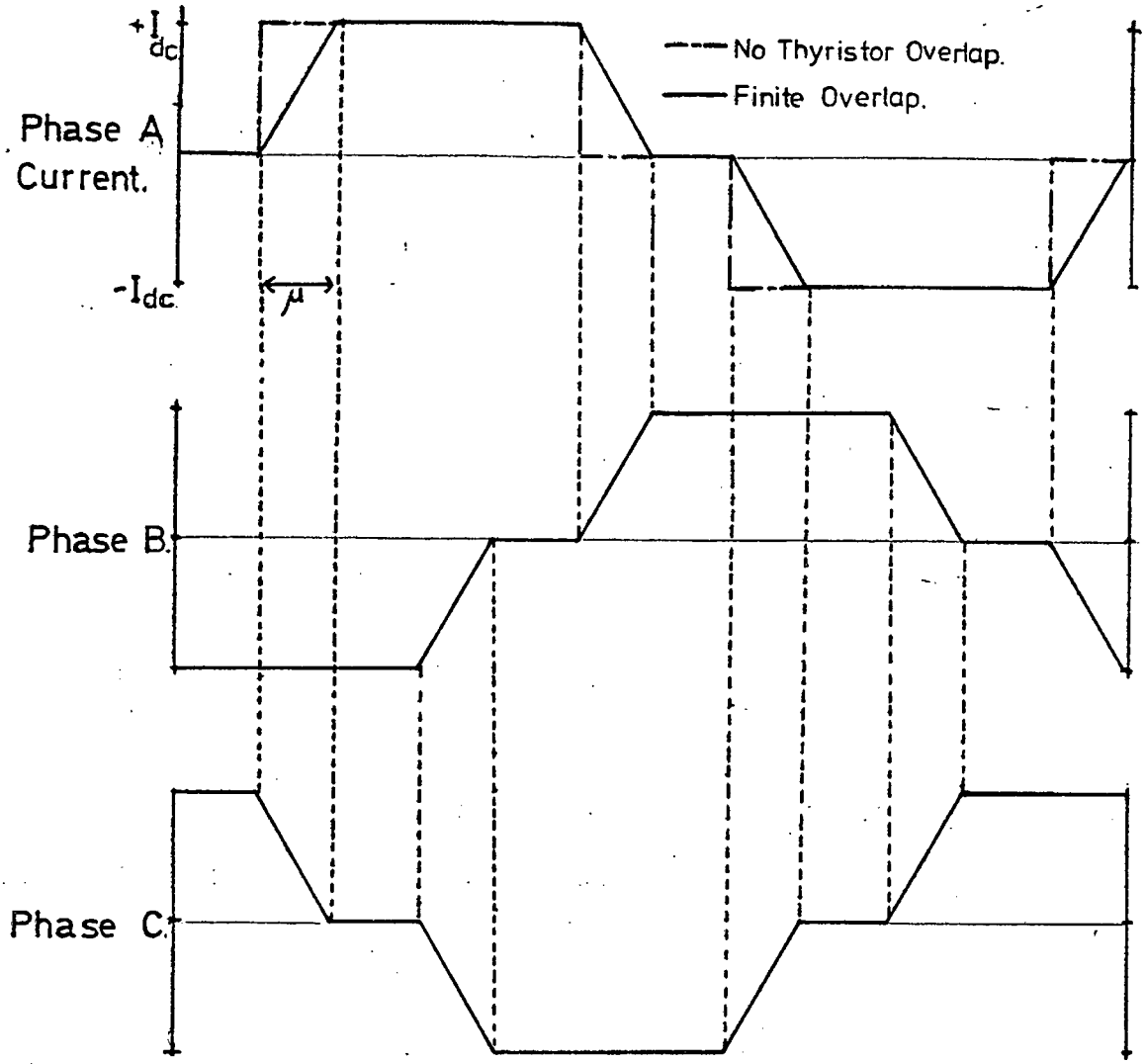

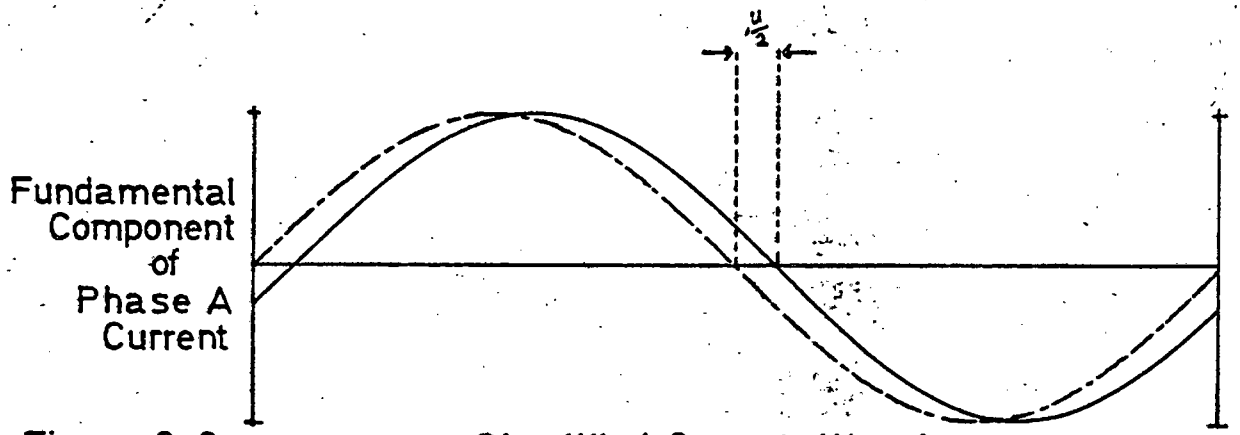

Figure 3.3a Simplified Current Waveforms.

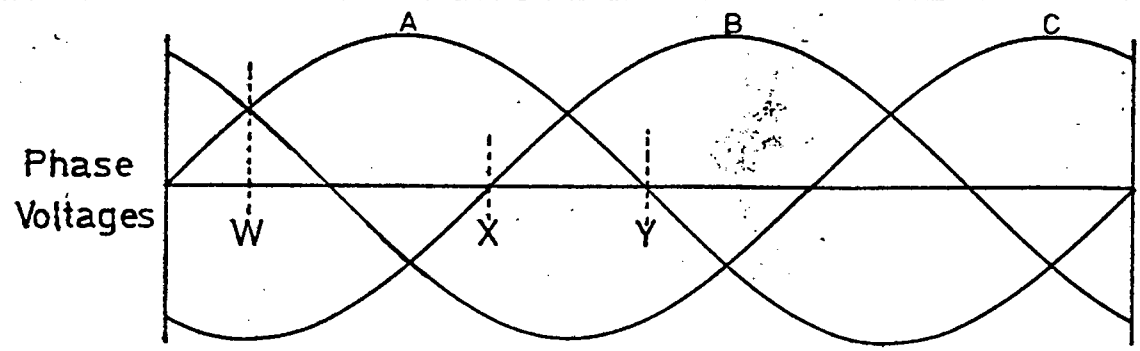

Figure 3.3b Thyristor Firing (Section 3.3)

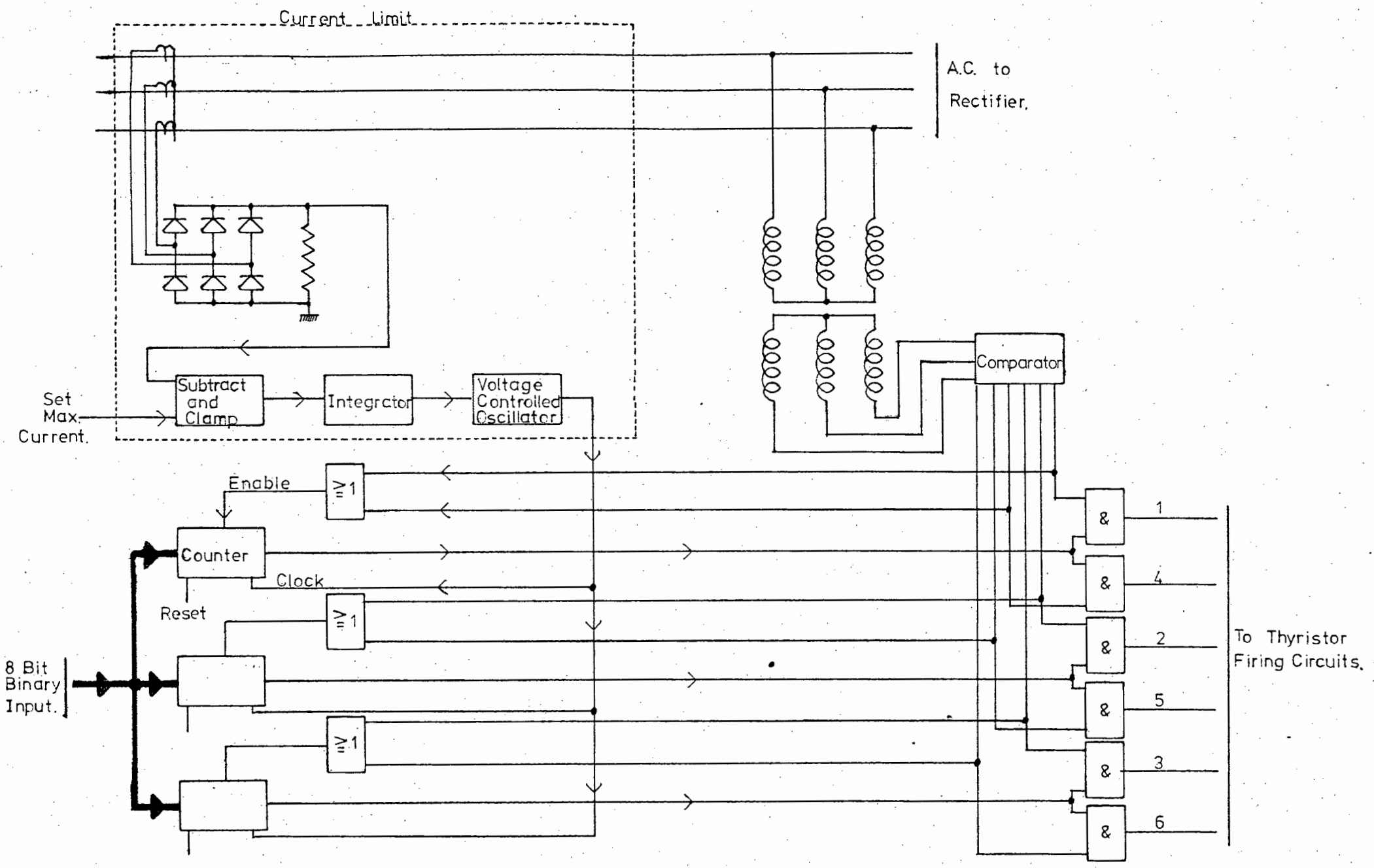

Figure 3.4

Block Diagram of Rectifier Control Logic.

$$\text{Delay angle:} \quad = \frac{377_8 - (\text{input number})_8}{(\text{clock frequency})} \times \frac{360^o}{0.02} \quad \ldots\ldots 3.5$$

The delay angle is linearly related to the eight bit input number and inversely proportional to the clocking frequency.

3.2 Cross-Over Detectors

The rectifier needs to be synchronized to the 50 Hz mains supply. This is accomplished using cross-over detectors. Fig. 3.5 shows these comparators and associated decoding logic.

The RC networks provide noise suppression, low pass filters and introduce an insignificant delay of 33 μS (0.6°). The comparators provide all zero-crossing points for phase and line voltages. The logic gates decode these outputs to give the thyristor firing ranges shown in Fig. 3.1.

Fig. 3.6 shows the relationship between the various waveforms.

3.3 Thyristor Firing

Although a single gate pulse is adequate to trigger a forward biased thyristor, in this case two thyristors need to be triggered to allow current flow and therefore thyristor latching. Thyristors may be turned on by the application of a D.C. current to the gate. This should not cause the allowable average power dissipation of the gate junction to be exceeded. Alternatively, a string of shorter pulses of higher instantaneous power but equal or lower average power may be applied. The

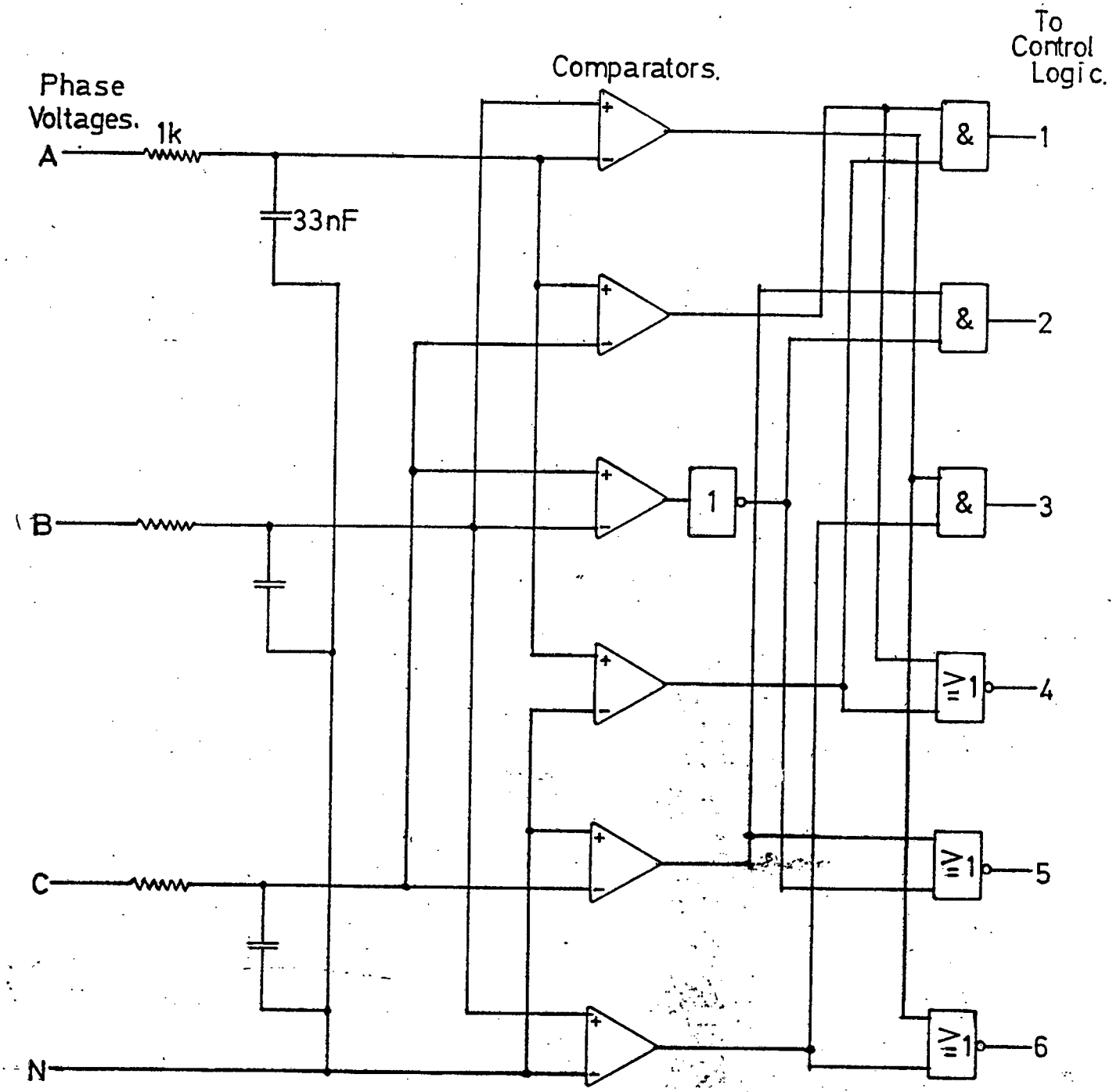

Cross-over Detectors

Figure 3.5

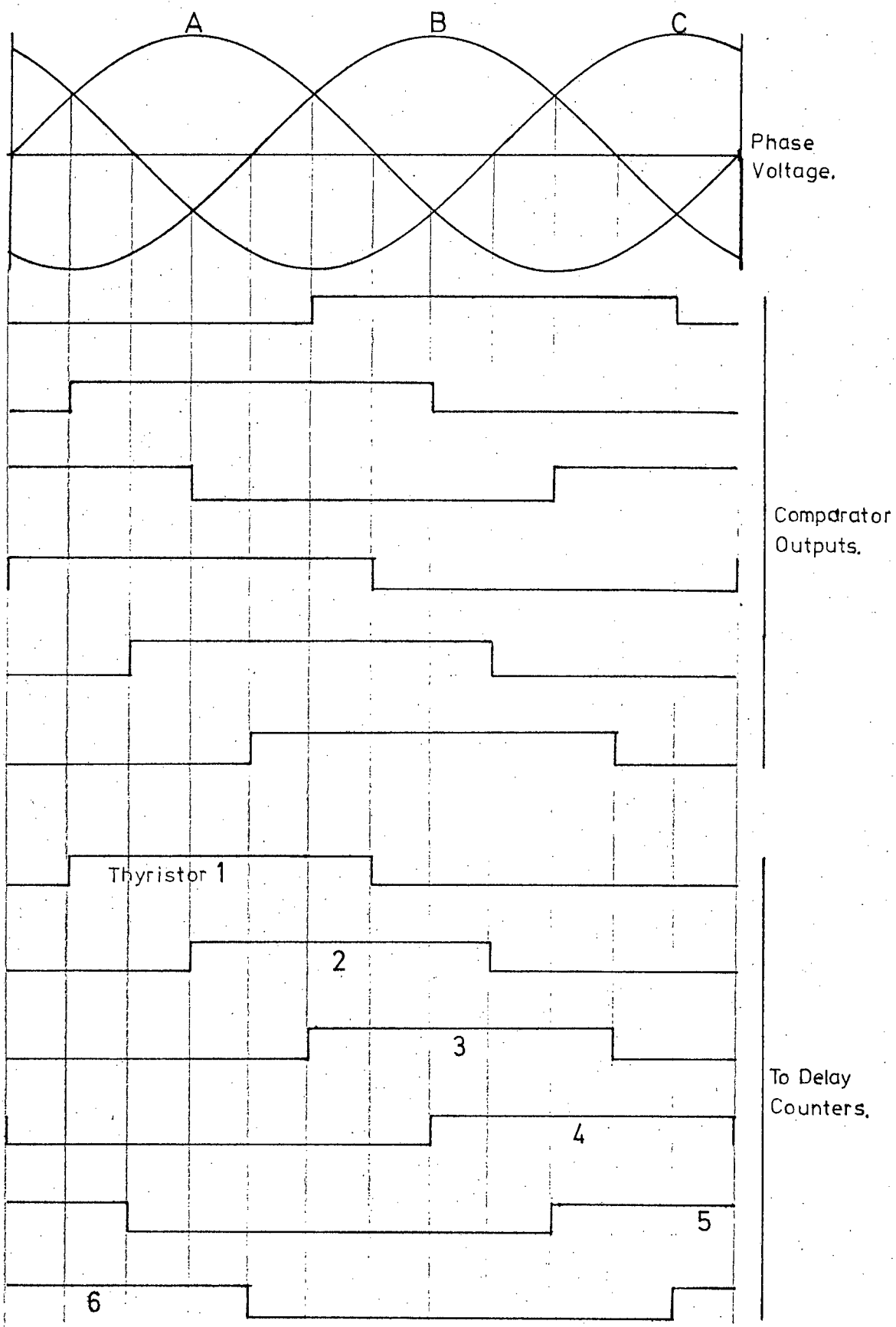

Firing Pulse Synchronization.

Figure 3.6

second method gives more reliable triggering and was the procedure used in this project.

The following paragraph refers to Fig. 3.3(b). For close to zero output D.C. voltage thyristor 1 must be fired at point X and thyristor 2 at point Y. For these firing pulses to overlap so that both thyristors 1 and 2 receive gate pulses simultaneously it is necessary for the gate pulse of thyristor 1 to extend as far as point Y. The earliest instant that thyristor 1 can be fired is at point W. The possible range of gate pulses for thyristor 1 is therefore from point W to point Y or 150°. Under operating conditions thyristor 1 gets a gate pulse α degrees after point W and the gate pulses remain until point Y.

The pulse train applied to the gates of the thyristors for this thesis was a square wave of 30 kHz and 50% duty cycle.

Fig. 3.7 shows the firing circuits used.

An inhibit input is shown and its use will be explained later. The inhibit input, when high, prevents any gate pulses from being delivered to the bridge.

3.4 Current Limit

A semi-digital current control circuit was incorporated into the rectifier firing control to limit the D.C. output current to a presettable level.

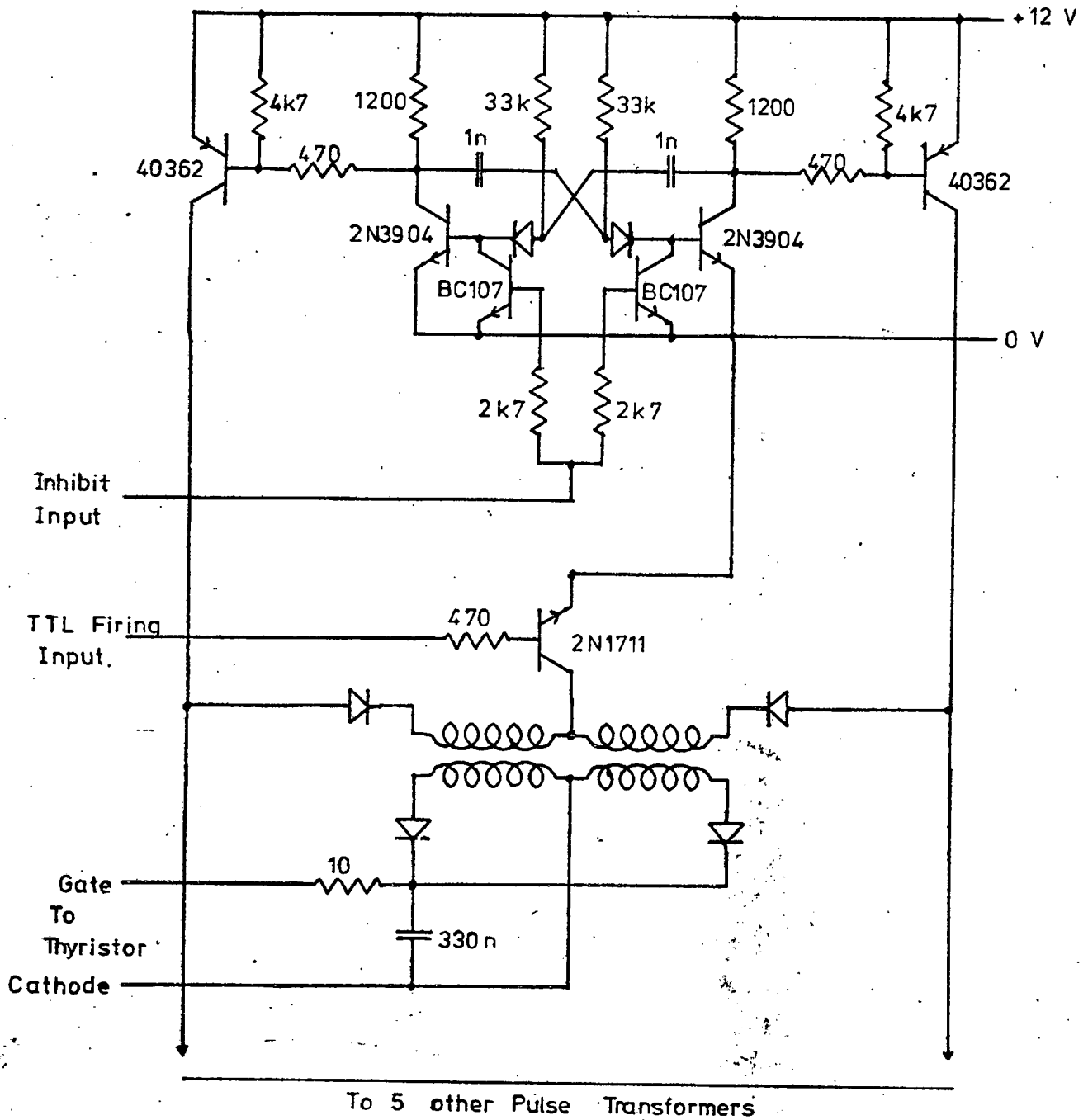

Thyristor Firing Circuit.

Figure 3.7

Equation 3.5 shows that the delay angle is inversely proportional to the counter clocking frequency. The rectifier output voltage is a function of the cosine of the delay angle (see Equation 3.3). By decreasing the clock frequency, the delay angle is increased and so the D.C. voltage and therefore the D.C. current is reduced.

The D.C. inductor is essential to the successful operation of the current limiter because once a thyristor has been fired the current through it could continue to rise for a period of 6.7 mS (even if no other thyristors are fired subsequently) if circuit conditions allowed. The D.C. inductor limits the maximum rate of rise of current to prevent large current surges under adverse conditions.

Current sensing was by means of 3 current transformers in the A.C. lines to the rectifier. The output of these was rectified and used to produce a voltage proportional to the D.C current. If this feedback voltage exceeded a given input voltage the difference between the two was amplified, processed and fed to a voltage controlled oscillator in such a way that the frequency dropped linearly with increasing control voltage. This frequency was used to clock the delay counters.

Initially the processing of the error signal referred to above, consisted of filtering (low pass) and amplifying only. This proved unsatisfactory because the large gain required (to cause a sharp cut-off at the current limit) caused instability and oscillation of the system.

The processor was then made to be a proportional plus integral controller and this gave a sharp current cut-off but was not fast enough to prevent a large (typically 100%) initial current overshoot which lasted for about 10 mS after the application of a short circuit on the rectifier output.

A bang-bang (on-off) digital controller was then added to supplement the above analog current limiter. This circuit inhibited the rectifier firing circuits as soon as the current exceeded the preset limit by a small amount. This only operated on transients after which the more accurate integral controller limited the current.

The digital controller also acted as a back-up protection unit in case of a logic failure in the control circuitary.

Fig. 3.8 shows the main components of the current limit circuit.

The voltage controller oscillator had a maximum frequency of 38 250 Hz which was the clock frequency needed to produce a delay angle of 120^{o} for an octal input of zero.(on the 8 bit input lines). See Appendix D.

It is clear from equations 3.5 and 3.3 that to obtain zero output voltage (and therefore current limiting when under short-circuit conditions) the clock frequency is a function of the input number. The control logic would not operate correctly with a clock frequency close to or equal to zero and so additional circuitary was added to prevent the binary input

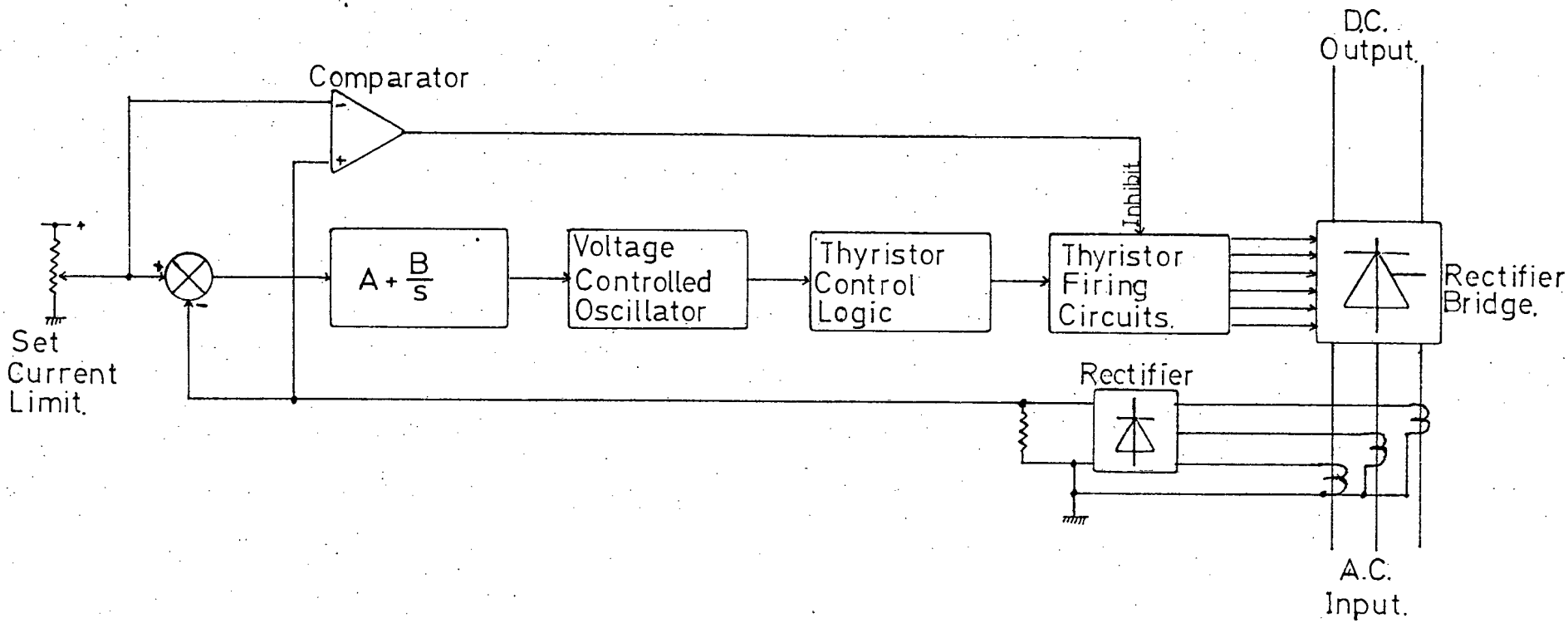

Figure 3.8

Block Diagram of Current Controller.

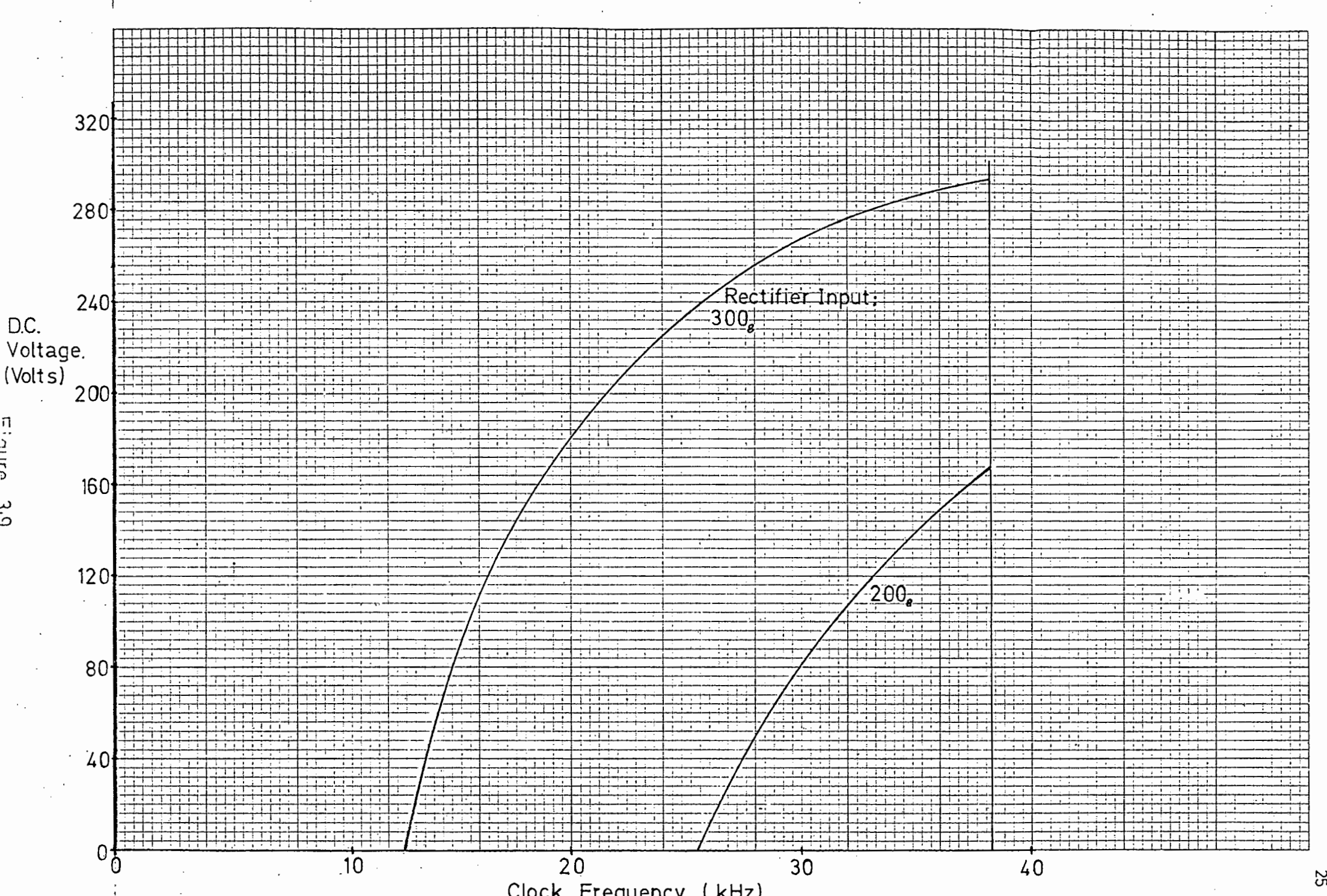
320
280
240
200
160
120
80
40
0
D.C.
Voltage.
(Volts)
Rectifier Input;
300v
200v
0
10
20
30
40
Clock Frequency (kHz)

Figure 3.9

number from exceeding 317_8. This made the lowest necessary clock frequency 9.6 kHz. The D.C. output level was, however, then limited to 93% of the maximum possible output.

Fig. 3.9 shows output voltage vs. clock frequency for different binary inputs.

3.5 Test Results

The rectifier and control circuitary was tested using a resistive load. (The D.C. smoothing inductor was considered to be part of the rectifier).

The average output voltage corresponded very closely to the expected output shown in Fig. 3.2.

Fig. 3.10 shows photographs of the rectifier voltage and current waveforms. The oscilloscope was triggered on the same point for all waveforms and so the phase relationships between the waveforms can also be seen. These photographs were taken later in the project and were recorded with the inverter driving the motor thus slight irregularities and "spikes" due to inverter firing can be seen in the current waveforms.

The D.C. output voltage is directly from the rectifier terminals and not smoothed by the inductor. The thyristor voltage shown is cathode with respect to the anode. The conditions under which the photographs were taken were:

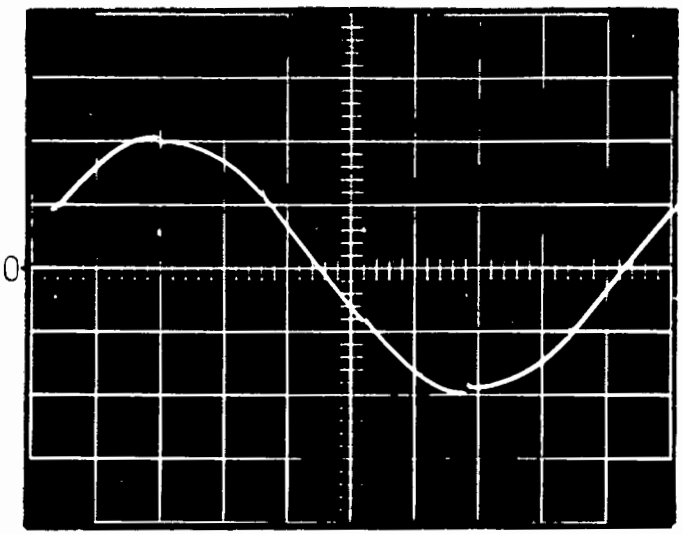

AC. Phase Voltage. 100 V/div.

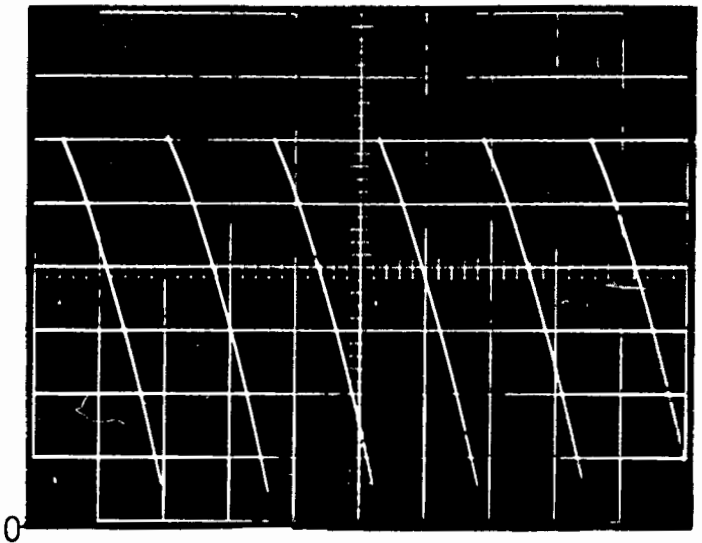

DC. Voltage. 50 V/div.

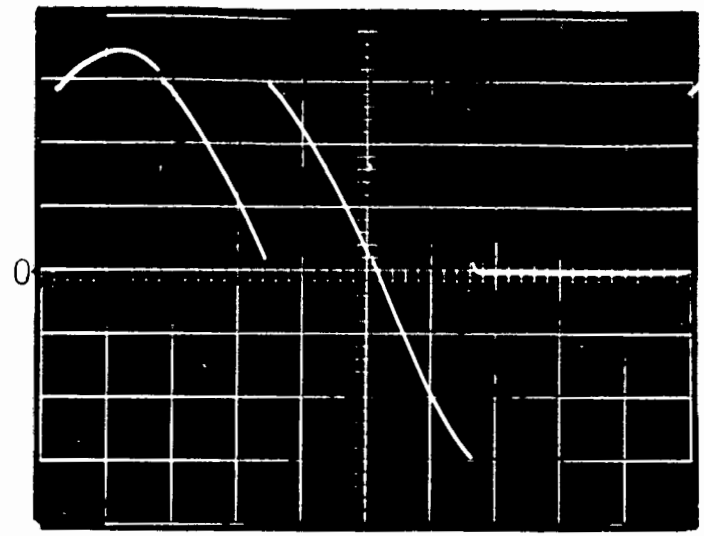

Thyristor Voltage. 100 V/div.

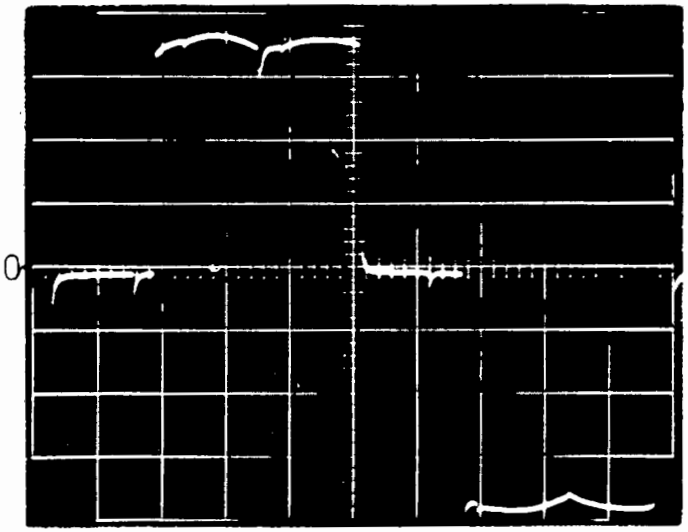

AC. Line Current. 7A./div.

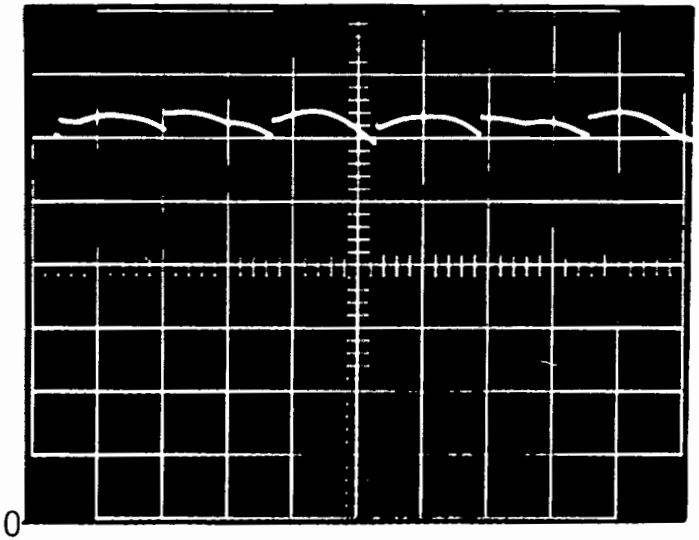

DC. Current. 4A./div.

Figure 3.10

Rectifier Voltage and Current Waveforms.

Horz. scale. 2ms./div.

V_{ac} phase	:	135 V
V_{dc}	:	172 V
I_{dc}	:	25 A
Delay Angle	:	57^{o}
Octal Input Number	:	206_{8}.

Fig. 3.11 shows the response of the current controller after the application of a short circuit to the output from the rectifier and smoothing inductor. The output voltage was maximum prior to the short circuit occurring.

Fig. 3.12 shows the steady state output voltage vs. current for a fixed delay angle.

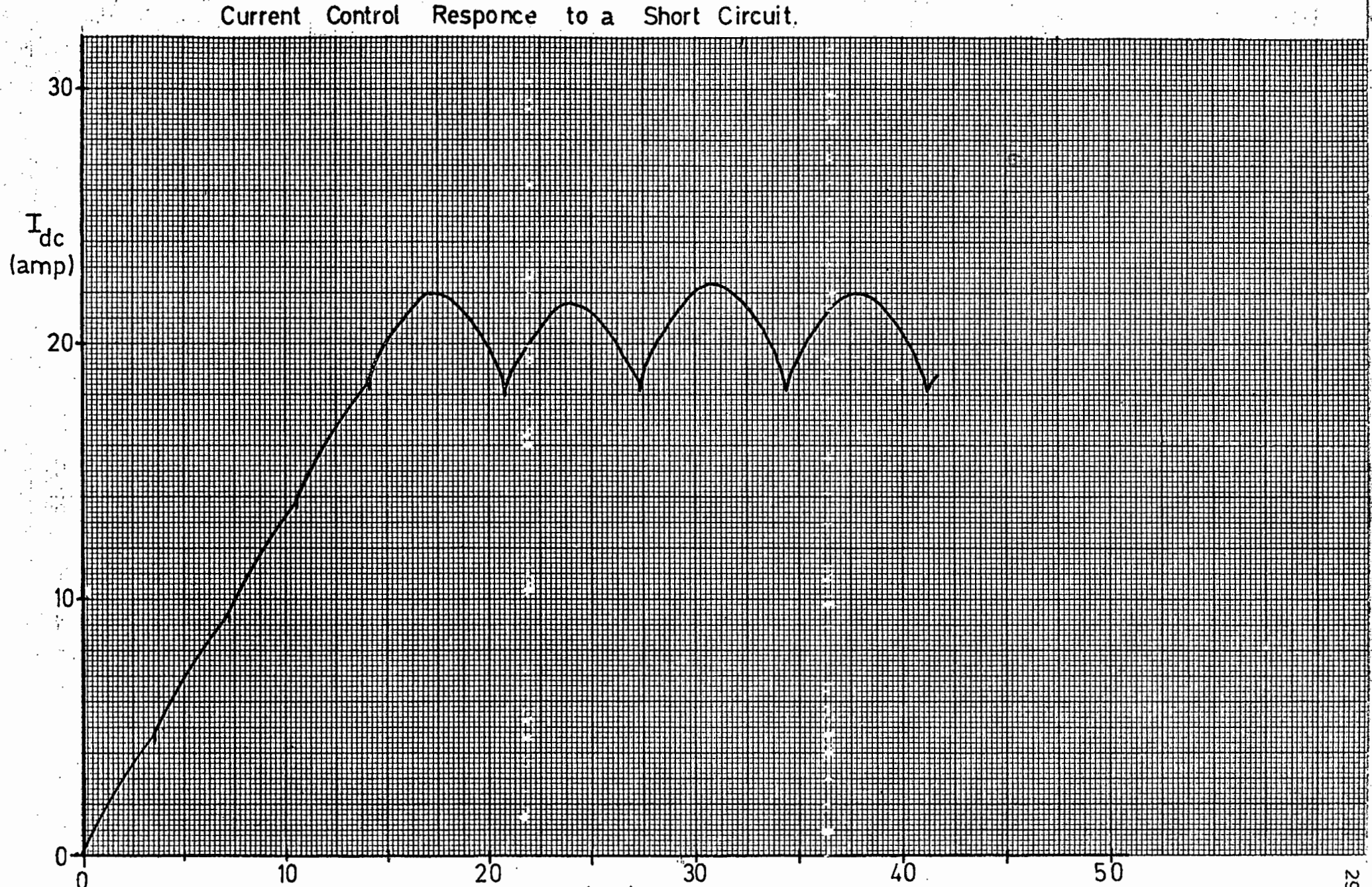
Current Control Responce to a Short Circuit.
I_{dc} (amp)
30
20
10
0
0
10
20
30
40
50

Figure 3.11

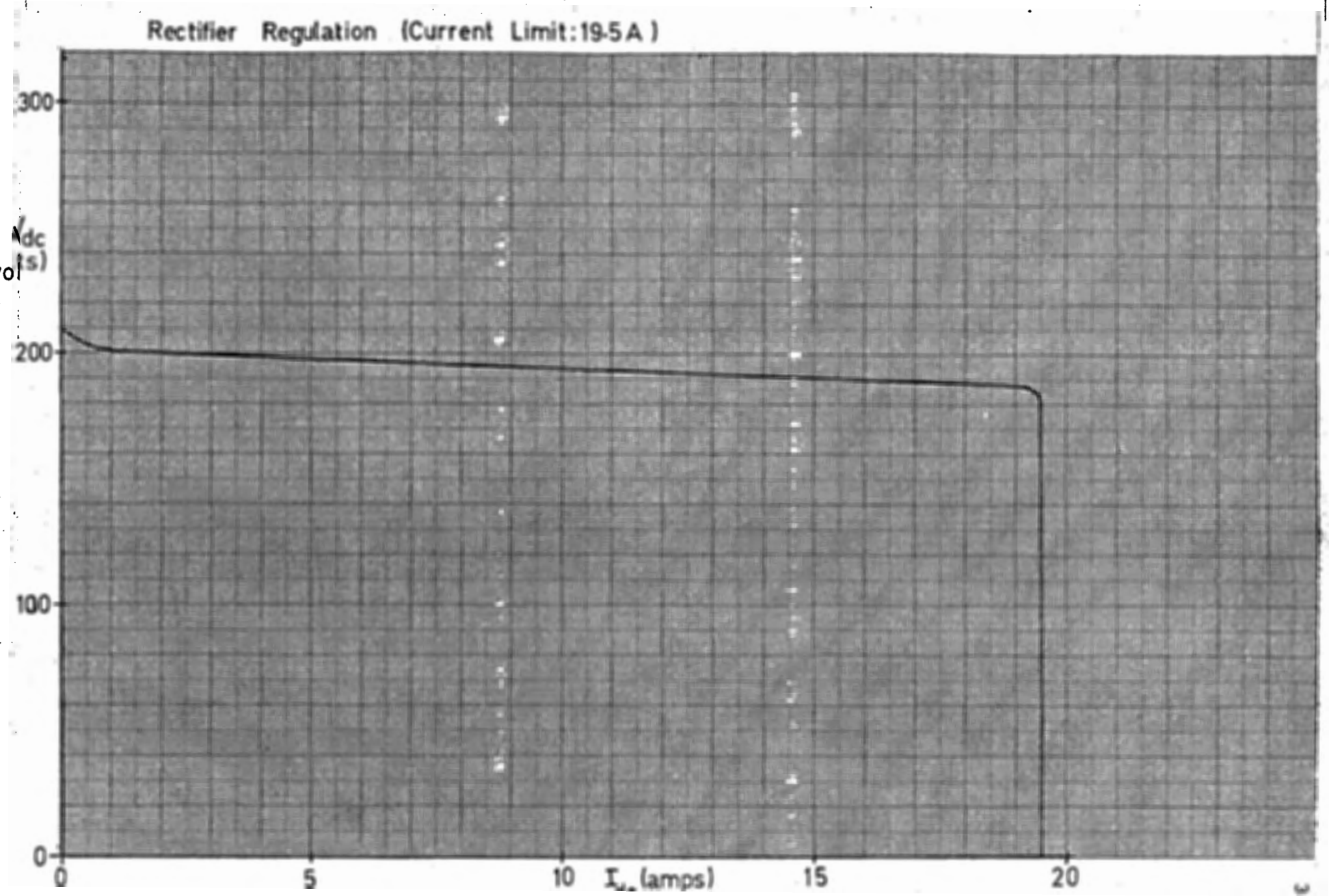
Rectifier Regulation (Current Limit: 19-5 A)
300
200
100
0
0
5
10
15
20
(amps)

Figure 3.12

CHAPTER 4.

THE INVERTER

The inverter is a 3-phase, 6 pulse thyristor bridge identical to the rectifier except for a difference in firing instants. The gate pulses are synchronized to the motor rotor position, and therefore to the induced field electromotive force. It is the resultant motor emf. that is used to naturally commutate the inverter thyristors. Thus although the inverter is synchronized to the field emf., the resultant emf. commutates the thyristors. The difference between the field emf. and the resultant emf. is due to armature reaction. The effects of this will be discussed in Chapter 5 and for the remainder of this chapter armature reaction is assumed to be zero.

Fig. 4.1 shows the inverter power circuits together with the possible range of thyristor firing pulses.

As was the case for the rectifier, variation of the firing delay angle caused a corresponding change in the ratio of A.C. to D.C. voltage. As the D.C. voltage is fixed (from the rectifier) the A.C. output voltage varies with delay angle.

There are two modes of operation rectification and inversion. As current can only be passed in one direction through the thyristors it is assumed to be always positive on the D.C. side of the bridge. For delay angles of between zero and 90^{o} the

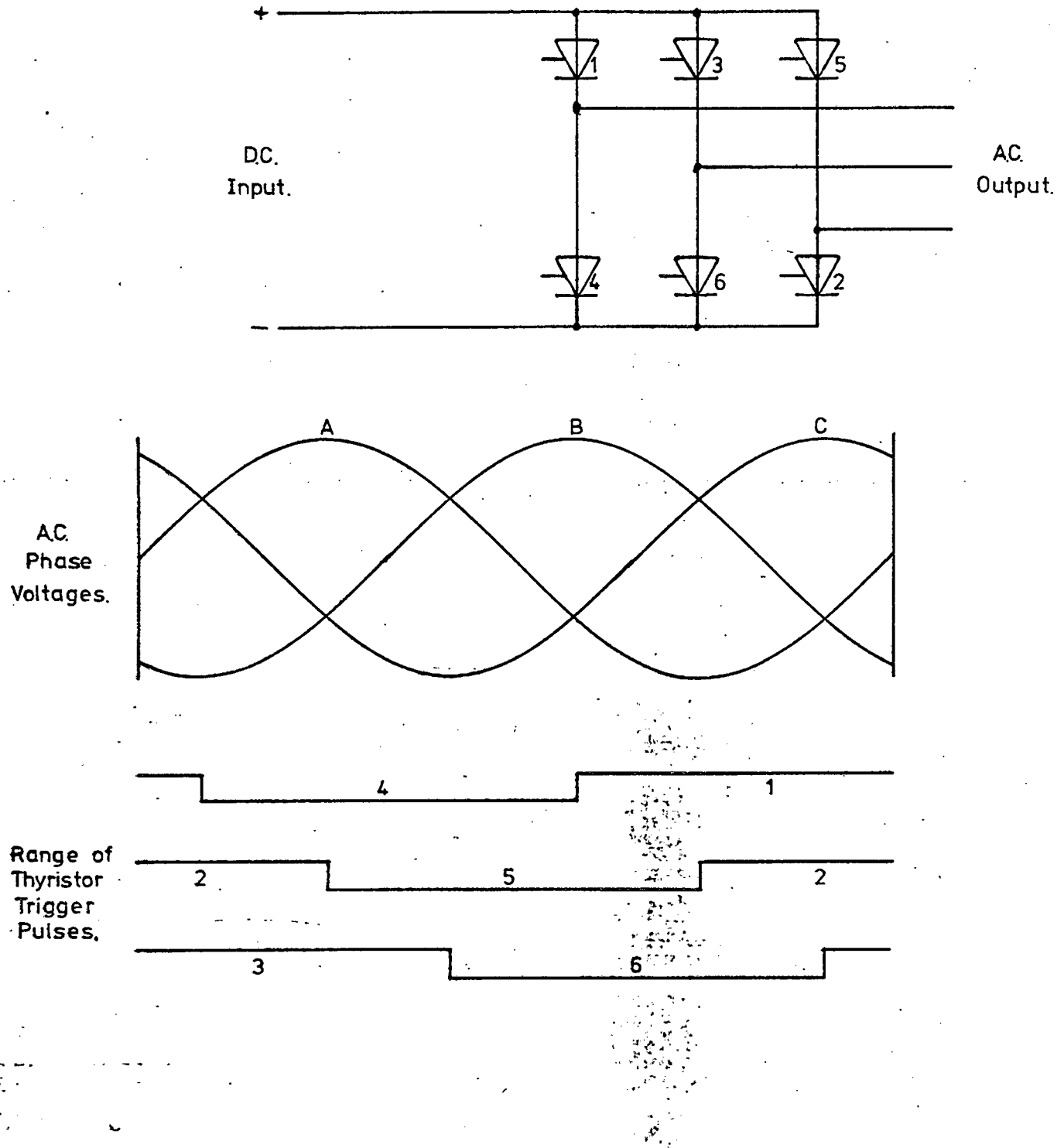

Inveter Circuit Diagram and
Thyristor Firing Range.

Figure 4.1

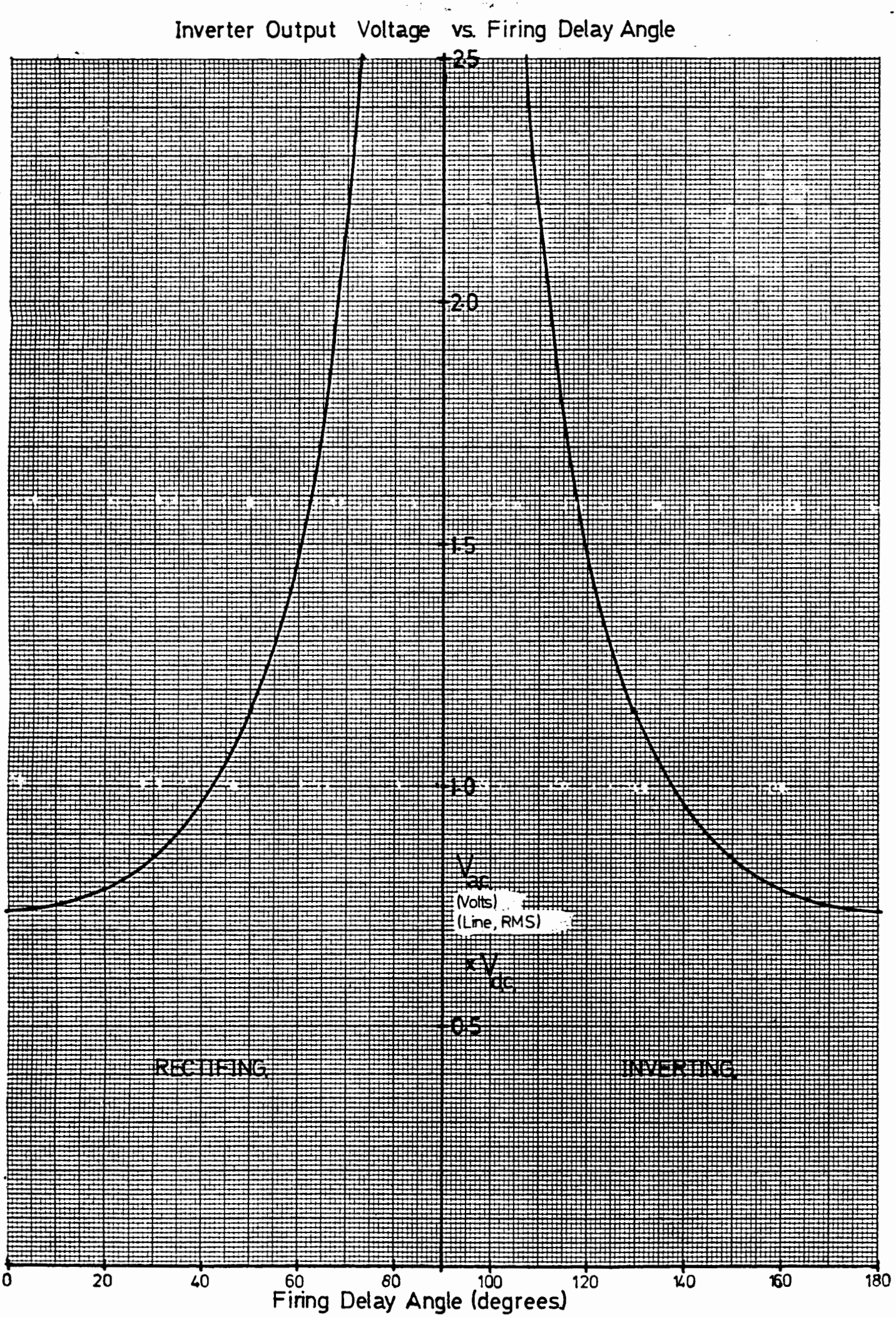
Inverter Output Voltage vs. Firing Delay Angle
2.5
2.0
1.5
1.0
0.5
V_{ac} (Volts) (Line, RMS)
$\times V_{dc}$
RECTIFING
INVERTING
0
20
40
60
80
100
120
140
160
180
Firing Delay Angle (degrees)

Figure 4.2

D.C. voltage is such that power is flowing from the A.C. side to the D.C. side of the bridge, thus rectification is occurring. For a delay angle of 90^{o} to 180^{o} a power flows from the D.C. side to the A.C. side of the bridge and inversion occurs.

Fig. 4.2 shows the output voltage for different delay angles and fixed D.C. voltage.

The equation relating A.C. and D.C. voltage is the same as that for the rectifier but rearranged so that the D.C. voltage is the input and the A.C. voltage the output.

$$V = \frac{\pi \cdot V_{dc}}{3\sqrt{6}\cos(180 - \beta)} = \frac{\pi \cdot V_{dc}}{3\sqrt{6}\cos(\alpha)} \quad \ldots\ldots 4.1$$

where β is the delay angle and α is the inverter advance angle.

$$\beta + \alpha = 180^{o} \quad \ldots\ldots\ldots 4.2$$

It should be noted that whereas the rectifier operated with a positive delay angle and therefore had a lagging power factor, the inverter has a positive advance angle and therefore a leading power factor. Changing the advance angle changes the power factor with unity power factor at zero advance angle. The simplified phasor diagram of Fig. 4.3b shows this.

conditionally true

Under normal operation, power with lagging power factor flows from the supply to the D.C. link and then to the motor, this time with leading power factor. For regeneration the "inverter" rectifies taking leading power from the "motor" ($\alpha > 90^{o}$,

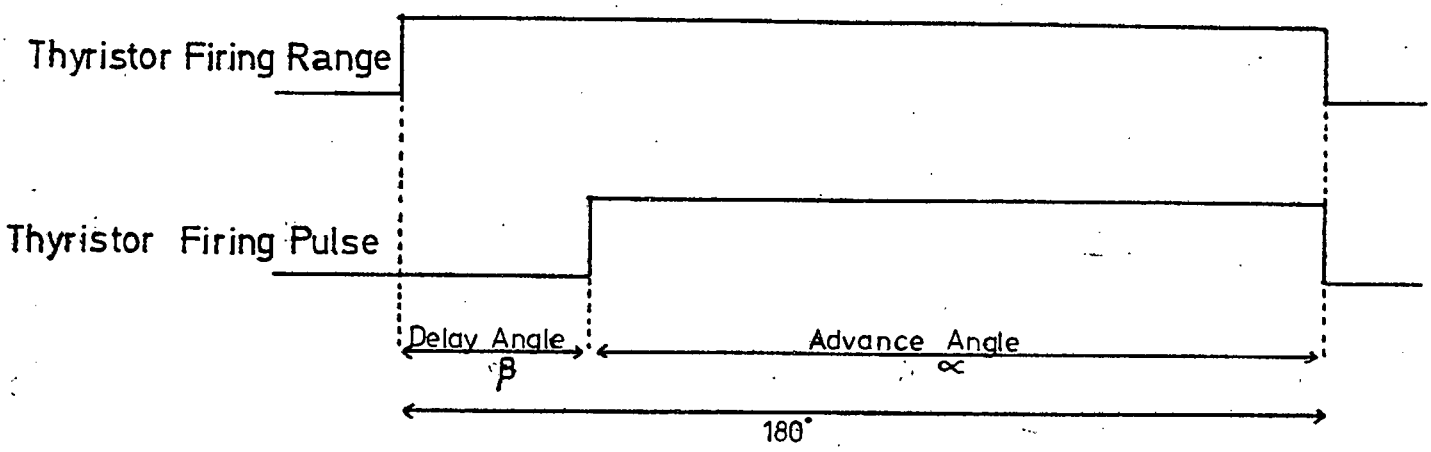

Thyristor Firing Pulse.

Figure 4.3a.

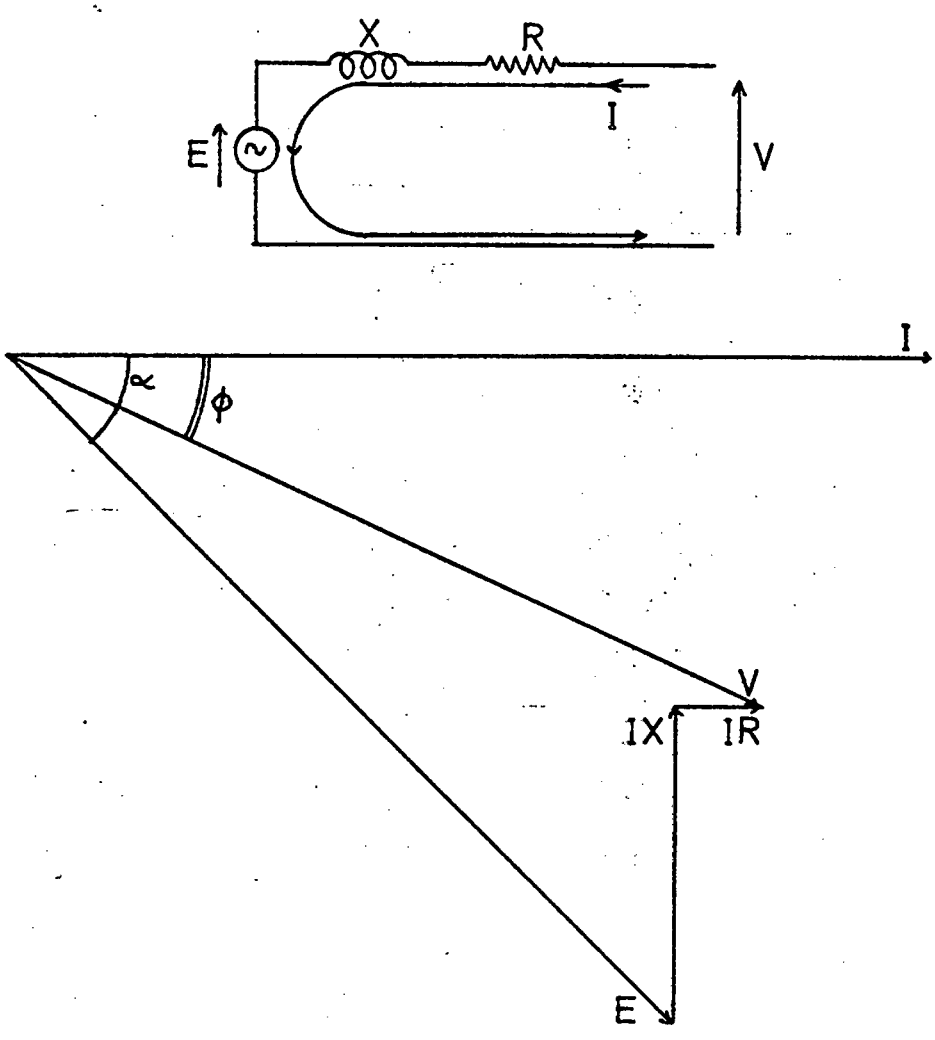

Simplified Phasor Diagram.

therefore cos (α) is negative, i.e. power flow into the motor is negative) and the "rectifier" inverts supplying lagging power to the A.C. supply ($\gamma > 90^{o}$ therefore cos (γ) is negative, i.e. power flow from the A.C. supply is negative).

In this thesis investigation of regeneration was omitted.

Fig. 4.4 shows a typical voltage waveform of a thyristor. For commutation to occur, the period for which the thyristor is reverse biased (the extinction angle) should be greater than the thyristor turn-off time. Clearly, as the advance angle is reduced so the extinction angle is reduced, until at zero advance angle the thyristor does not become reverse biased at all. Thus for commutation to occur there must be sufficient reverse voltage, for the necessary time, to allow the circuit (and thyristor) current to fall to zero.

As was the case for the rectifier, reactance in the A.C. system causes finite thyristor turn-on and turn-off times. In this case the reactance is mainly due to armature winding subtransient leakage reactance and damper winding inductance (if any). This overlap angle is not insignificant and there must be compensation for it.

Fig. 4.5 shows simplified thyristor and line current waveforms. At any instant the sum of the thyristor currents, the sum of the line currents and the D.C. current are all equal and remain approximately constant due to the D.C. smoothing inductance.

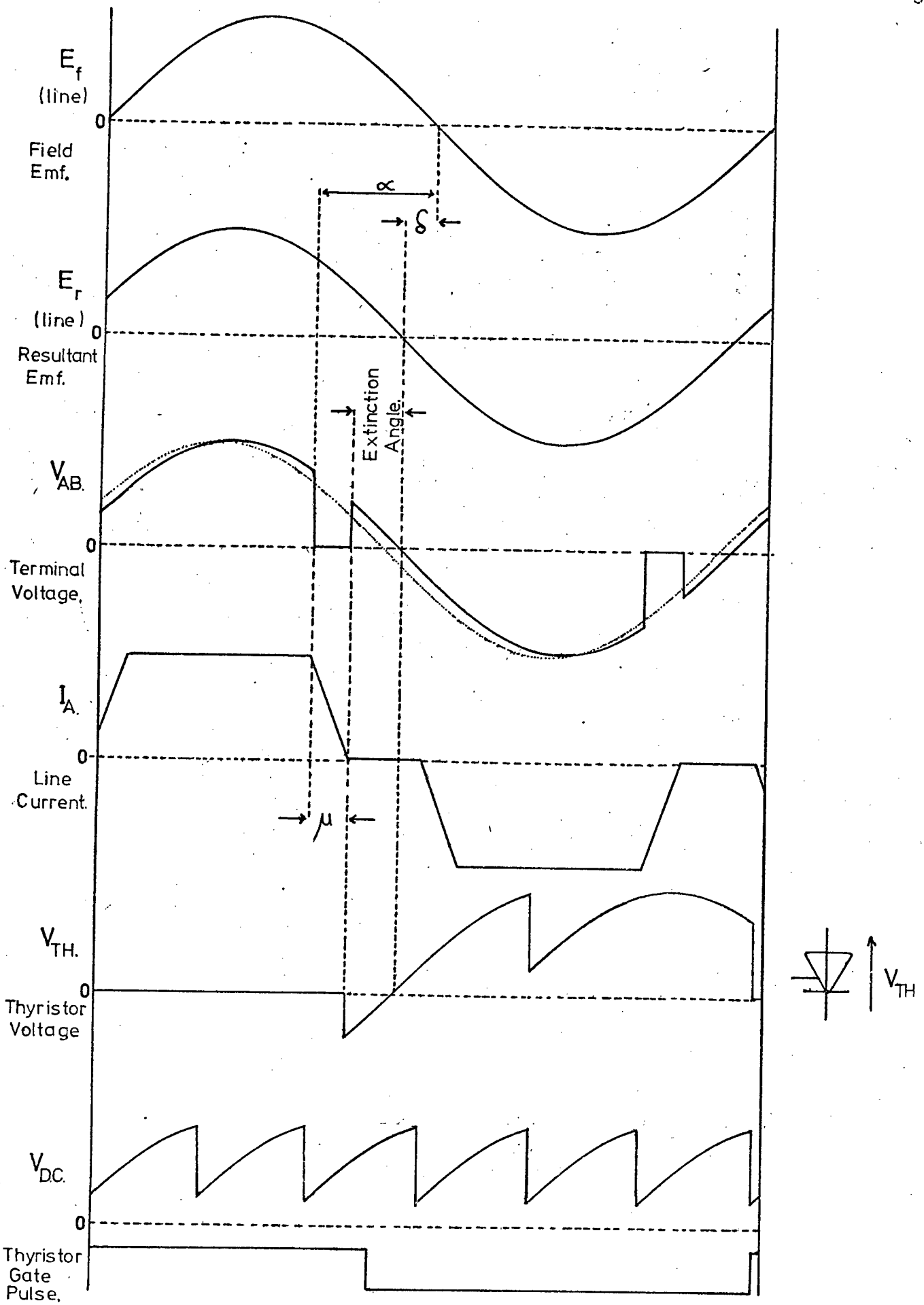

Simplified Voltage and Current Waveforms.

Figure 4.4.

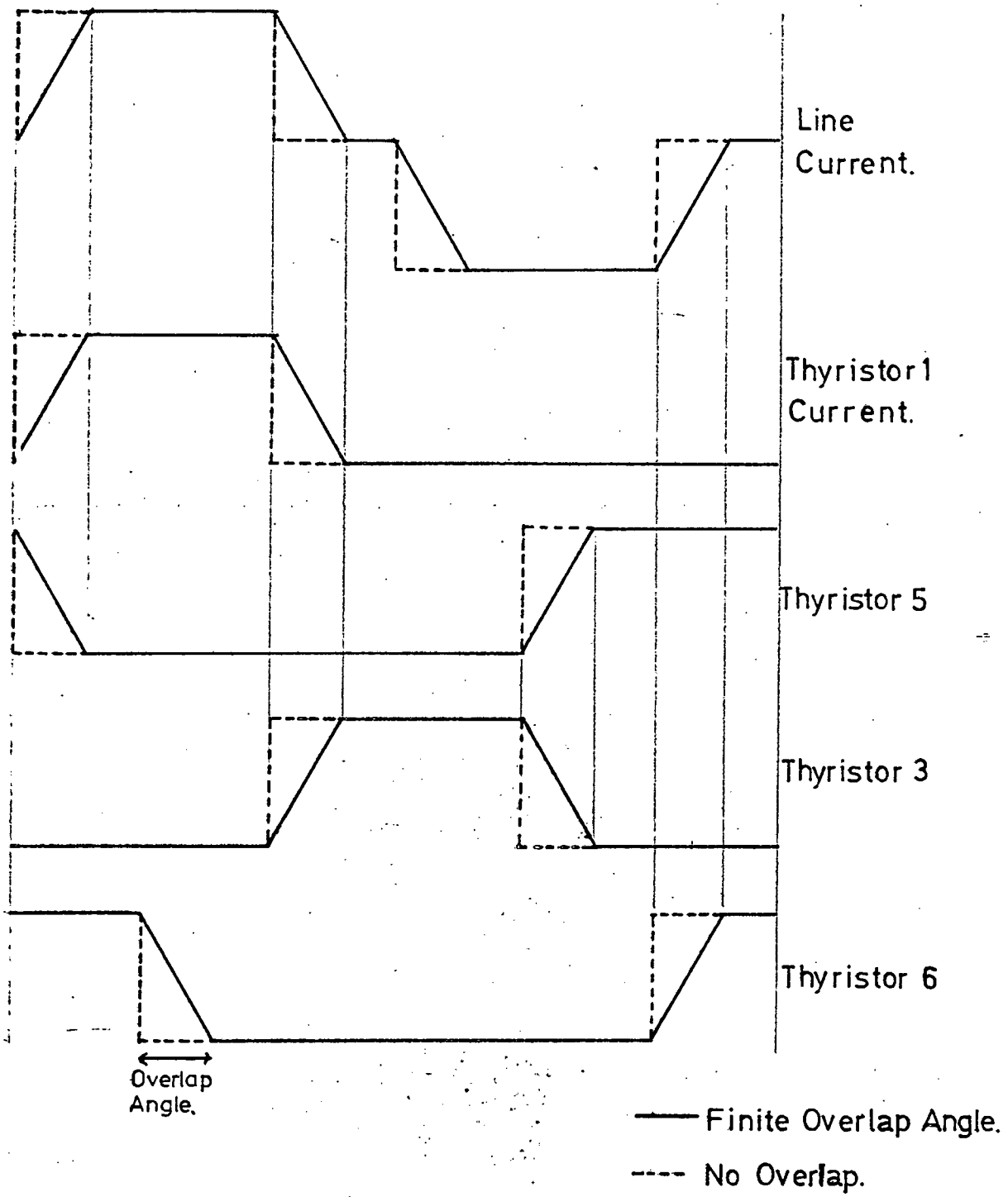

Simplified Current Waveforms.

Figure 4.5.

A block diagram of the main components of the control logic is shown in Fig. 4.6.

Operation of the delay counters is the same as that of the rectifier control circuits. The counters are synchronized to the rotor position and the counter clock frequence is directly related to the motor speed.

At zero and low speeds the motor emf. is insufficient to ensure reliable commutation, and a different method of turning the thyristors off is used. This method will be discussed later.

If regenerative operation was to be incorporated into the drive, simple logic circuits could change the rectifier and inverter thyristor firing instants so that their roles are reversed and power flows from the motor load to the A.C. mains supply.

Reversal of the direction of rotation of the motor could also be controlled by electronically swopping the firing pulses to the thyristors connected to two of the motor phases. This effectively changes the phase rotation of the motor supply.

4.1 Shaft Encoder

A slotted disc was fitted onto the machine rotor. Photo-transistors close to the disc are switched by light shining through the disc slots. Fig. 4.7 shows the circuits used to synchronize the control logic to the motor shaft position.

A buffer transistor mounted close to the photo-transistor, and

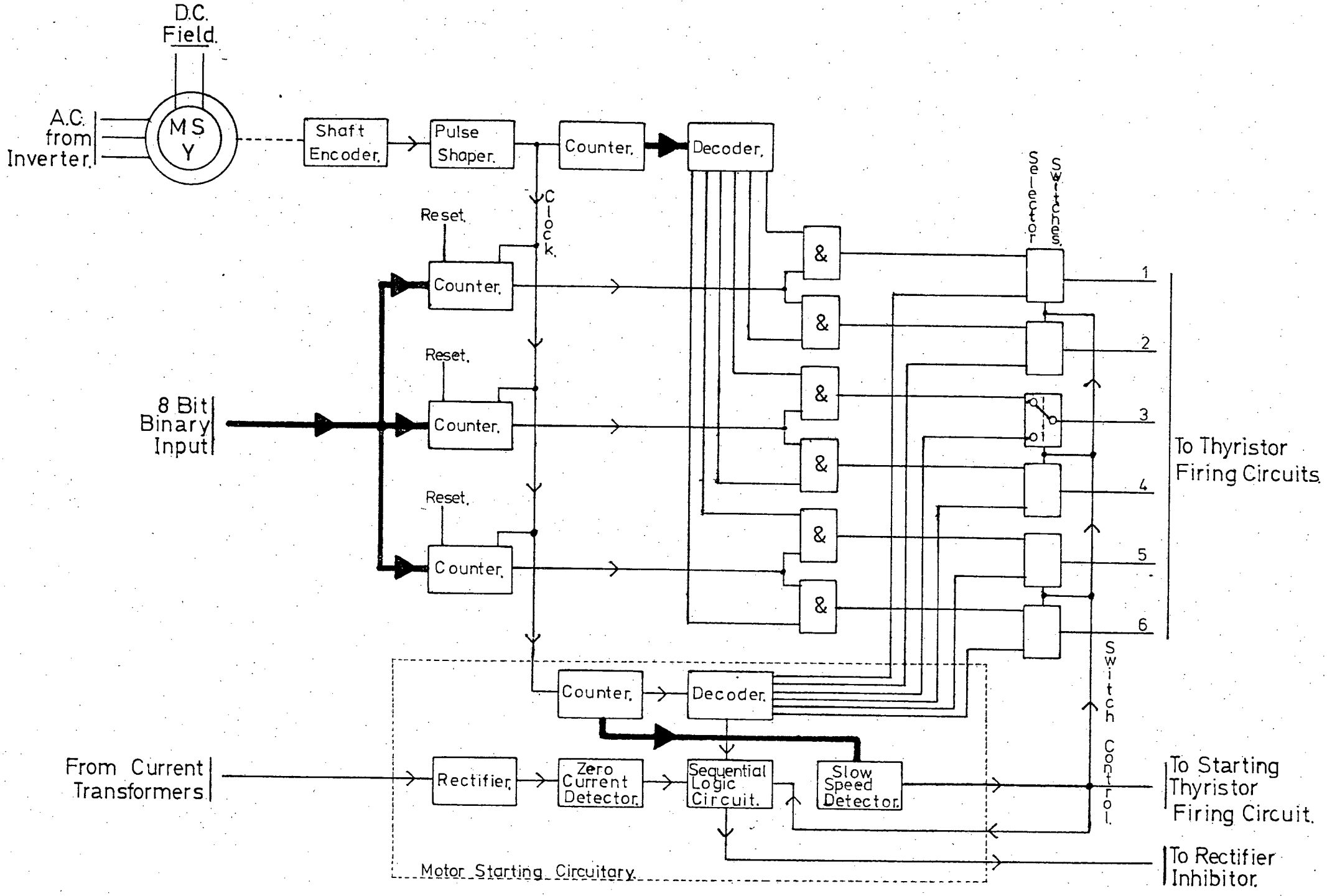

Figure 4.6

Block Diagram of Inverter Control Logic

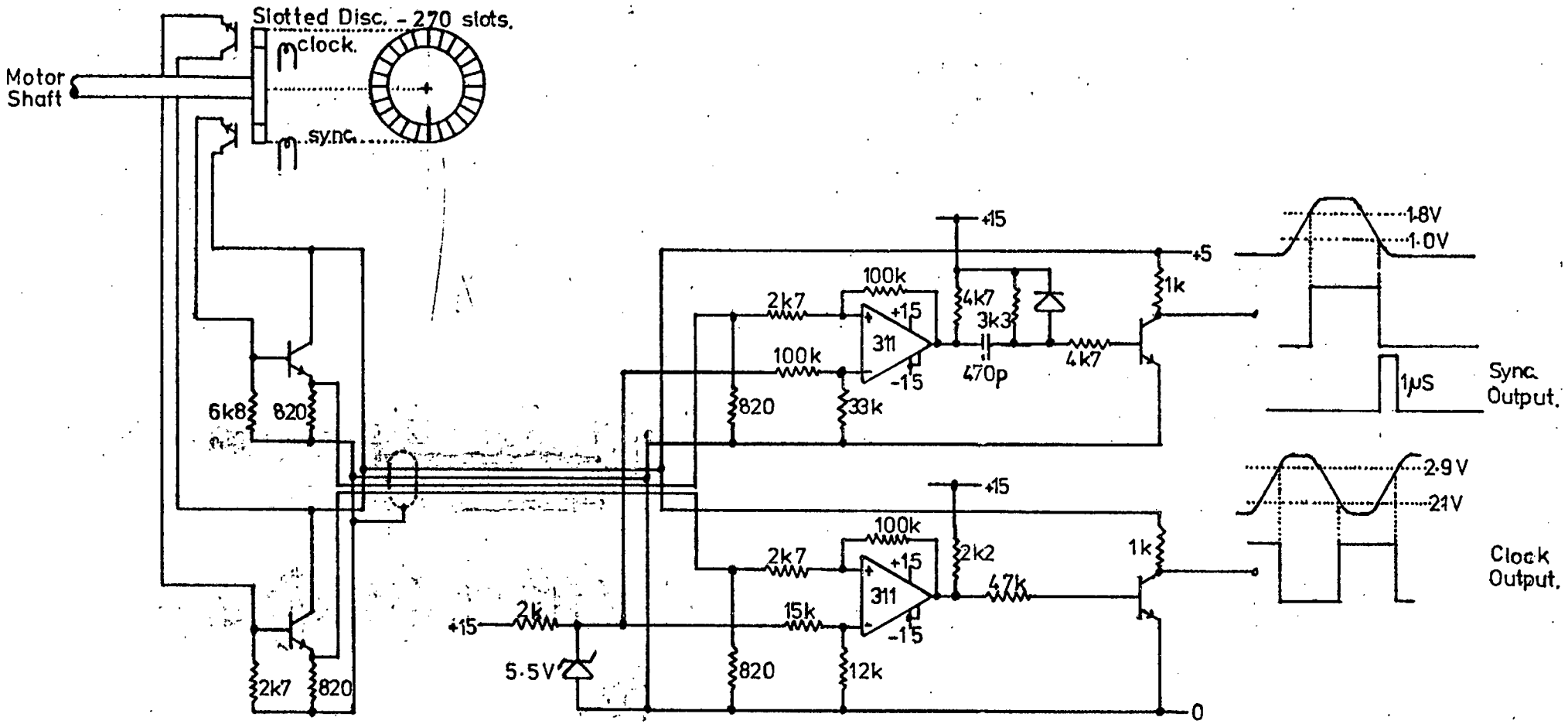

Shaft Encoder and Pulse Shaper Circuit.

Figure 4.7

screened cable from the motor frame to the logic circuitary is used to reduce spurious signals. Schmitt triggers shape the signals and produce TTL compatable outputs.

The position of the disc was adjusted so that the synchronization pulse occurs at the instant that the phase A voltage of the motor emf. is a minimum.

4.2 Motor Starting and Slow Speed Operation

Commutation of the inverter at slow speeds is accomplished by turning off the rectifier until the D.C. current has dropped to zero. This ensures that all the inverter thyristors are in a blocking state. The relevant gate pulses are applied and the rectifier inhibit pulse removed. This causes the rotor to rotate and the process is repeated when it becomes necessary for a new set of inverter thyristors to be gated.

When starting, the thyristors are fired so as to produce maximum torque, and the firing instants are independent of the 8 bit binary input. The advance angle for maximum torque is zero.

The rectifier is switched off and new inverter thyristors selected every 1/6 of an electrical cycle.

When the motor has reached approximately 10% of rated speed the control logic automatically switches over to the normal mode of operation.

Fig. 4.8 shows the thyristor firing positions and the position

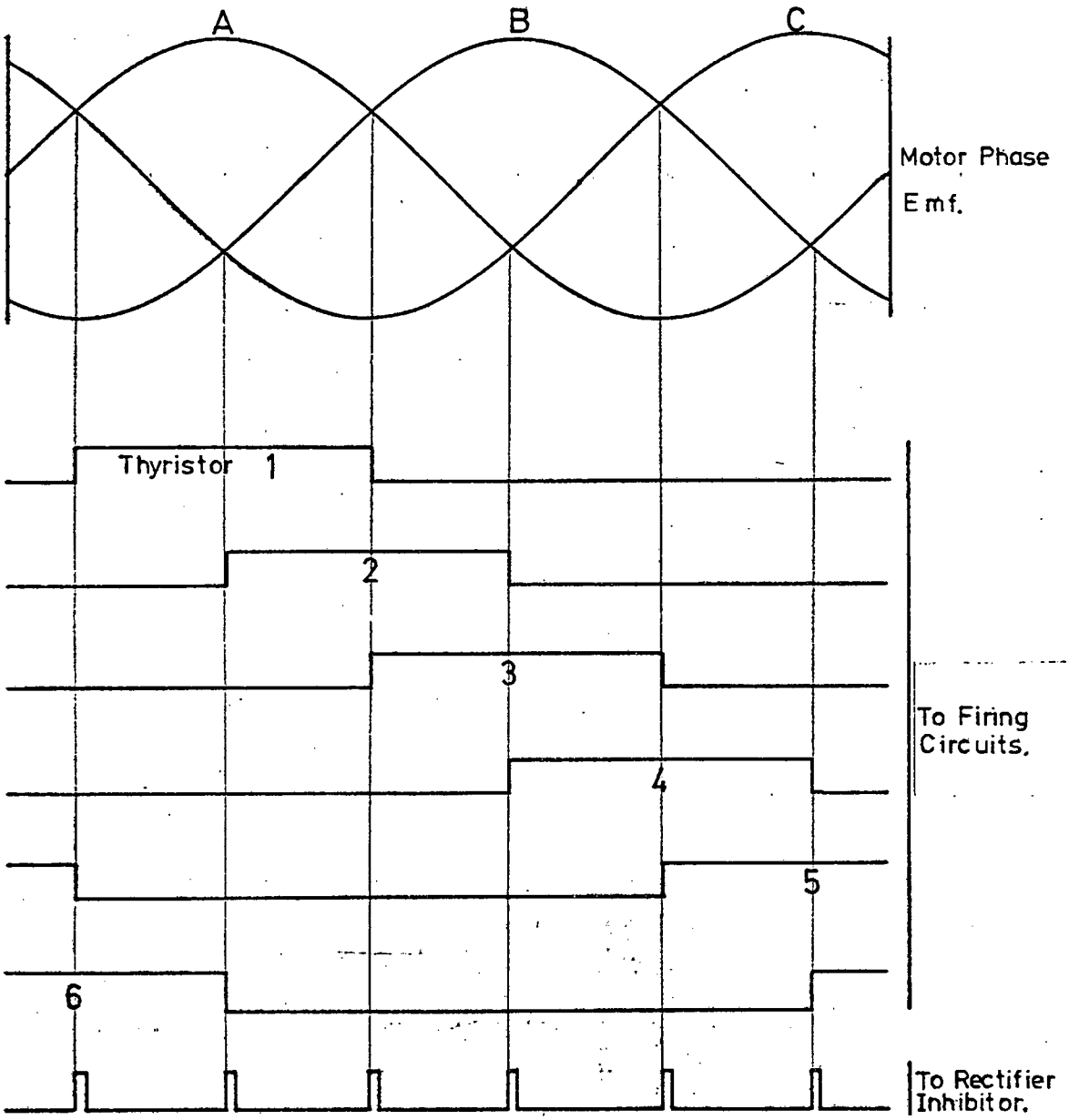

Firing Pulses for Motor Starting.

Figure 4.8

at which the rectifier is inhibited in relation to the motor emf. (or position).

When the above system was tested it was found that noise and the jerky movement of the rotor was causing the system to lose synchronization and so cause a malfunction and motor stalling. At high currents it took a relatively long time for the D.C. current to drop to zero because of the energy stored in the D.C. smoothing inductor.

The operation of the motor at slow speed was made smoother and more reliable by the addition of an extra thyristor, placed across the D.C. smoothing inductor and fired continuously during slow speed and starting operation.

Fig. 4.9 shows the basic power circuits with the additional thyristor. This thyristor has no effect under normal operating conditions because it is then in the blocking state.

The extra thyristor improves inverter commutation in two ways.

(a) When the rectifier receives an inhibit pulse, the current through the inductor continues to circulate through the starting thyristor. The current through the rectifier and inverter is, however, zero. The time taken for the inverter current to fall to zero is much less than previously because the energy stored in the smoothing choke does not need to be removed. Thus inverter commutation is made much faster.

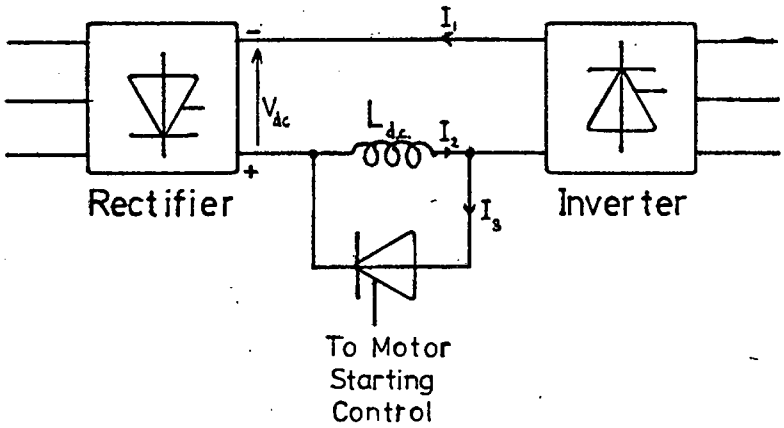

Motor Starting Circuit.

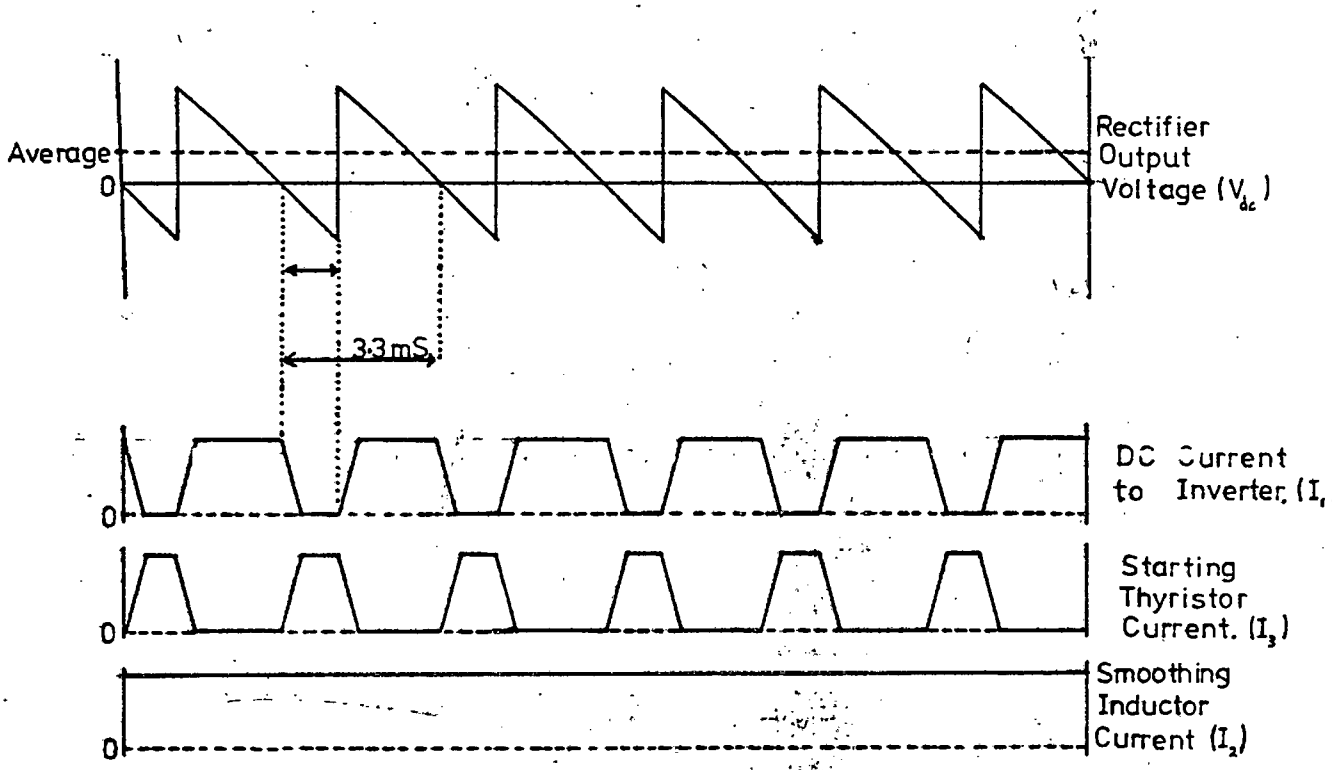

Simplified Voltage and Current Waveforms

Figure 4.9.

(b) During slow speed operation the D.C. voltage is small (current limit circuit ensures this). Although the average value is positive, the output of the rectifier does have substantial periods of negative output voltage occurring every 3.3 mS. These cause the "starting" thyristor to be forward biased and so are conducted to the inverter input. The negative voltage reverse biases the inverter thyristors and enables commutation to take place. The inverter is therefore commutated every 3.3 mS. Once the rectifier output voltage goes positive again the "starting" thyristor becomes reverse biased and commutates and the full D.C. current again flows into the inverter. Thus current build-up in the inverter is fast, as the D.C. smoothing inductor does not limit the rate of rise of current.

Unfortunately the motor used could not be loaded at low speeds and so starting torque could not be measured directly. Speed/time graphs, however, show that the acceleration (and hence torque) of the motor is greater during the starting process than just after switching to the normal operating mode.

4.3 Thyristor Firing

As is the case for the rectifier, it is necessary for two inverter thyristors to be gated for a current to flow. If the inverter is operating with an advance angle close to zero, (the most common condition as the power factor is then close to unity) then it is necessary to extend the firing pulse by 60° from this

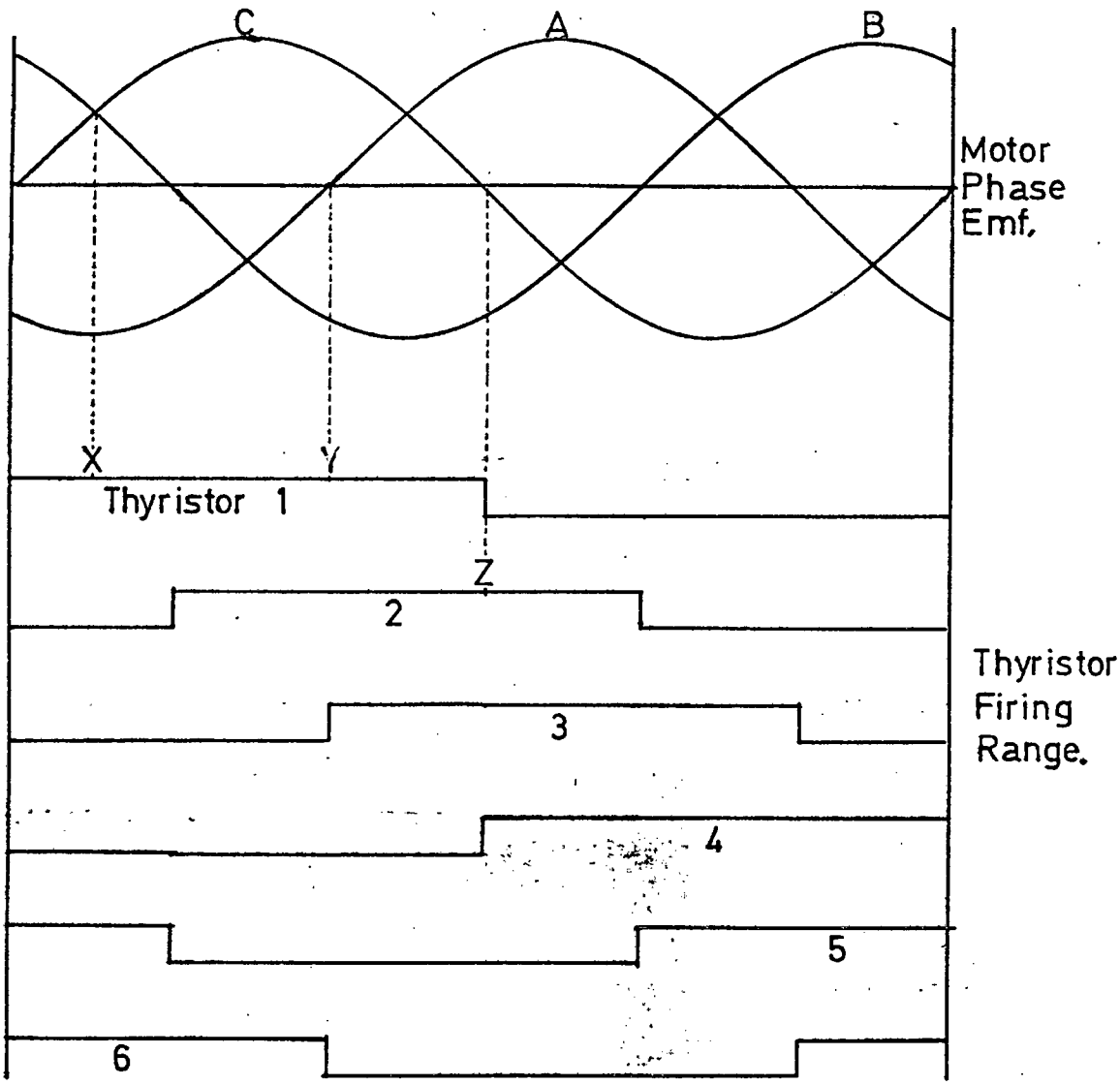

Inverter Bridge Firing Range.

Figure 4.10

point to enable two gate pulses to overlap. As the regeneration aspect of operation is not investigated in this project, the condition for a delay angle of between zero and sixty degrees is not necessary. It was therefore decided to "shift" the range of thyristor trigger pulses by 60° as shown in Fig. 4.10. 30° is shown in fig 4.10 ?

Point X corresponds to an advance angle of 90° and point Y to an angle of 0°. Under normal inverter operation the thyristor initial gate pulse occurs between points X and Y. For zero advance angle thyristor 1 is fired at point Y and thyristor 2 at point Z. These two pulses must overlap and the gate pulse of thyristor 1 therefore extends 60° from point Y to point Z.

4.4 Test Results

Initial tests were performed by connecting the inverter to an alternator and operating the inverter with an advance angle of greater than 90°, i.e. rectifying. This enabled synchronization and logic problems to be eliminated before inversion was attempted.

Fig. 4.11 shows photographs of the inverter voltage+current waveforms. The oscilloscope was triggered on the same point for all of the photographs and so phase relationships can be observed. These photographs were taken later in the project but are useful to the explanation of the inversion process and so they have been presented here. The conditions under which the photographs were taken were:

V_{dc}	:	172 V
V	:	87 V
I_{dc}	:	25 A
Advance angle	:	60^{o}
Octal input number	:	360_{8}
Operating frequency	:	37 Hz.

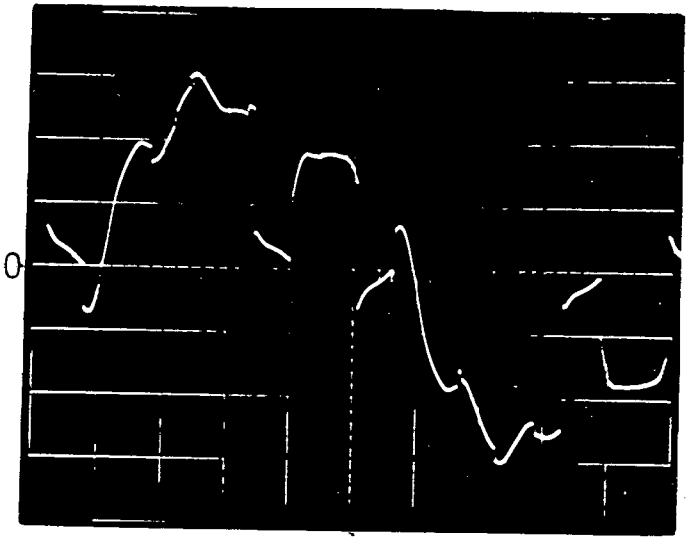

Motor Phase Voltage. 50V/div.

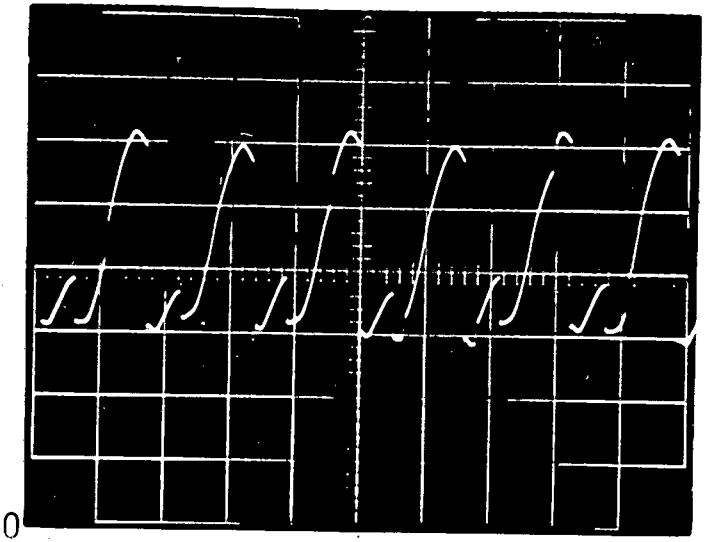

DC. Voltage. 40V/div.

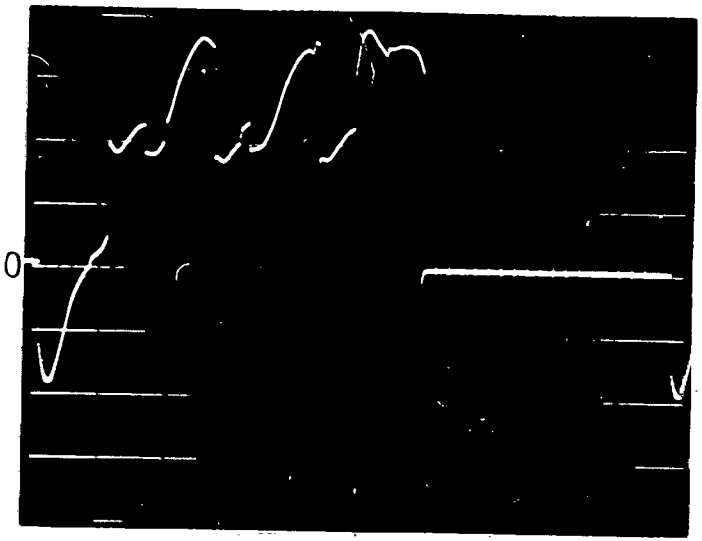

Thyristor Voltage. 60V/div.

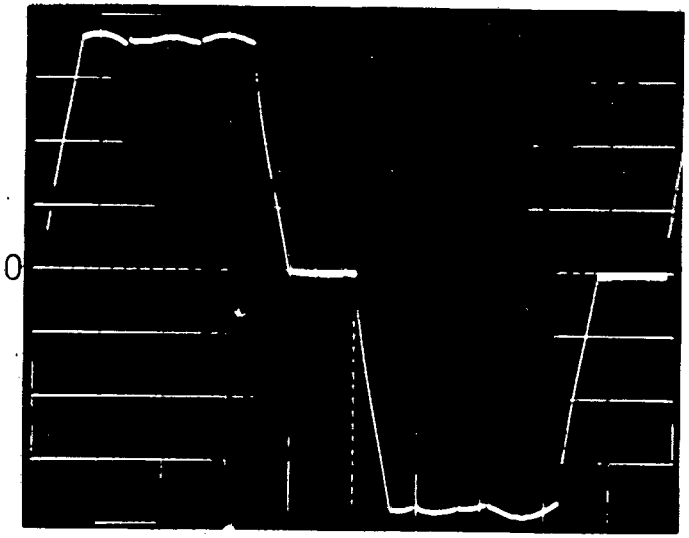

Motor Line Current. 7A./div.

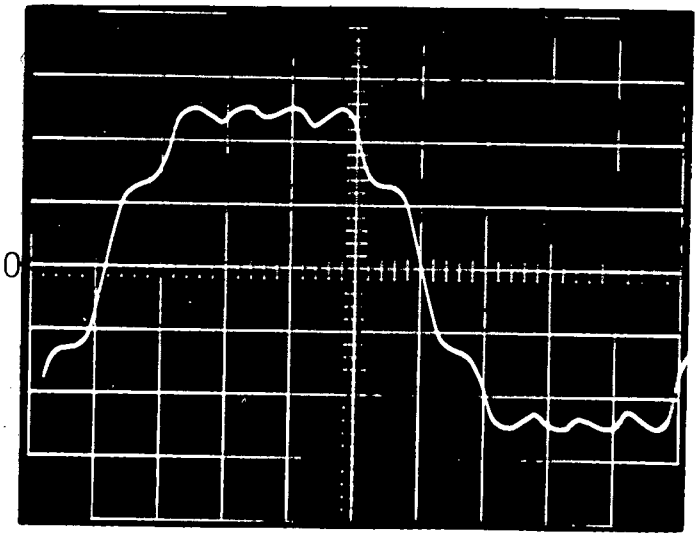

Motor Phase Emf. 50V/div.

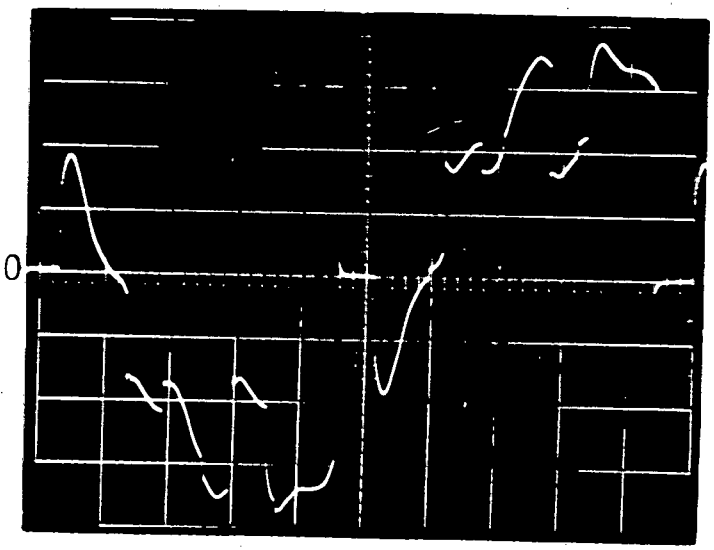

Motor Line Voltage. 100V/div.

Figure 4.11

Inverter Voltage and Current Waveforms. Horz. scale. 2·7 ms/div.

CHAPTER 5.

THE OVERALL SYSTEM

Up until this point the rectifier, D.C. link, and inverter have all been considered ideal. This was done to simplify the explanation of the operation of the system. The most important deviations from an ideal system will be discussed below.

5.1 Impedance in the Rectifier A.C. Lines

This impedance is made up of the supply impedance, the transformer primary and secondary resistance and leakage reactance and the impedance of the connecting cables.

The resistive component causes IR voltage drops and therefore reduces the rectifier output voltage.

As already described in Chapter 3, the reactance causes thyristor overlap to occur. During overlap two phases of the A.C. supply are short circuited and the result is a reduced D.C. output voltage. It can be shown (Davis, 1971) that :

$$V_{dc} = \frac{3\sqrt{6}}{\pi} \cdot V_{ac} \cdot \cos(\gamma) - \frac{3 \cdot I_{dc} \cdot X_{ac}}{\pi} \qquad \ldots\ldots\ldots 5.1$$

$$X_{ac} \cdot I_{dc} = \sqrt{6} \cdot E \cdot \left(\sin^2\left(\frac{\gamma+\mu}{2}\right) - \sin^2\left(\frac{\gamma}{2}\right)\right) \qquad \ldots\ldots 5.2$$

where μ = overlap angle.

With the transformer and leads used in this project, the effect

of resistance and reactance in the A.C. supply is small and has been disregarded in future calculations.

The overlap angle is less than 5^{o} at full load current.

5.2 D.C. Link Impedance

Series resistance of the D.C. link (including the smoothing inductor) causes an IR voltage drop in the D.C. input voltage to the inverter.

5.3 Series Impedance of Motor Armature

Armature and connecting lead resistance cause IR voltage drops and need to be included in theoretical calculations. As the motor current is not sinusoidal, accurate calculations of the effects become complex. In the analysis of this system the armature resistance has been transferred to the D.C. side of the inverter as an effective resistance for some of the calculations. This has made calculations of the expected inverter output voltage easier.

$$R_{dc.eff} = R\left(2 - \frac{3\mu}{2\pi}\right) \qquad \ldots\ldots\ldots 5.4$$

where R = motor armature and A.C. lead resistance

μ = overlap angle

See Appendix E.

Series reactance of the inverter A.C leads and the motor sub-transient armature reactance cause thyristor overlap. It can

be shown (Davis, 1971) that for the inverter

$$V_{dc} = \frac{3\sqrt{6}}{\pi} .E.\cos(\alpha) + \frac{3\ I_{dc}X''}{\pi} \quad \ldots\ldots\ldots 5.4$$

$$I_{dc}X'' = \sqrt{6} \cdot E \cdot (\sin^2 (\frac{\alpha + \mu}{2}) - \sin^2 (\frac{\alpha}{2})) \quad \ldots\ldots 5.5$$

where X" is the machine subtransient armature leakage inductance.

The overlap also introduces a lagging phase shift in the current waveform of approximately $\mu/2$ and it is necessary to increase the inverter advance angle to compensate for this.

5.4 Armature Reaction

Armature reaction has the effect of not only reducing the motor emf. and therefore the thyristor commutating voltage, but it also reduces the extinction angle of the thyristors. This is because at high armature currents, the armature reaction mmf. wave causes the resultant mmf. wave to lead the field mmf. wave.

Thus under load conditions the motor resultant emf. leads the no-load emf., and, as the current leads the no-load (or field) emf. the angle between the current and the resultant emf. is reduced. This effectively reduces the inverter advance angle. It is therefore necessary to increase the advance angle at high currents to compensate for armature reaction phase shift and to prevent commutation failure.

At low currents the motor now operates at a low power factor. The power factor increases as current increases.

The effects mentioned in Sections 5.2 to 5.4 are compensated for in the following manner.

(a) The rectifier output voltage needs to be increased to counteract resistive and inductive voltage drops and the reduction in voltage due to thyristor overlap. The rectifier voltage needs to be reduced to compensate for a reduced motor emf. due to armature reaction.

(b) The inverter angle of advance must be increased to allow for thyristor turn-off and turn-on times and also to compensate for armature reaction reducing the angle between the current and the motor emf.

Reference to the phasor diagram of Fig. 5.1 will help clarify the abovementioned effects.

5.5 Initial Testing

Initial testing of the system as a whole was performed using a small synchronous alternator with a "V" belt drive to a small D.C. motor. At this stage the inverter did not incorporate the starting control logic and the D.C. motor was used for that purpose as well as for a load once the A.C. motor/inverter was operational.

Fig. 5.2 shows the original test system.

The synchronous alternator specifications are given in Appendix F.

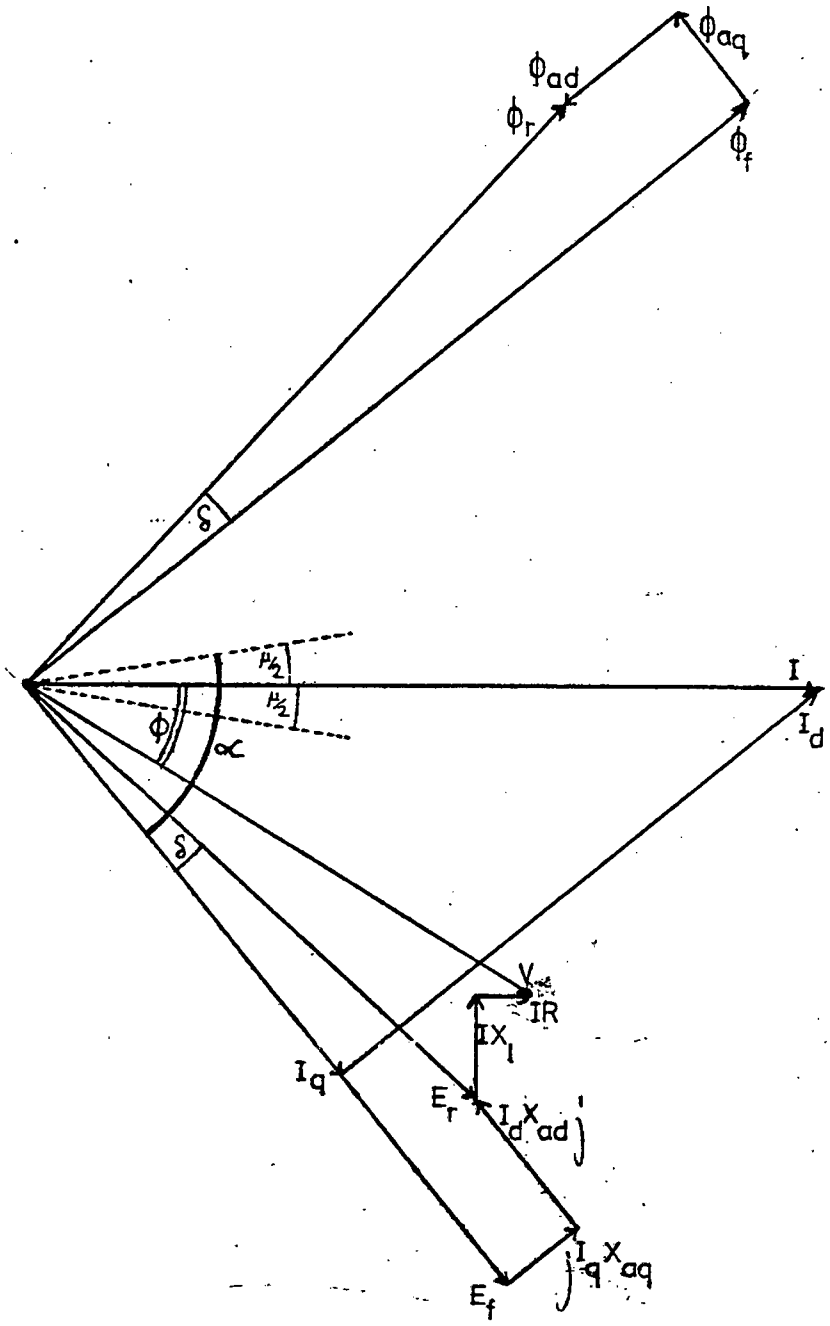

Scale: 1cm.=2A.
1cm.=10V.

Typical Motor Phasor Diagram.

Figure 5.1

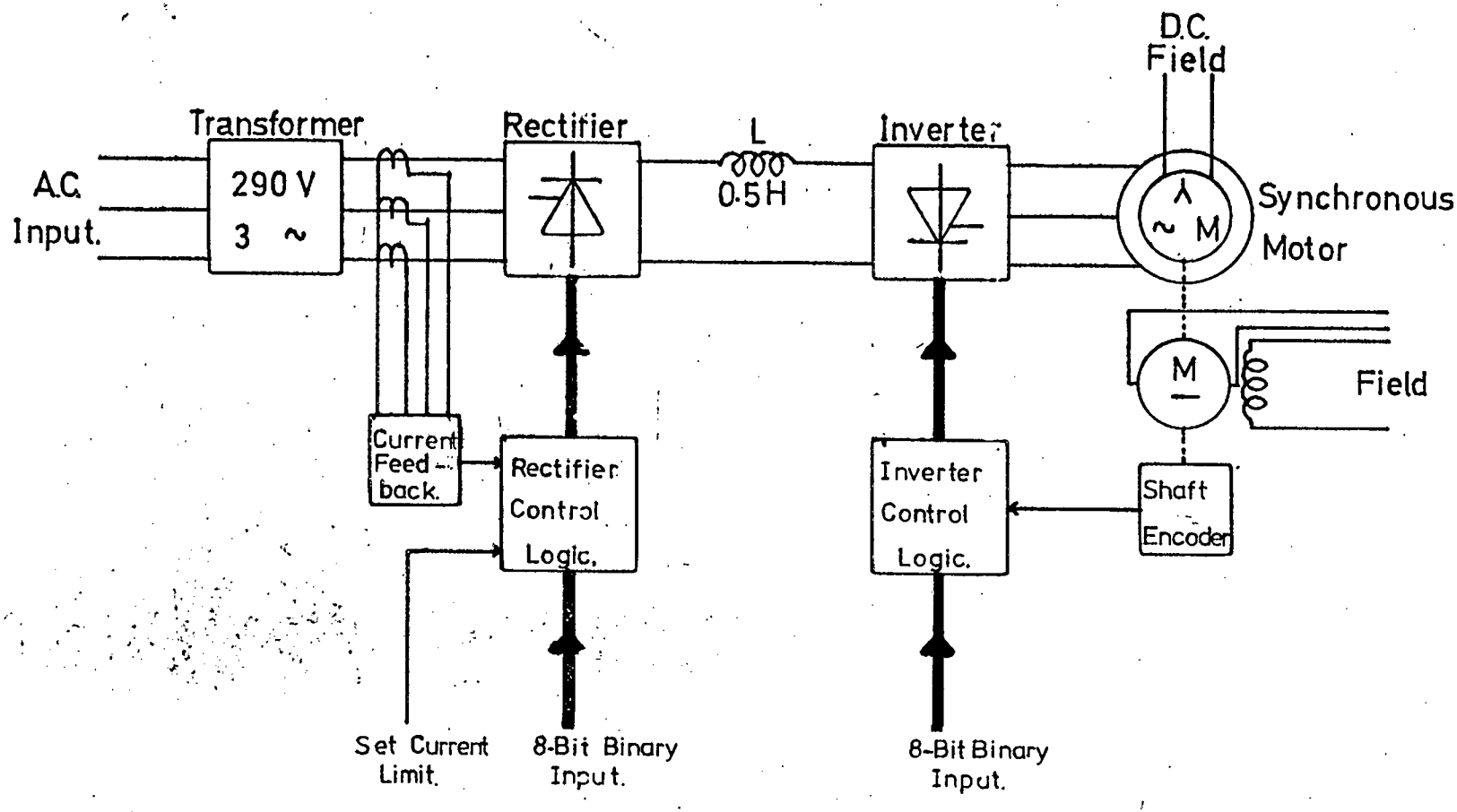

Figure 5.2

Block Diagram of Test System

The thyristors used for both bridges were BTX 48-1200.

The drive operated satisfactorily over a speed range of 300 r.p.m. to 3800 r.p.m. A typical set of results being:

Rectifier:	phase voltage	:	170 V
	line current	:	0.7 A
	power factor	:	0.77 lagging
D.C. Link:			300 V
			0.9 A
Motor:	phase voltage	:	156 V
	line current	:	0.7 A
	power factor	:	0.85 leading
	frequency	:	70 Hz.

This low power system was used to help iron out problems in the apparatus and also used to develop the starting and slow speed operation control logic.

Unfortunately, the no-load current demanded by the A.C. motor was close to its rated value and so load tests could not be performed. In addition, the rated voltage of the transformer was not sufficiently high to enable the motor to operate close to rated speed with the inverter advance angle close to zero (i.e. high speed operation at high power factor was not possible).

The shaft encoder on this motor consisted of a gear wheel with

96 slots. As the motor had 4 poles, 48 slots corresponded to one electrical cycle (i.e. 1 slot = 7.5^{o} electrical). It was found that this did not allow sufficient accuracy in the inverter control.

As stated in Section 3.4, the current limit circuit was improved using this low power device.

Because of these limitations it was decided to move to a bigger machine. A 5 kW salient pole alternator was available in the laboratory and was used. See Appendix B for specifications.

5.6 Final System

Minor modifications to the system were required to allow for the motor being a 6 pole machine instead of the previous 4 pole motor. A more accurate 270 slotted disc was made and fitted to the machine shaft as the shaft encoder.

Larger thyristors for both bridges were necessary and 50A silicon controlled rectifiers, type number IR36REA120 were available and used.

A 250 V, 3 phase transformer of adequate rating and two 0.2H 14 A iron cored inductors (used in parallel) replaced the smaller units in the test system.

Switches were still used for setting the inputs to the rectifier and inverter control logic.

A number of problems were encountered before the whole system operated satisfactorily. At high currents, pickup on the cables to the thyristor gates caused spurious firing. Screened cable for the gate connections was found to be necessary to prevent this. Slight irregularities in the slot widths of the shaft encoder and axial movement of the rotor caused modulation of the photo-transistor outputs. Modification of the Schmitt triggers in the pulse shaping circuitry and incorporation of a single transistor preamplifier reduced these errors and also decreased spurious noise signals.

A Schrage motor mounted on the same bedplate and which could be coupled to the synchronous motor was used as a load. Unfortunately this motor had a minimum speed of 375 r.p.m. and could not be switched in when being driven because of synchronization problems. Once running, however, the load could be changed by means of a hand operated brush shifting gear. Full load tests could only be performed above 400 r.p.m. because of the limitation in speed of the Schrage motor.

The high subtransient leakage inductance caused overlap angles to be large (greater than 20^{o} at high currents) and the effects of large armature reaction necessitated operation with a high value of inverter advance angle (typically 50^{o} to 60^{o}) to enable the rated power output to be obtained. This resulted in a substantial "droop" of the speed vs. current (with constant D.C. voltage) curve of the inverter/motor set.

Fig. 5.3 to 5.5 show the effects of the 3 control variables

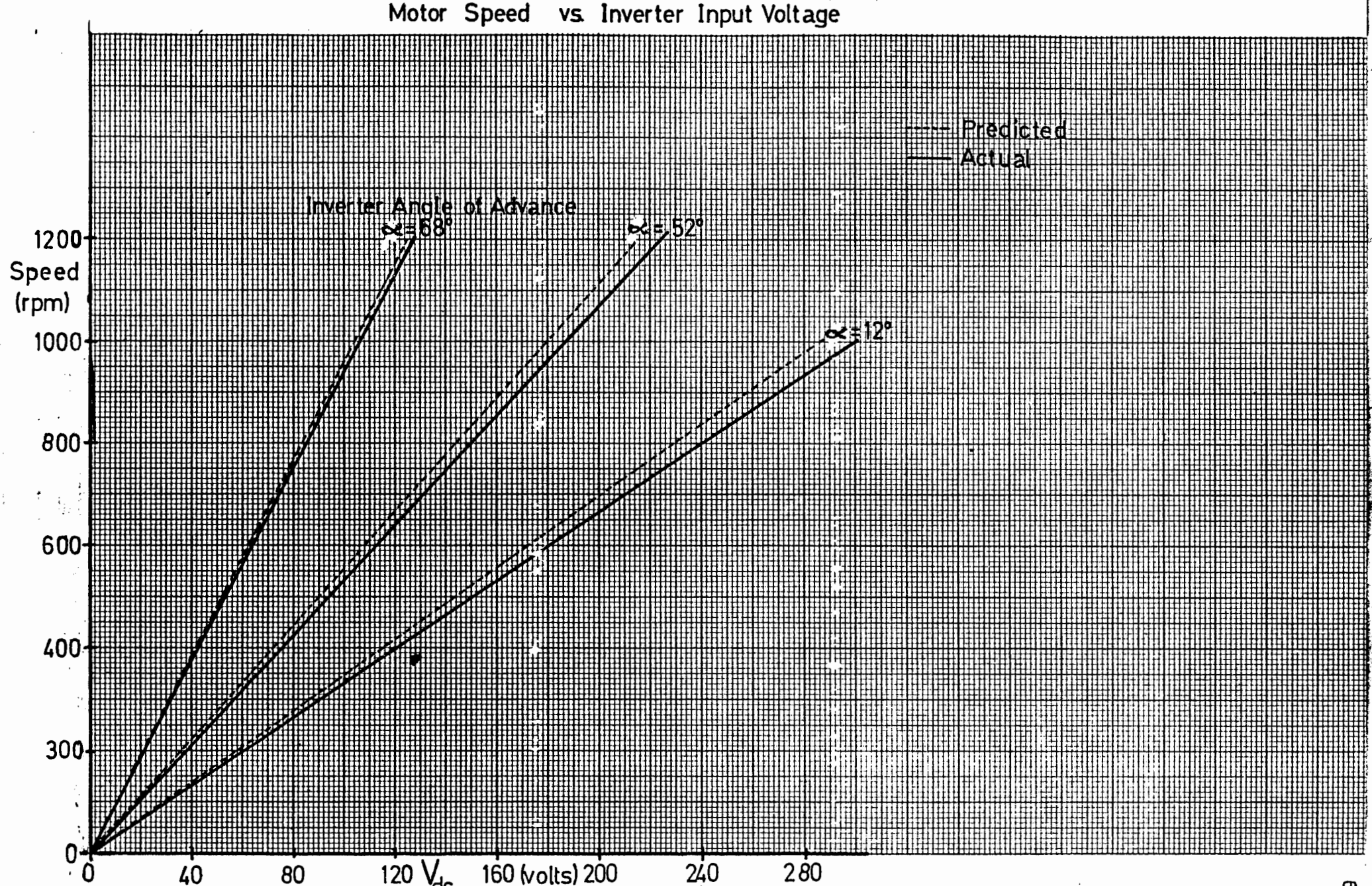
Motor Speed vs. Inverter Input Voltage
Predicted
Actual
Inverter Angle of Advance
∝=68°
∝=52°
∝=12°
Speed (rpm)
1200
1000
800
600
400
300
0
0
40
80
120 V_{dc}
160 (volts) 200
240
280

Figure 5.3

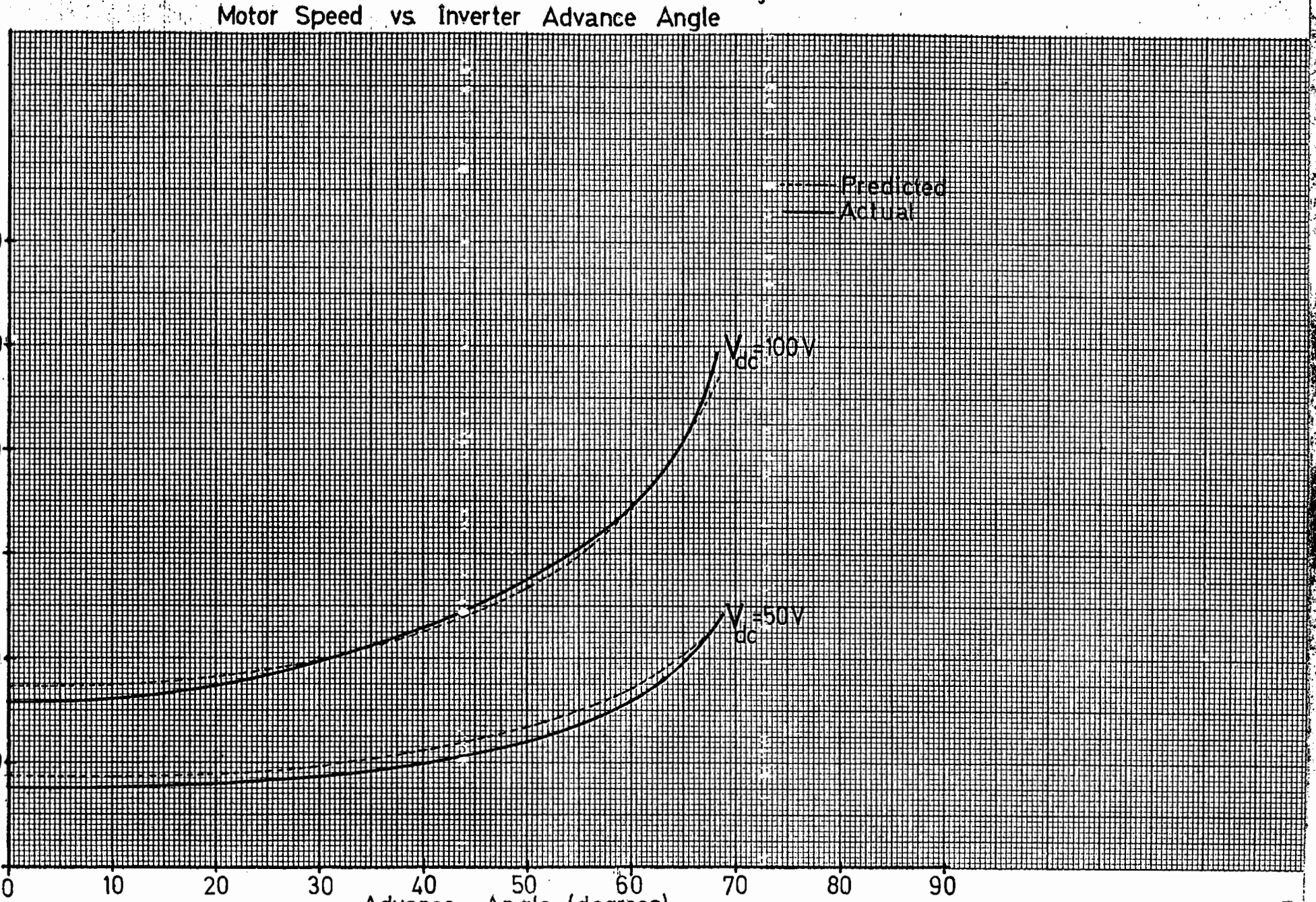
Motor Speed vs Inverter Advance Angle
Predicted
Actual
Speed (rpm)
1200
1000
800
600
400
200
0
V_{dc}=100V
V_{dc}=50V
0
10
20
30
40
50
60
70
80
90

Figure 5.4

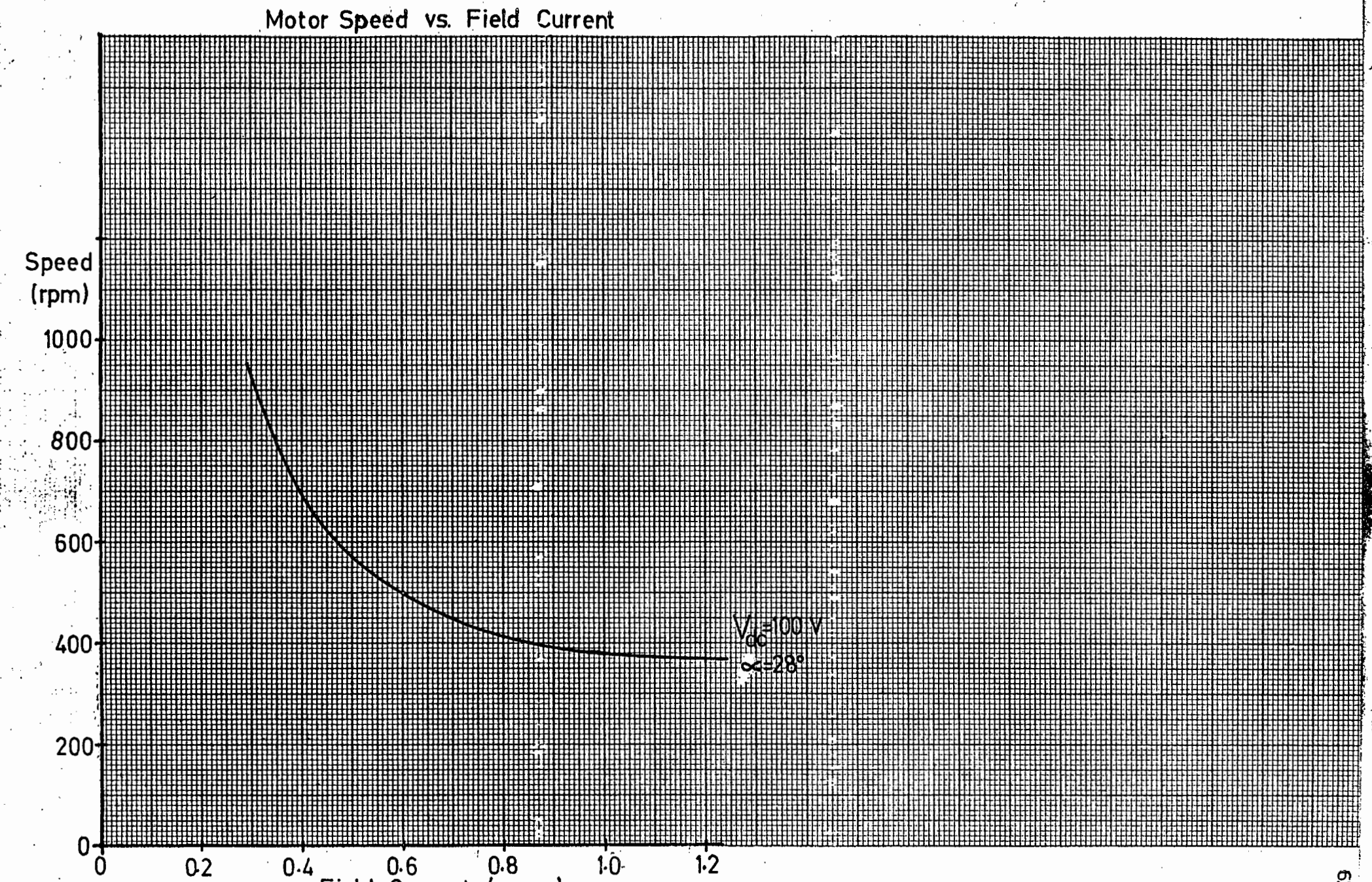
Motor Speed vs. Field Current
Speed (rpm)
1000
800
600
400
200
0
0
0·2
0·4
0·6
0·8
1·0
1·2
V_{dc}=100 V
∝=28°

Figure 5.5

(D.C. voltage, inverter advance angle and field current) on the speed of the motor under light load conditions. These correspond closely with expected results calculated using Equations 2.2 to 2.4.

Under load conditions it is necessary to account for armature reaction, resistive losses and thyristor overlap in trying to predict the steady state characteristics of the system. As stated earlier these equations become involved, and so prediction has only been done for a few sets of conditions. An itterative process of solving the system equations, given in Appendix C, was used to predict the torque/speed curves given in Fig. 5.6. As can be seen, the actual measured results correlate fairly well with predicted results for high torques. For light loads prediction became inaccurate because it was assumed that once the current became discontinuous it ceased to flow at all. This is not the case in reality as torque is produced and the system operates with a discontinuous D.C. current. Measurement of the air gap torque produced at light loads is also difficult because it is difficult to determine losses due to friction and windage and also losses in the Schrage motor load. Accurate measurement and prediction of these quantities is not an essential part of this thesis, and only varification of the basic system equations was desired. This has been done by the correlation of results at large loads, and it was decided it was unnecessary to try and improve prediction and measurement methods for the light load cases.

Fig. 5.7 and 5.8 show the measured effects of loading on the

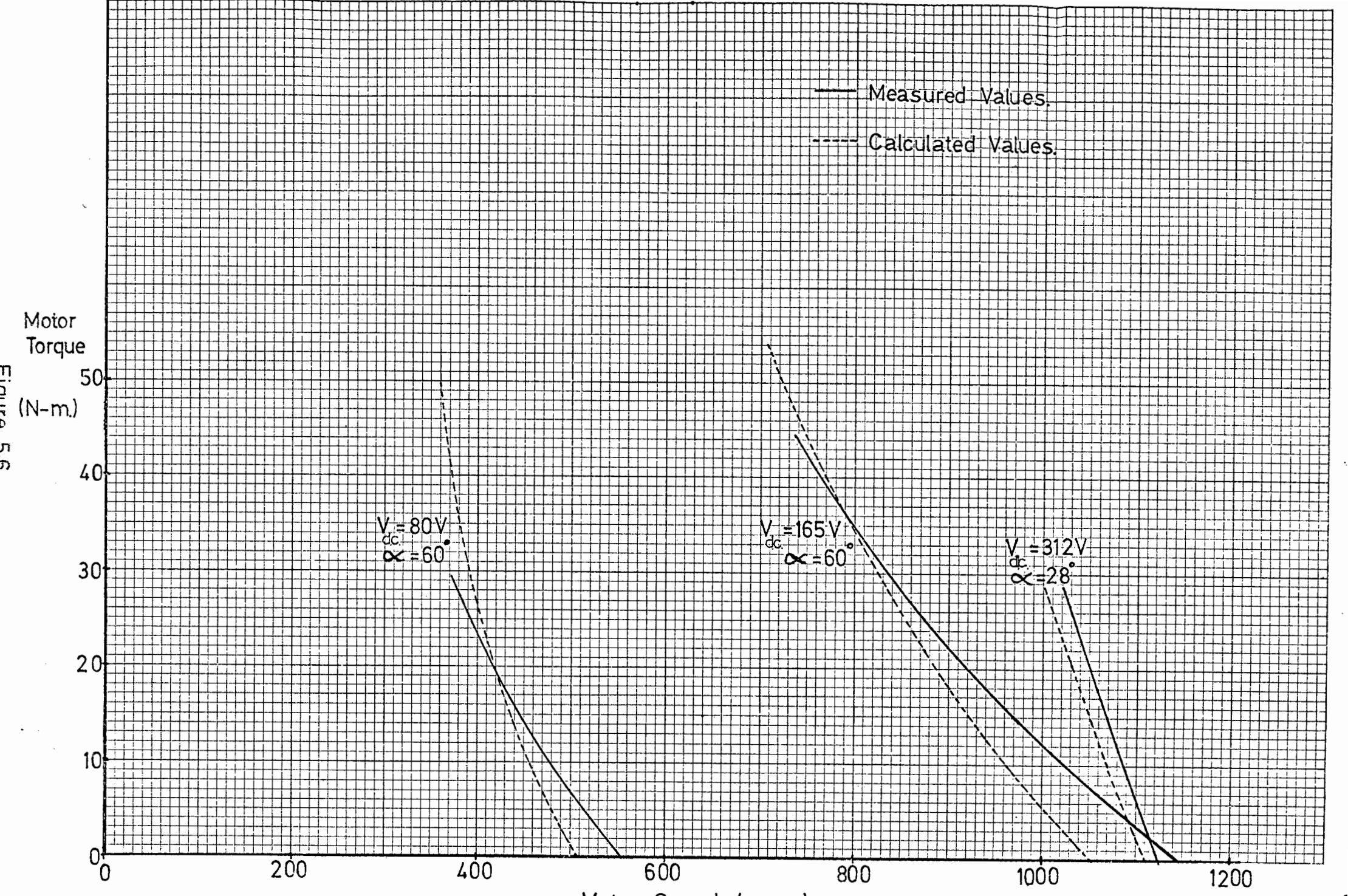
Measured Values.
Calculated Values.
Motor Torque (N-m.)
50
40
30
20
10
0
0
200
400
600
800
1000
1200
V_{dc} = 80V
α = 60°
V_{dc} = 165V
α = 60°
V_{dc} = 312V
α = 28°

Figure 56

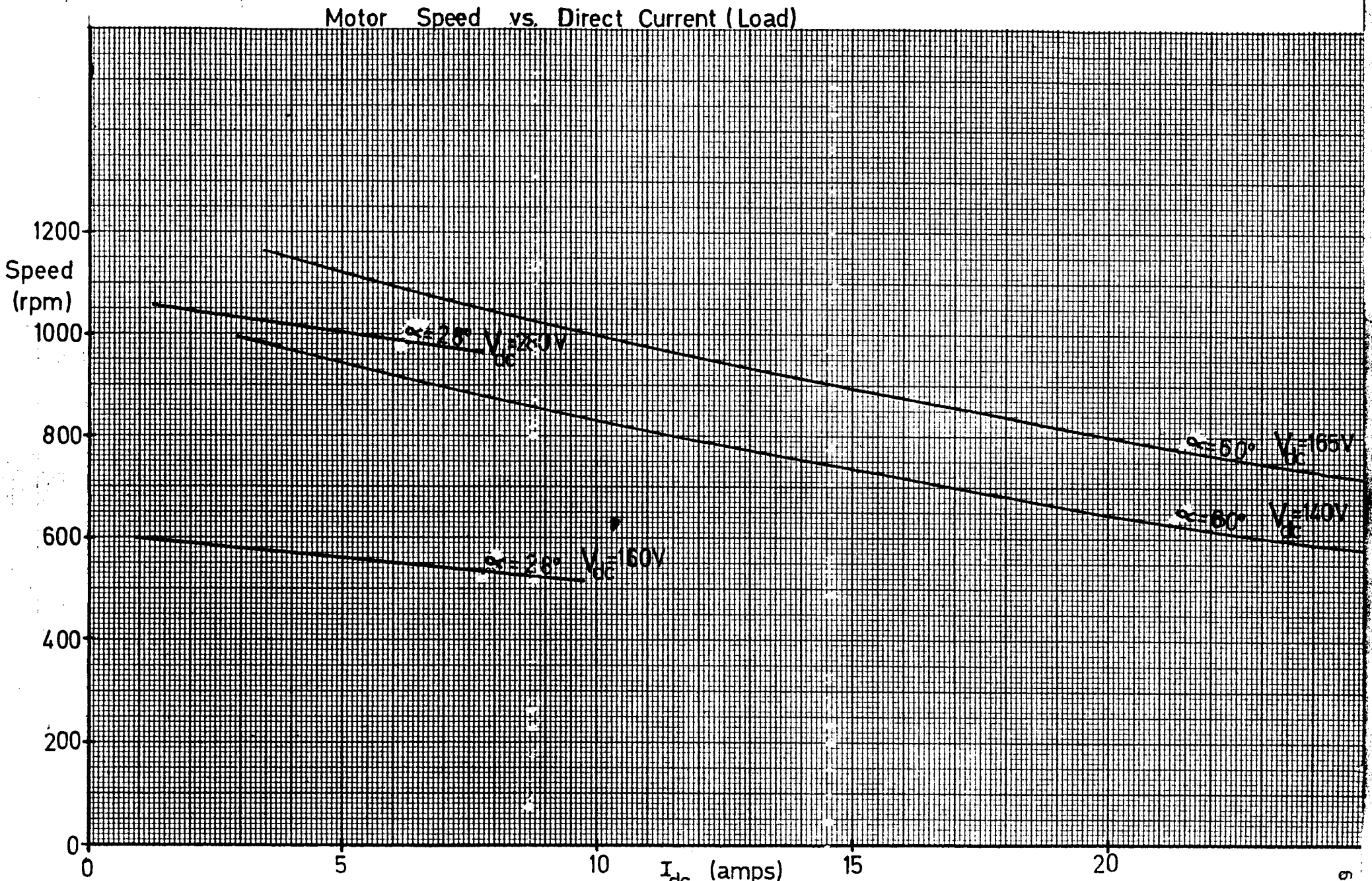
Motor Speed vs. Direct Current (Load)
Speed (rpm)
1200
1000
800
600
400
200
0
0
5
10
15
20
I_{dc} (amps)
$\alpha = 26°$ $V_{dc} = 226V$
$\alpha = 60°$ $V_{dc} = 165V$
$\alpha = 60°$ $V_{dc} = 140V$
$\alpha = 26°$ $V_{dc} = 160V$

Figure 5.7

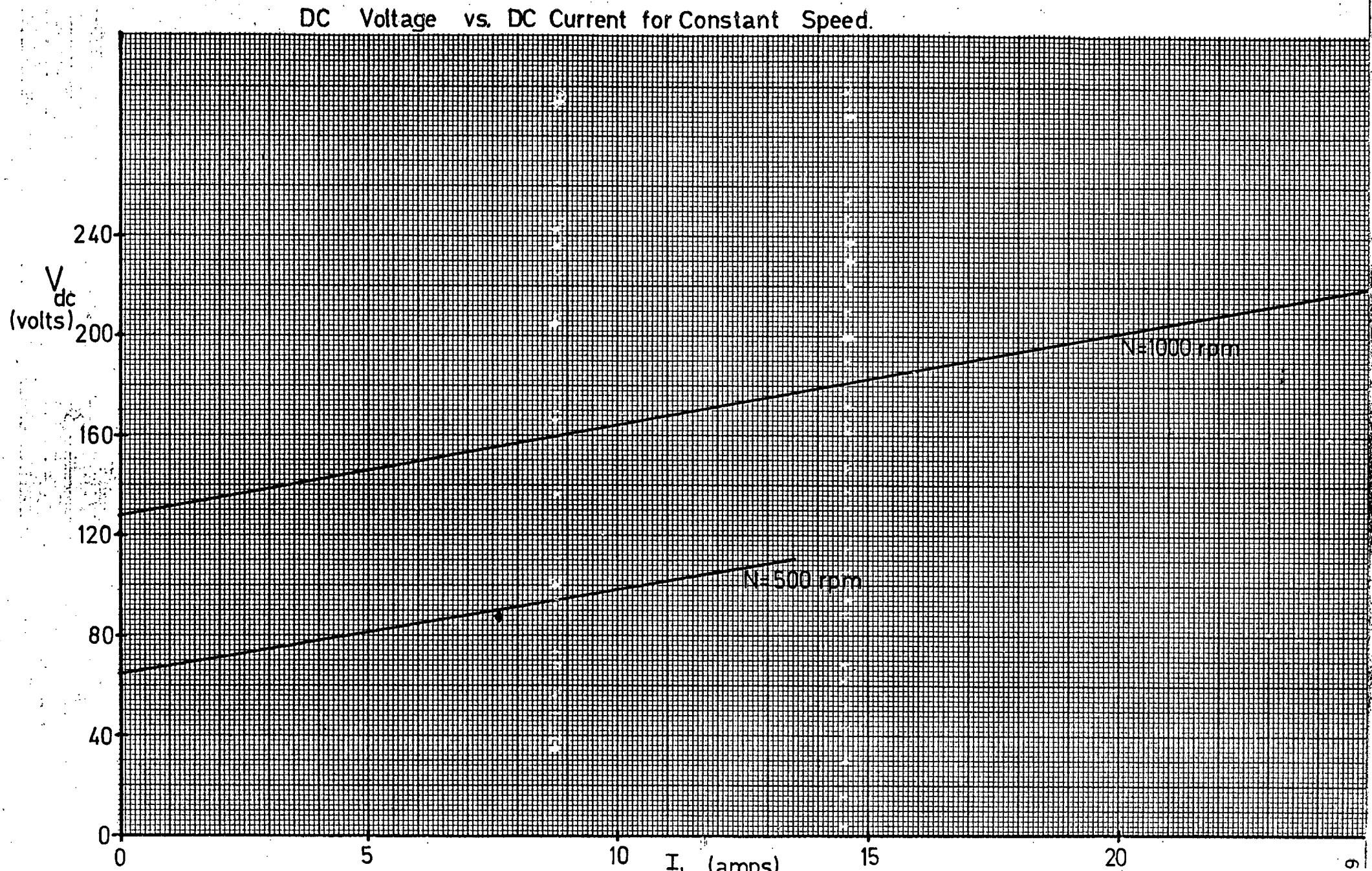
DC Voltage vs. DC Current for Constant Speed.
V_{dc} (volts)
240
200
160
120
80
40
0
0
5
10
15
20
I_a (amps)
N=1000 rpm
N=500 rpm

Figure 5.8

performance of the motor/inverter set.

5.7 System Transcient Response

There are two methods available to increase the power output of the system. The current may be increased or the power factor may be increased. The latter is achieved by reducing the motor power angle, i.e. the inverter advance angle.

$$T = k.I_f.I.\cos(\alpha) \qquad \ldots\ldots\ldots\ldots\ldots\ldots 5.6$$

These, however, are conflicting requirements in terms of inverter stability because an increase in current requires a corresponding increase in the inverter advance angle to ensure adequate thyristor extinction angle.

The optimum values of thyristor advance angle and field current will depend on motor speed, inverter D.C. voltage, motor current and motor load. This optimisation of the inverter performance is outside the scope of this thesis and has not been attempted.

The main aim of the project is to show that the system as a whole is amenable to speed control of a general synchronous motor and that a variety of types of response may be obtained without optimising the motor/inverter combination.

The motor/inverter was therefore considered as a single unit with one input (D.C. voltage) and one output (motor speed). To enable a closed loop control system to be developed it was necessary to determine the transfer function of this "black

box" consisting of the motor and inverter. Analytical means of doing this become very tedious, with many non-linear, simultaneous equations to be solved (Appendix C). It was therefore decided to determine the transfer function by experimental means. This was done for each of 3 different inverter advance angles so that the effect of varying this angle on the overall transfer function could be observed.

The 3 inverter advance angles chosen, and the corresponding maximum allowable line current to ensure proper inverter commutation under all load and speed conditions were:

Advance Angle	Max. Line Current
68°	27 A
44°	15 A
20°	5 A

The response of the motor/inverter to a small change (such that no current limiting occurred) in D.C. voltage was recorded for each of the 3 advance angles. The response was found to closely resemble an underdamped second order system with different time constants for the different advance angles. Appendix G shows the graphical means used to obtain the transfer functions.

Figs. 5.9 to 5.11 show the motor speed and line current responses to a step change in inverter D.C. voltage.

The transfer functions obtained were as follows:

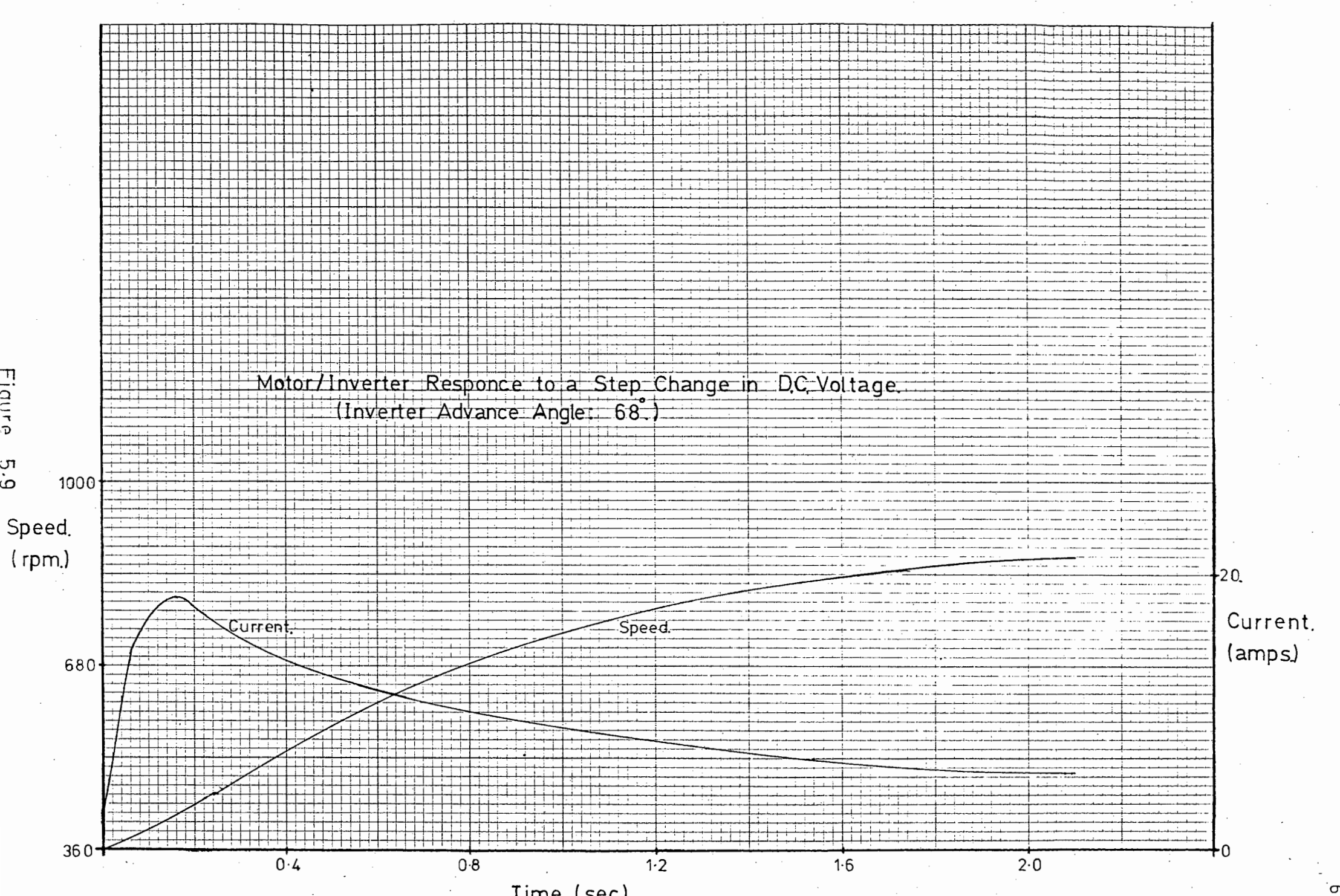
Motor/Inverter Responce to a Step Change in D.C. Voltage.
(Inverter Advance Angle: 68°.)
1000
680
360
Speed.
(rpm.)
20.
0
Current.
(amps.)
Current.
Speed.
0·4
0·8
1·2
1·6
2·0
Time (sec)

Figure 5.9

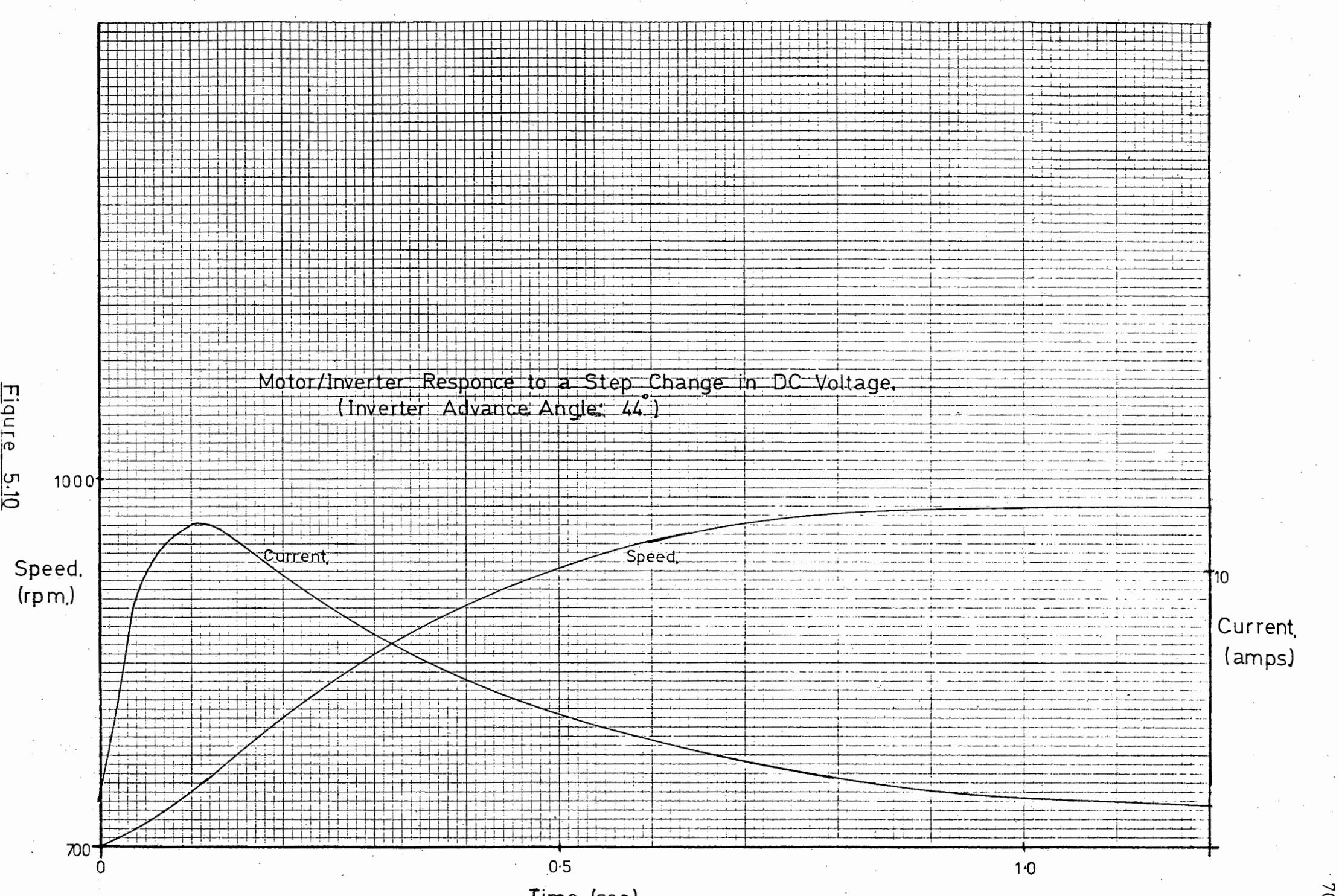
Motor/Inverter Responce to a Step Change in DC Voltage.
(Inverter Advance Angle: 44°)
1000
700
Speed.
(rpm.)
Current.
Speed.
10
Current.
(amps)
0
0·5
1·0
Time (sec)

Figure 5.10

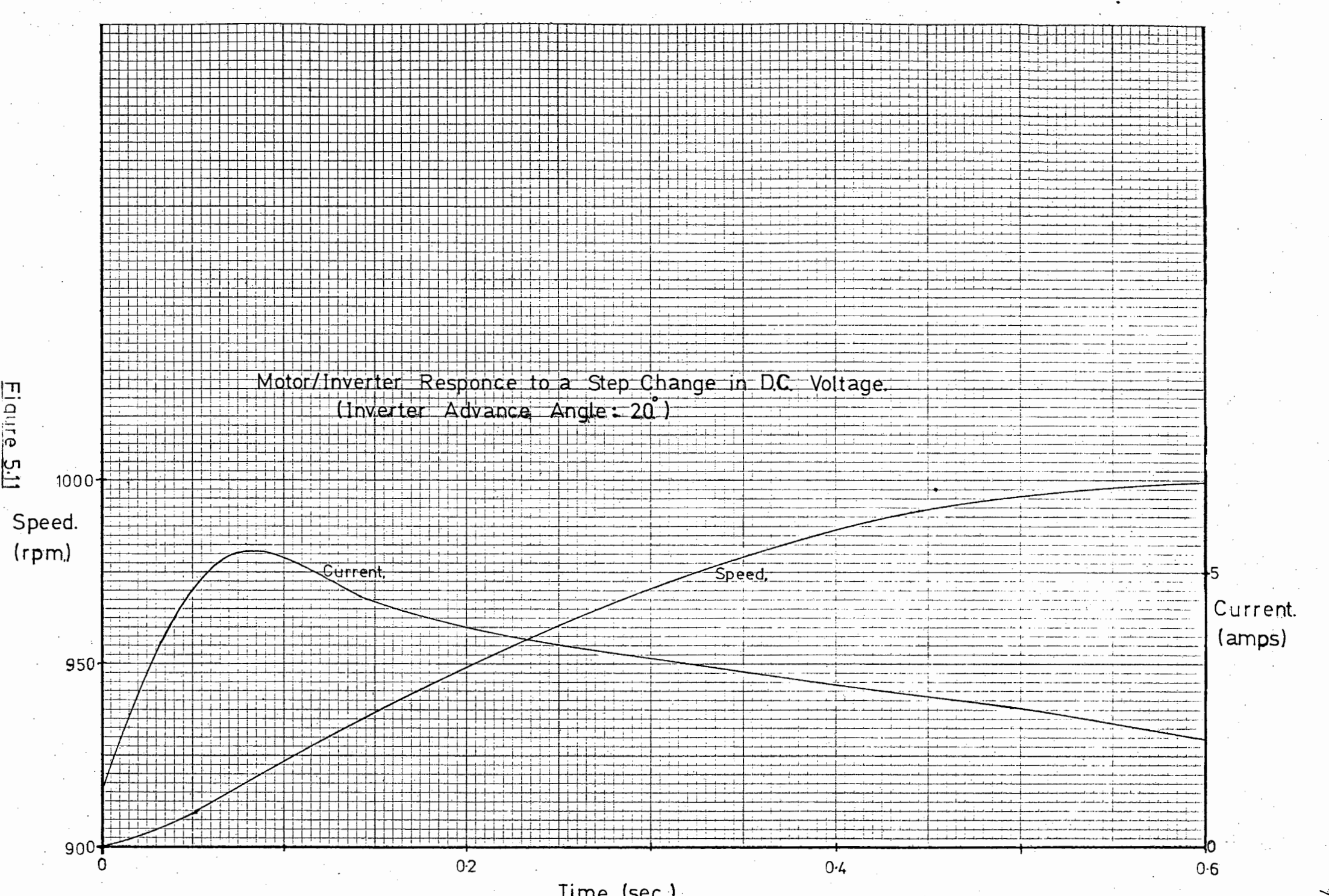
Motor/Inverter Responce to a Step Change in D.C. Voltage.
(Inverter Advance Angle: 20°)
Speed. (rpm.)
1000
950
900
Current.
Speed.
5
0
Current. (amps)
0
0·2
0·4
0·6
Time (sec.)

Figure 5.11

$$\alpha = 68^{\circ} \quad T(S) = \frac{13.6}{S^2 + 15.35 + 13.6} \quad (\zeta = 2.1, \omega_n = 3.7) \quad .. \quad 5.7$$

$$\alpha = 44^{\circ} \quad T(S) = \frac{60.8}{S^2 + 21.3S + 60.8} \quad (\zeta = 1.4, \omega_n = 7.8) \quad .. \quad 5.8$$

$$\alpha = 20^{\circ} \quad T(S) = \frac{84.6}{S^2 + 20.2S + 84.6} \quad (\zeta = 1.1, \omega_n = 9.2) \quad .. \quad 5.9$$

The current was also observed to very closely resemble the differential of the speed.

$$\text{i.e.} \quad N \simeq \frac{1}{S} \cdot I \qquad \ldots\ldots\ldots\ldots\ldots\ldots \quad 5.10$$

CHAPTER 6.

SYSTEM SIMULATION

To enable a closed loop speed control system to be developed, the open loop system presented so far was simulated on the analog computer.

For this purpose the rectifier was assumed to have a constant mean linear transfer function with the rectifier delay angle linearly related to the D.C. voltage output. This had a maximum of -12% error if correctly chosen, i.e. it was assumed that -

$$V_{dc} = k\ (90^{o} - \gamma) \qquad \ldots\ldots\ldots\ldots\ 6.1$$

The motor current was used to control the rectifier under current limit conditions. As regeneration did not occur in the real system the motor "coasted" down when deceleration was required. This was simulated by allowing a fixed but small "negative" current to flow into the inverter/motor simulator. The rectifier D.C. voltage was also clamped to a maximum level.

The rectifier and inverter control is by digital logic circuits, their transfer functions are not smooth but quantized. In addition, the speed feedback signal is sampled at regular intervals. These two effects were disregarded in the analog simulation.

The response of this simulation correlated very well with the

response curves of the real system shown in Fig. 5.9 to 5.11.

To enable closed loop motor speed control to be obtained, it was proposed that the actual motor speed be compared with the desired speed and the error signal thus generated be passed through a proportional plus integral controller and then on to the rectifier, inverter and motor simulation. This was simulated as shown in Fig. 6.1(a).

A satisfactory closed loop performance was obtained with the following transfer function for the error processor:

$$T_E(S) = (20 + \frac{20}{S}) \quad \ldots\ldots\ldots\ldots\ldots\ldots 6.2$$

When studied more carefully, however, it was found that this method could not be adequately adapted to the real system. The reason for this is that, because of the large gain in the error processor, a very accurate error signal would be necessary. It was estimated that a 12-bit error signal would be necessary. It would also have entailed 12-bit control of the rectifier. The digital system had been designed for 8-bit control logic and therefore another control method was examined.

The second method simulated was to accelerate the motor under constant maximum current until its speed was within a certain error band of the desired speed, after which integral control was used to give an accurate and stable final speed. The simulation diagram is shown in Fig. 6.1(b).

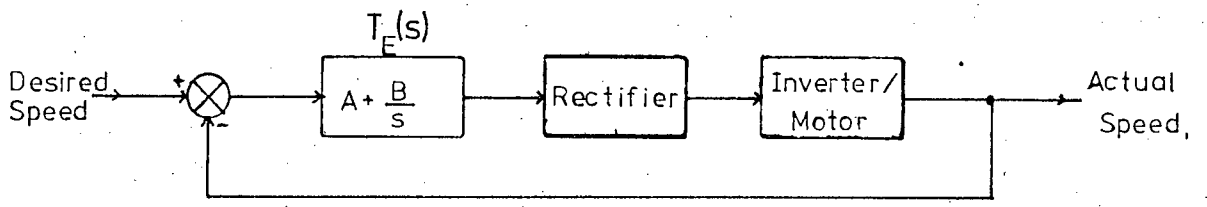

Block Diagram of Closed-Loop Simulation.

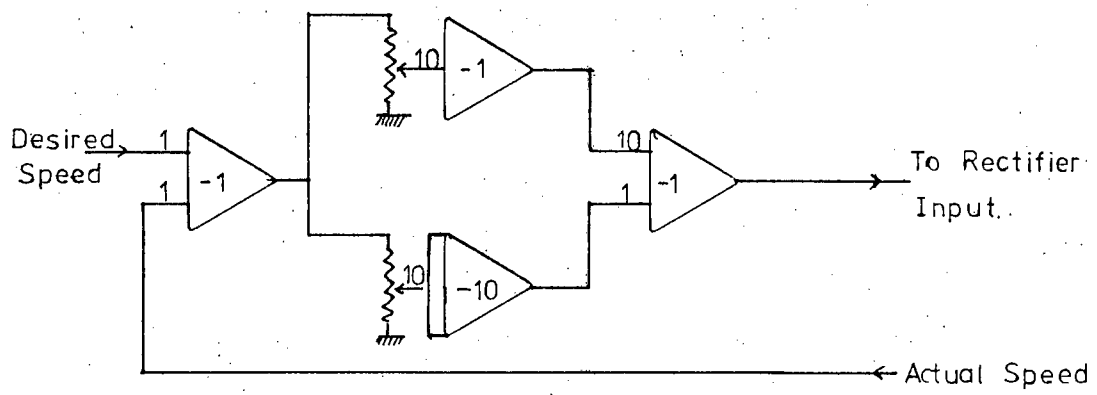

Computer Diagram of Rectifier Controller.

Figure 6.1a

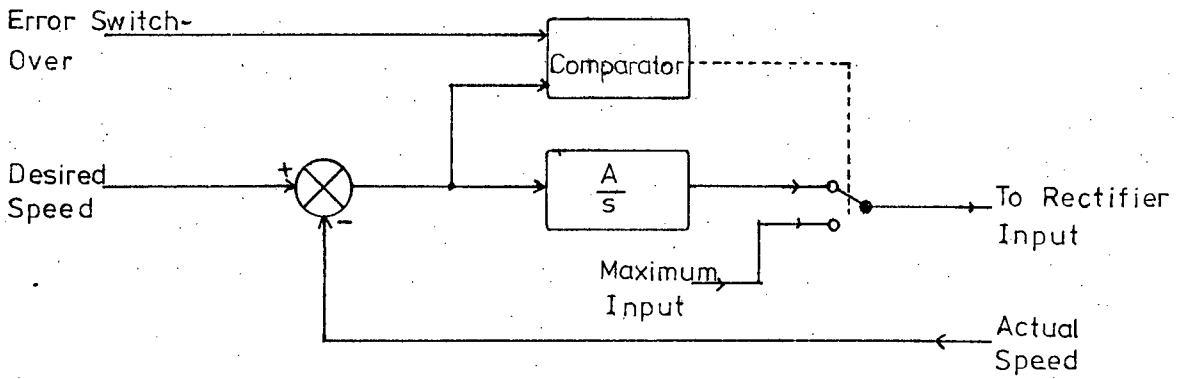

Block Diagram of Final Controller.

Figure 6.1b

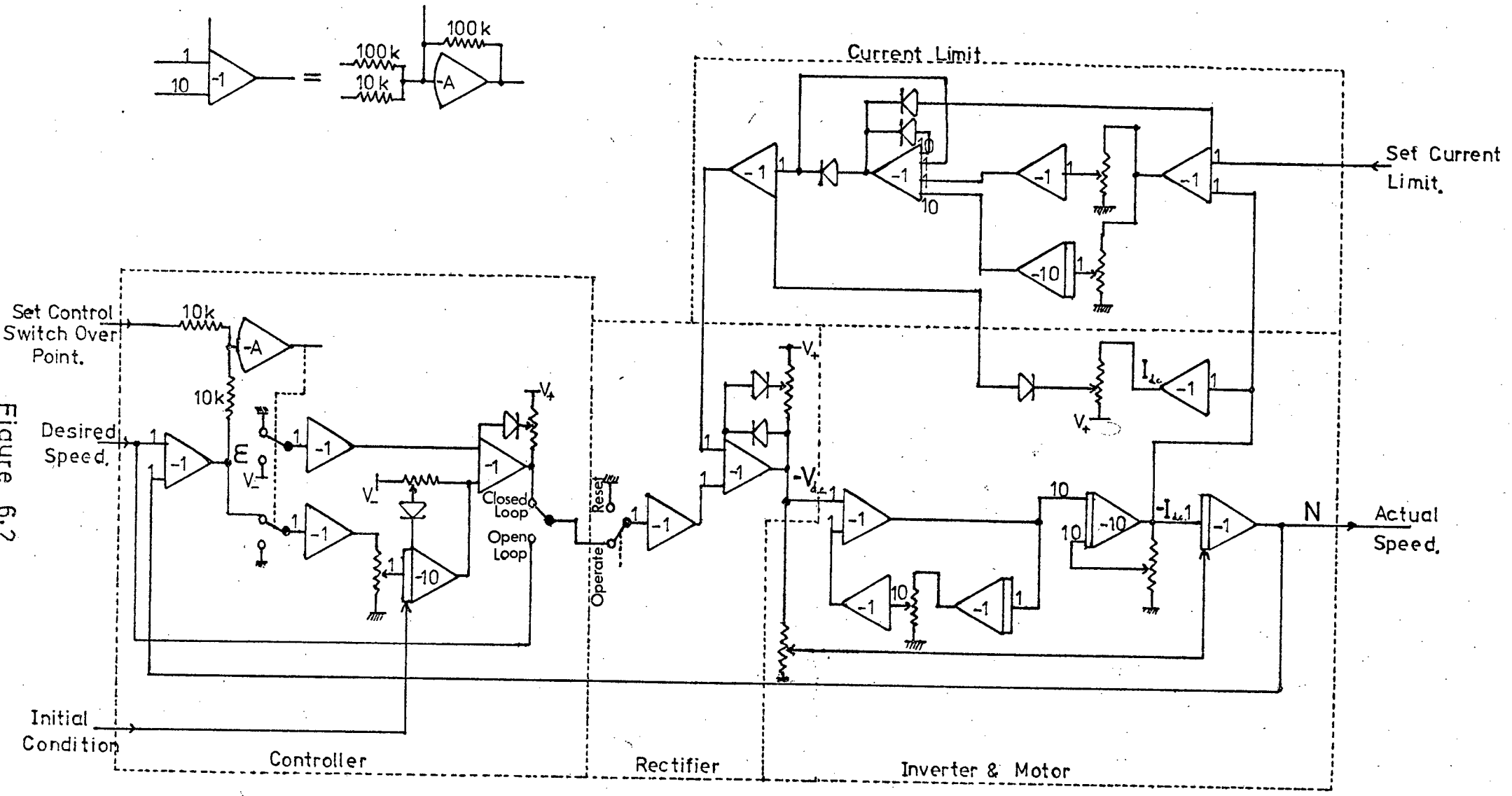

Figure 6.2

Diagram of Analog Computer Simulation

Satisfactory performance was obtained with the motor receiving maximum current until within 10% of the desired speed and then having a circuit with a transfer function of $\frac{5}{S}$ switched into the feedback path.

The amount of overshoot (damping) and the settling time of the closed loop speed controller could be controlled by changing the switch-over error, the gain of the integrator, and the integrator initial condition.

It was noted that the setting of the initial condition of the integrator could present a problem in the real system. This is because the initial condition would vary with load just as the D.C. voltage to the inverter varies with load (see Fig. 5.8). Therefore, to obtain the best response under loaded conditions a larger initial condition would be necessary.

It was decided that this method of control was feasible and that a corresponding digital feedback system could be easily realised.

Using Z transform analysis techniques, the response of the system with a digital control processor was analysed. The results of this, together with a Laplace transform analysis (assuming a linear feedback system) are shown in Fig. 8.1.

The details of these two analyses are given in Appendix H.

The design and construction of a digital feedback processor based on the abovementioned method was then initiated.

CHAPTER 7.

THE DIGITAL CONTROL SYSTEM

Fig. 7.1 shows a block diagram of the digital, speed feedback system.

The rotor speed is obtained by counting the number of clock pulses received from the shaft encoder in a fixed time interval. This time interval is in fact related to the overall gain of the feedback system. As the disc has 90 slots per motor electrical cycle, it is obvious that -

$$\text{Counter output} = 90.f.T \qquad \ldots\ldots\ldots\ldots\ldots\ldots \quad 7.1$$

where f = motor electrical frequency

T = counting time interval.

If T is large then one bit of the counter will represent only a small percentage of the total count, thus an error of one bit will be a small speed error. For small T, a one bit error will correspond to a much larger speed error.

The loop gain of the system is also a function of the inverter advance angle for the following reason. The rectifier is considered linear (i.e. a one bit change in the binary input will result in a fixed change in output D.C. voltage) but the gain of the inverter is highly dependent upon the advance angle. This is obvious by consulting Fig. 4.2. As the advance

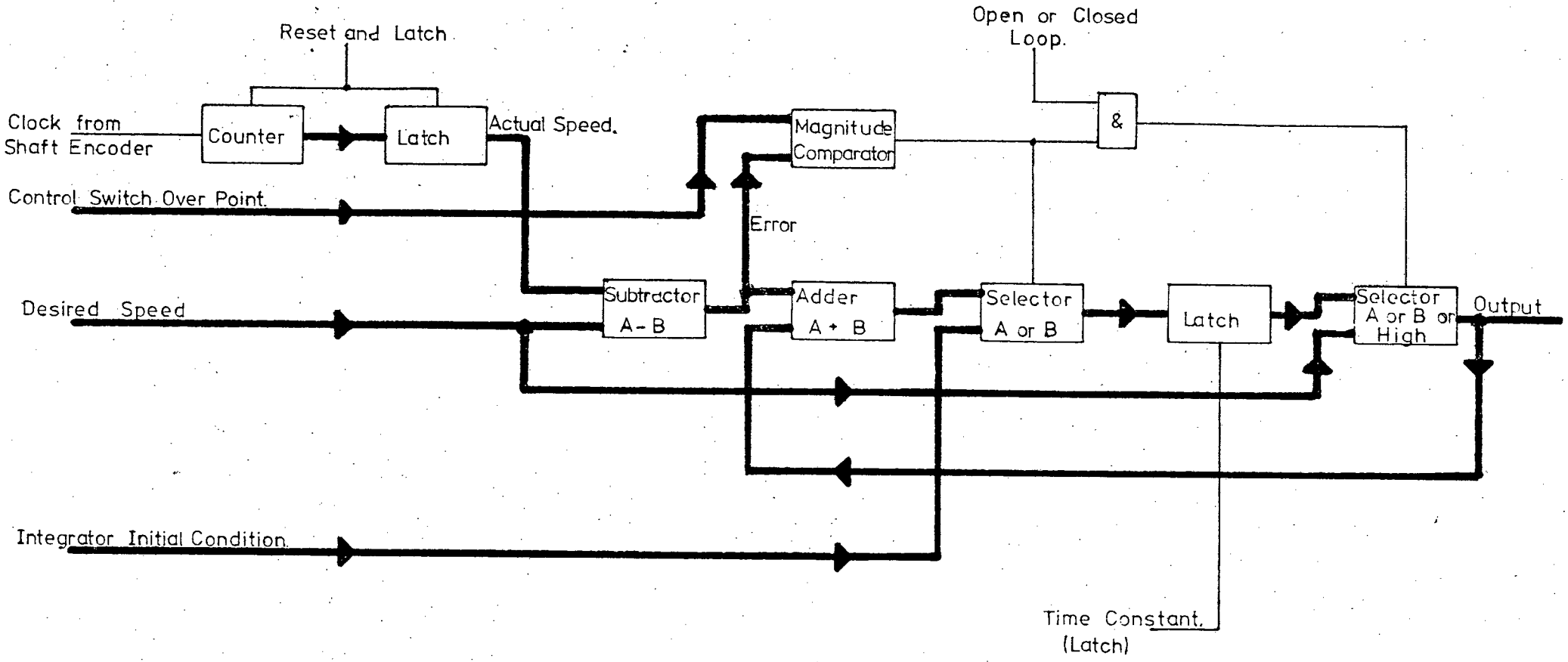

Figure 7.1

Block Diagram of Feedback System.

angle tends to 90^{o} the gain of the inverter tends to infinity. At zero advance angle (delay angle 180^{o}) the gain is zero.

The desired speed is fed into the system from eight switches, as is the integrator initial condition and the error switch-over point.

A single switch allows selection of open loop or closed loop control. In the former case the desired speed inputs are fed directly to the rectifier inputs.

The time constant of the integrator is controlled from an external clock and may be varied. Integration is performed by adding the output of the integrator to the input of the integrator at discrete time intervals. This new total then becomes the output of the integrator.

The selector switches consist of 2 sets of 8 tri-state buffers with a common set of 8 outputs. One set of the buffers always being in the high impedance state.

The second set of selector switches has pull-up resistors so that when both sets of buffers are in the high impedance state, logic high levels are on the outputs.

The arithmetic operations are performed in 2's complement form.

Additional circuitary is necessary to prevent the "speed counter" from overflowing and to prevent the output from over-

flow or underflow. In the latter case a negative number in 2's complement form would be incorrectly interpreted by the rectifier control logic.

CHAPTER 8.

RESULTS

Results given in this Chapter show that different types of motor response can be obtained using rectifier control only, and without optimization of the inverter/motor combination. It is not attempted to show that optimization of the inverter/motor is unnecessary for optimal system performance, but rather that the method of rectifier control does not rely on an accurately defined inverter and motor system, and that as a wide range closed-loop speed control system, this type of system is feasible.

A prediction of the performance of the system for a continuous control system and of that for a discrete time control system, together with the actual measured response is shown in Fig. 8.1. The assumption made here is that the motor is under pure integral control. The difference in rate of deceleration, is that the motor does not regenerate, while for prediction purposes, it was assumed that this did occur.

For all results the following nomenclature has been used:

α : Inverter advance angle

T : Integrator time constant in seconds

I.C. : Integeator initial condition in octal.

O.L. : The open-loop input required to obtain the same final speed (in octal)

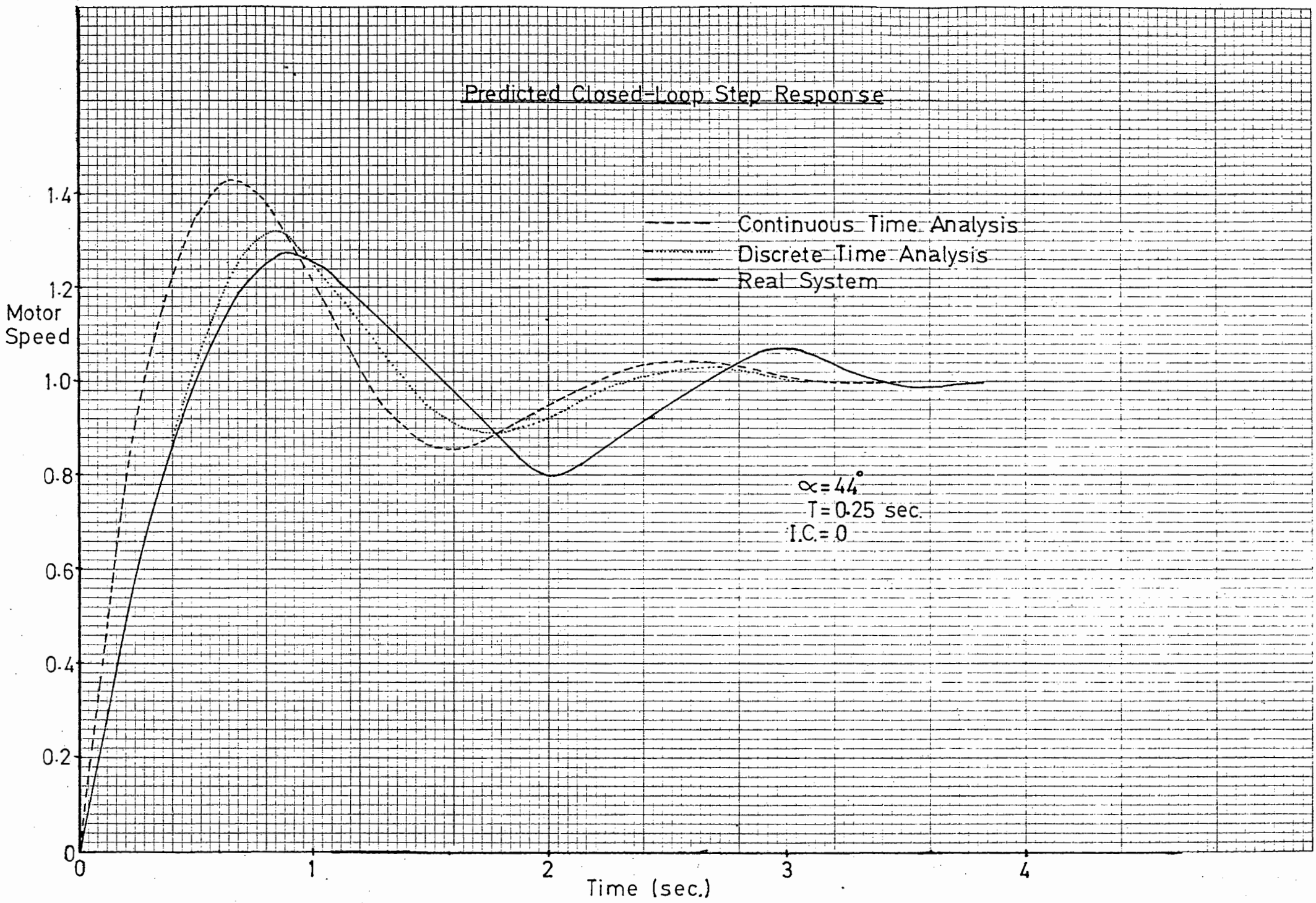
Predicted Closed-Loop Step Response
Continuous Time Analysis
Discrete Time Analysis
Real System
∝ = 44°
T = 0.25 sec.
I.C. = 0
Motor Speed
Time (sec.)
0
0.2
0.4
0.6
0.8
1.0
1.2
1.4
1
2
3
4

Fig. 8.1

C.L. : The closed-loop desired speed input (in octal)

ε : The error at which the control system switches to integral control (in octal).

Fig. 8.2 shows a comparison of the open-loop and closed-loop performance for a step change in input. The rise time of the closed-loop response is approximately half that of the open-loop system (0.53 sec. as opposed to 1 sec.).

Fig. 8.3 is similar except that a large step input is given. Rise time is improved with closed-loop control, but current limiting restricts the maximum acceleration of the motor in both cases.

Fig. 8.4 is again a comparison of open-loop and closed-loop performance, but this time under loaded conditions. The final motor output is 1.5 kW in both cases.

Fig. 8.5 to 8.8 are used to show the different types of responses obtainable, with a comparison to the simulated responses. They are all under no load conditions. Fig. 8.9 shows the onset of limit cycling in the system due to excessive loop gain. The magnitude of this oscillation is limited by the error switch over point.

Figs. 8.10 and 8.11 show different types of response obtainable under loaded conditions (load approximately 1 kW) for a different inverter advance angle to that of Fig. 8.4.

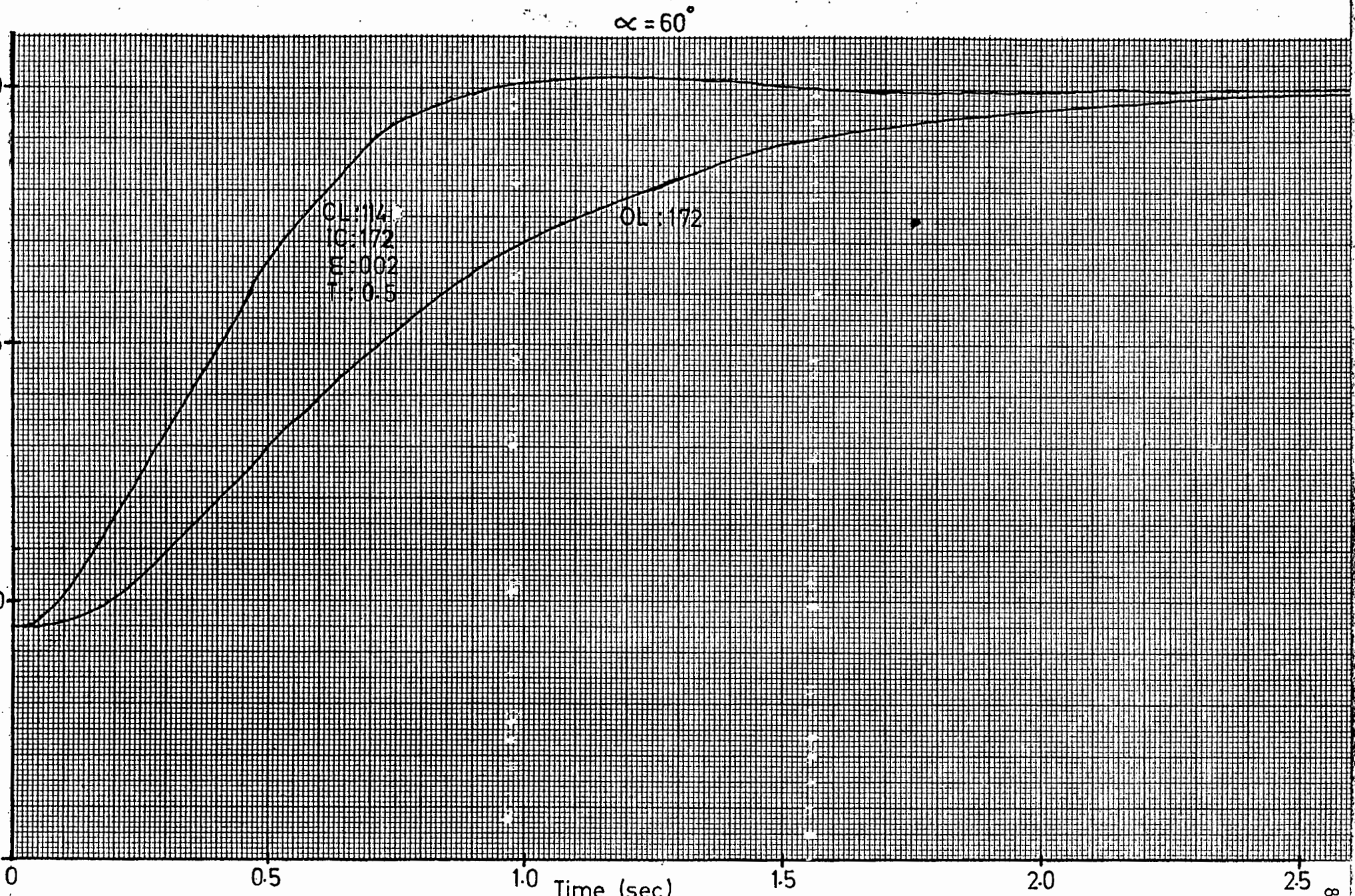
∝ = 60°
750
625
500
375
Speed (rpm)
OL:14
IC:172
E:002
T:0.5
OL : 172
0
0·5
1·0
1·5
2·0
2·5
Time (sec)

Figure 8.2

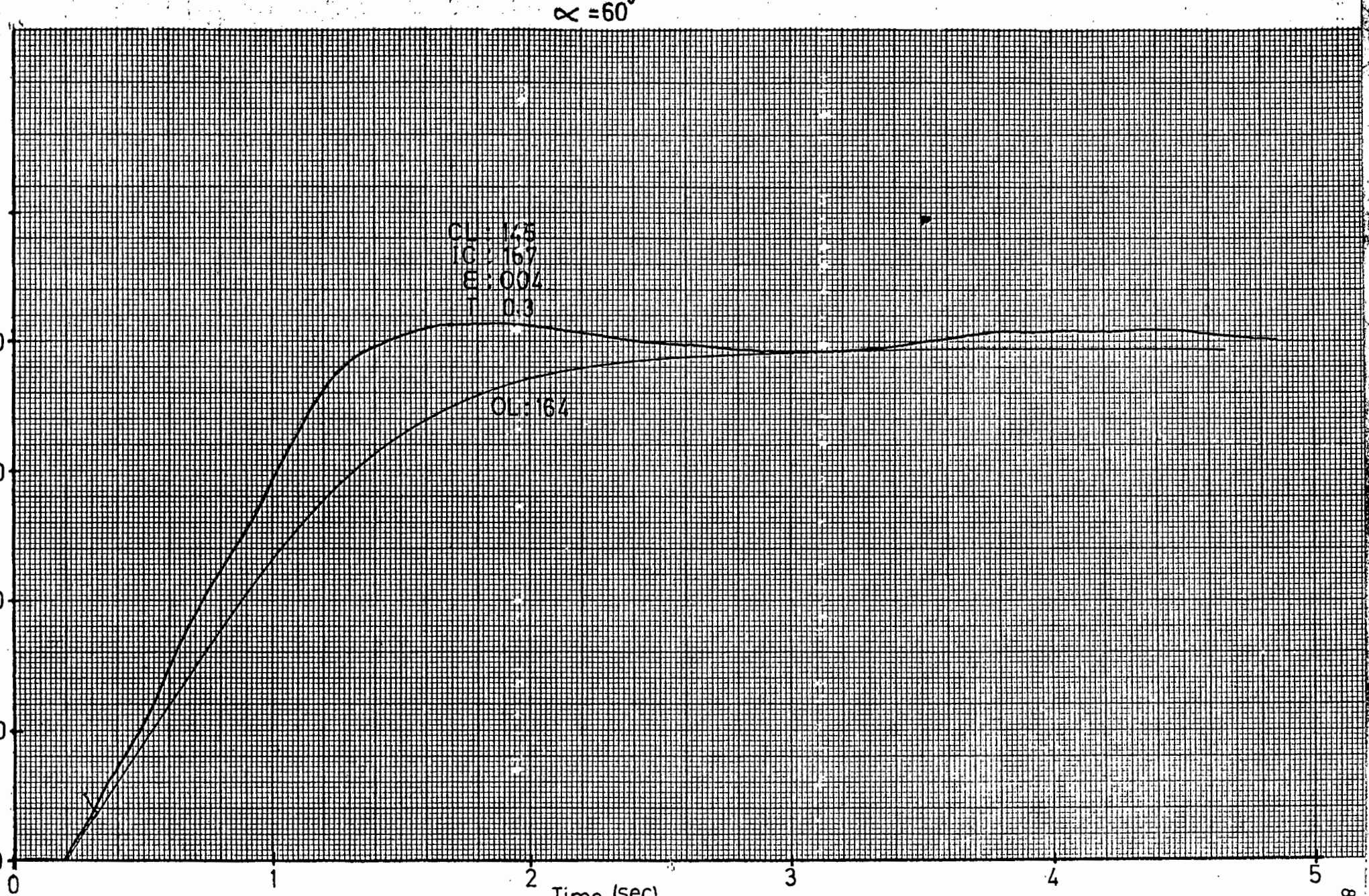
∝ =60°
CL: 145
IC: 167
E: 004
T 0.3
OL: 164
Speed (rpm)
1000
750
500
250
0
0
1
2
3
4
5
Time (sec)

Figure 8.3

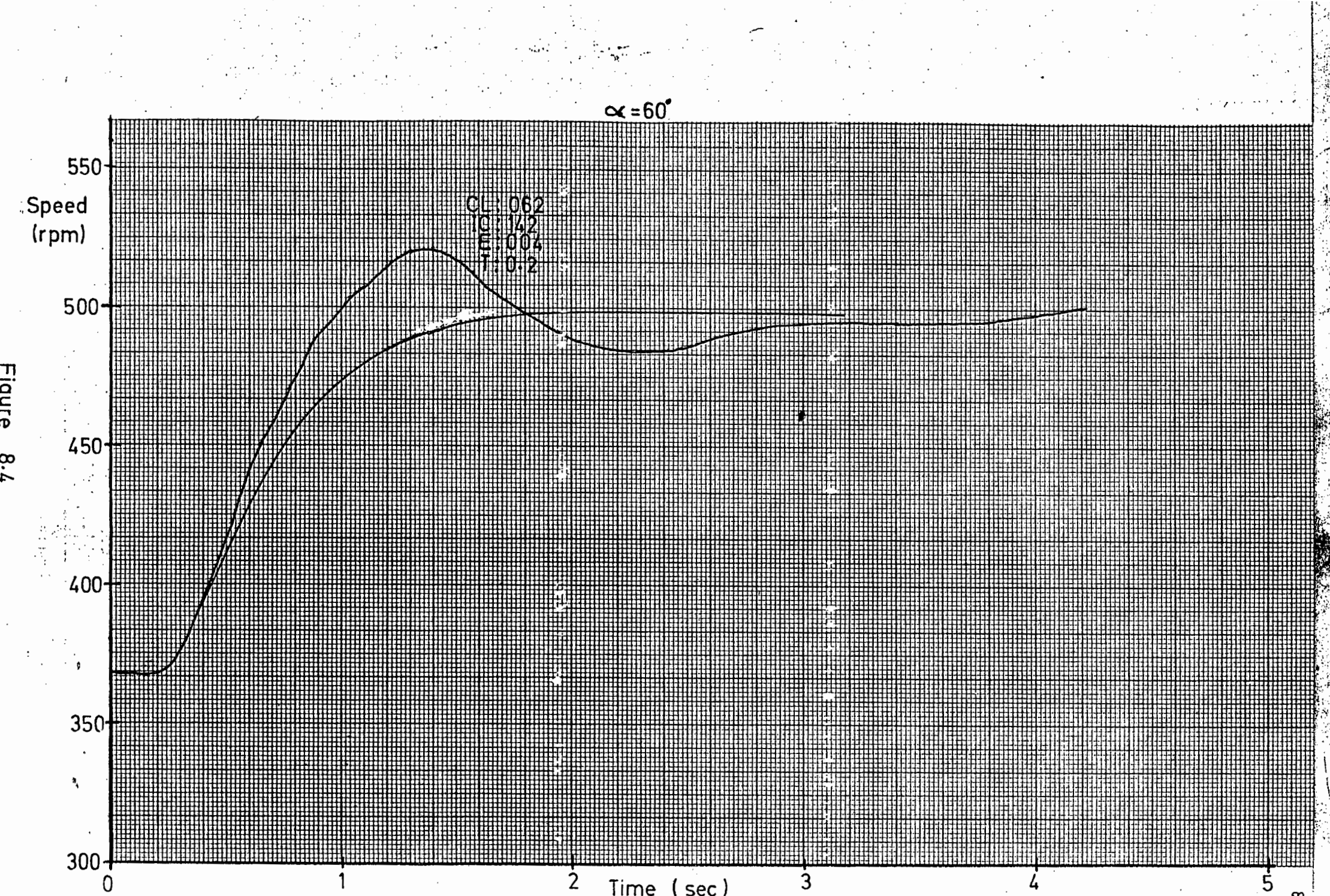
∝=60°
CL ; 062
IG ; 142
E ; 004
T ; 0.2
Speed (rpm)
550
500
450
400
350
300
0
1
2
3
4
5
Time (sec)

Figure 8.4

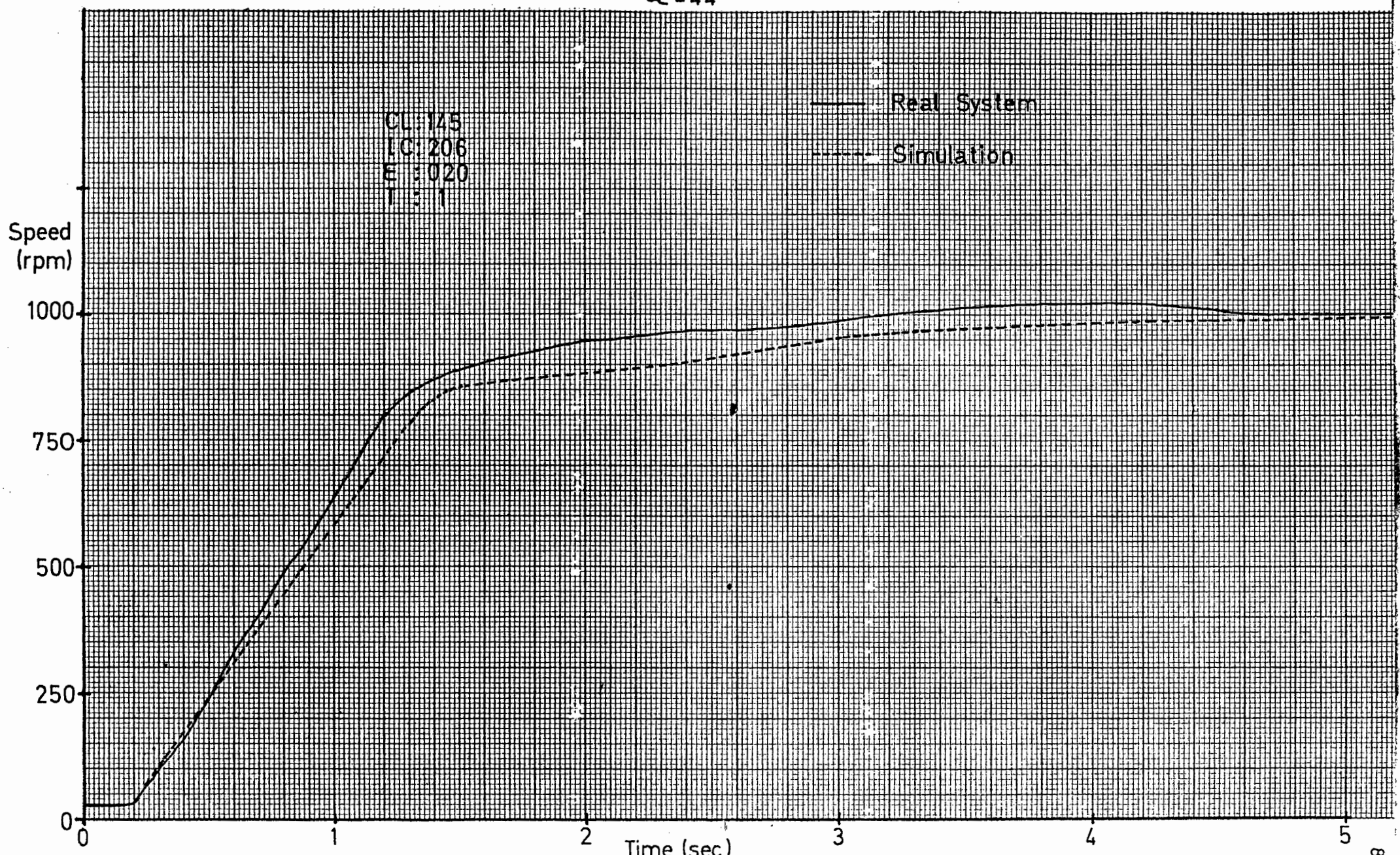
α = 44°
CL: 145
LC: 206
E : 020
T : 1
Real System
Simulation
Speed (rpm)
1000
750
500
250
0
0
1
2
3
4
5
Time (sec)

Figure 8.5

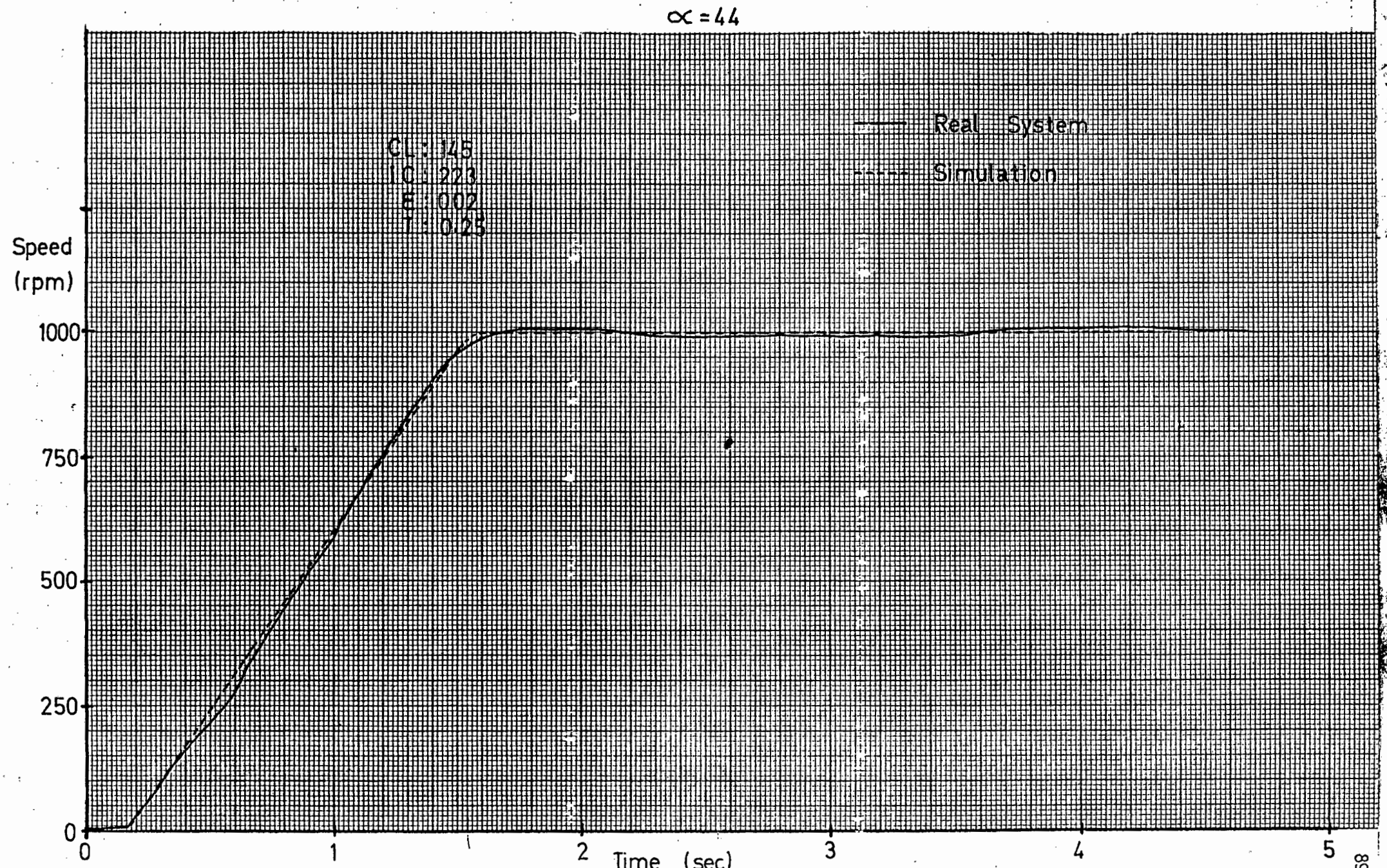
∝ = 44
CL : 145
IC : 223
E : 002
T : 0.25
Real System
Simulation
Speed
(rpm)
1000
750
500
250
0
0
1
2
3
4
5
Time (sec)

Figure 8.6

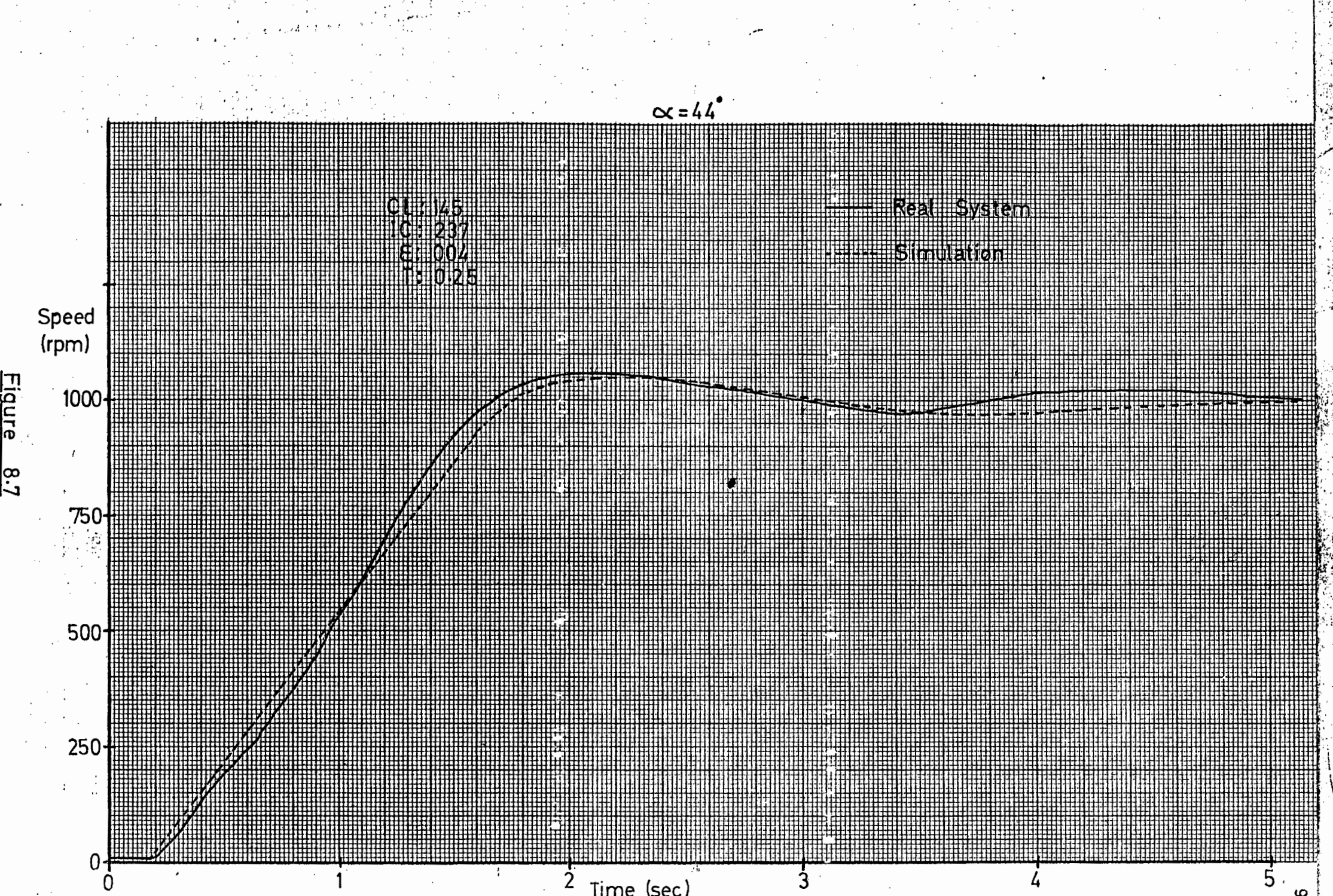
α = 44°
CL: 145
CD: 237
E: 004
T: 0.25
Real System
Simulation
Speed (rpm)
1000
750
500
250
0
0
1
2
3
4
5
Time (sec)

Figure 8.7

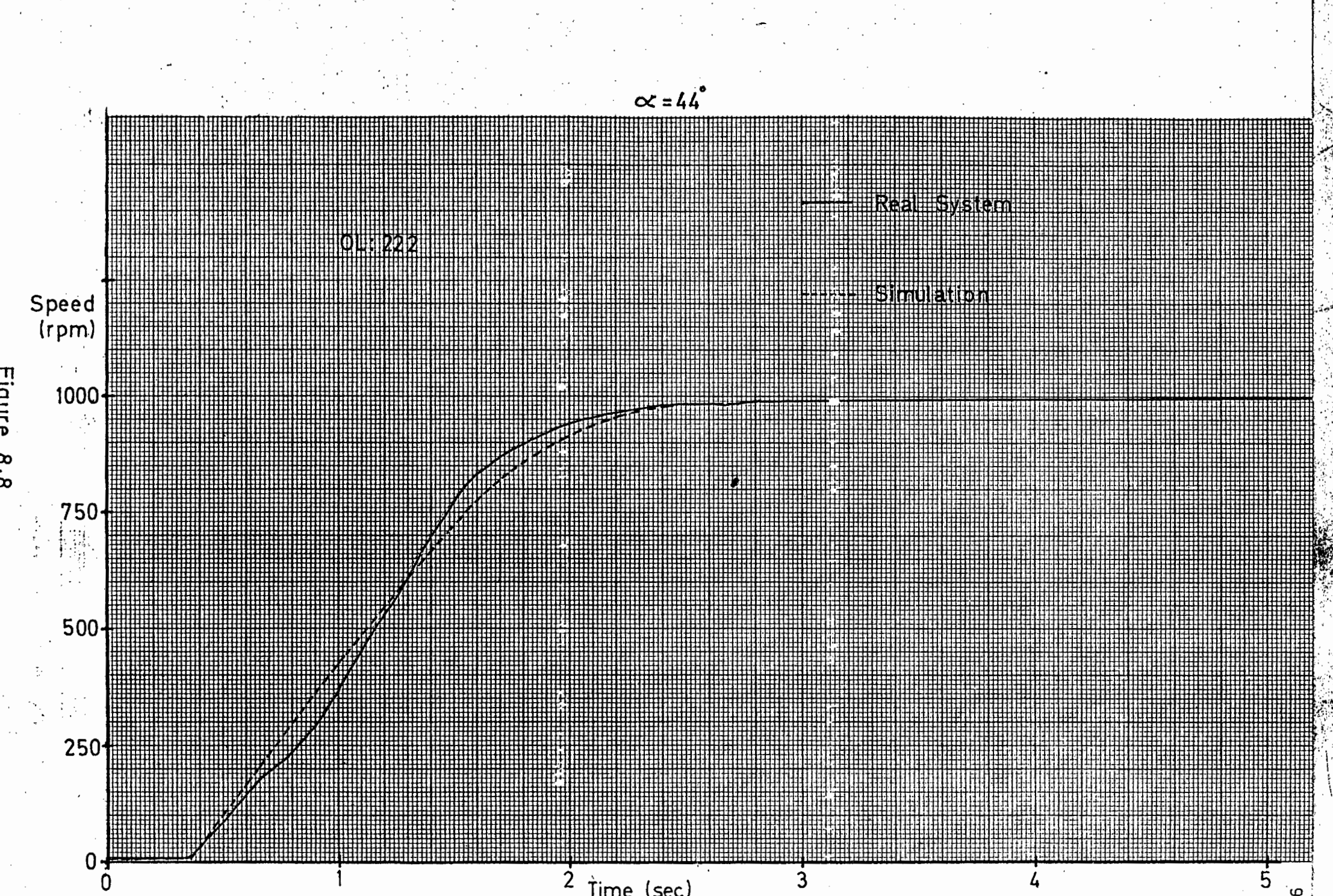
α = 44°
OL: 222
Real System
Simulation
Speed (rpm)
1000
750
500
250
0
0
1
2
3
4
5
Time (sec)

Figure 8.8

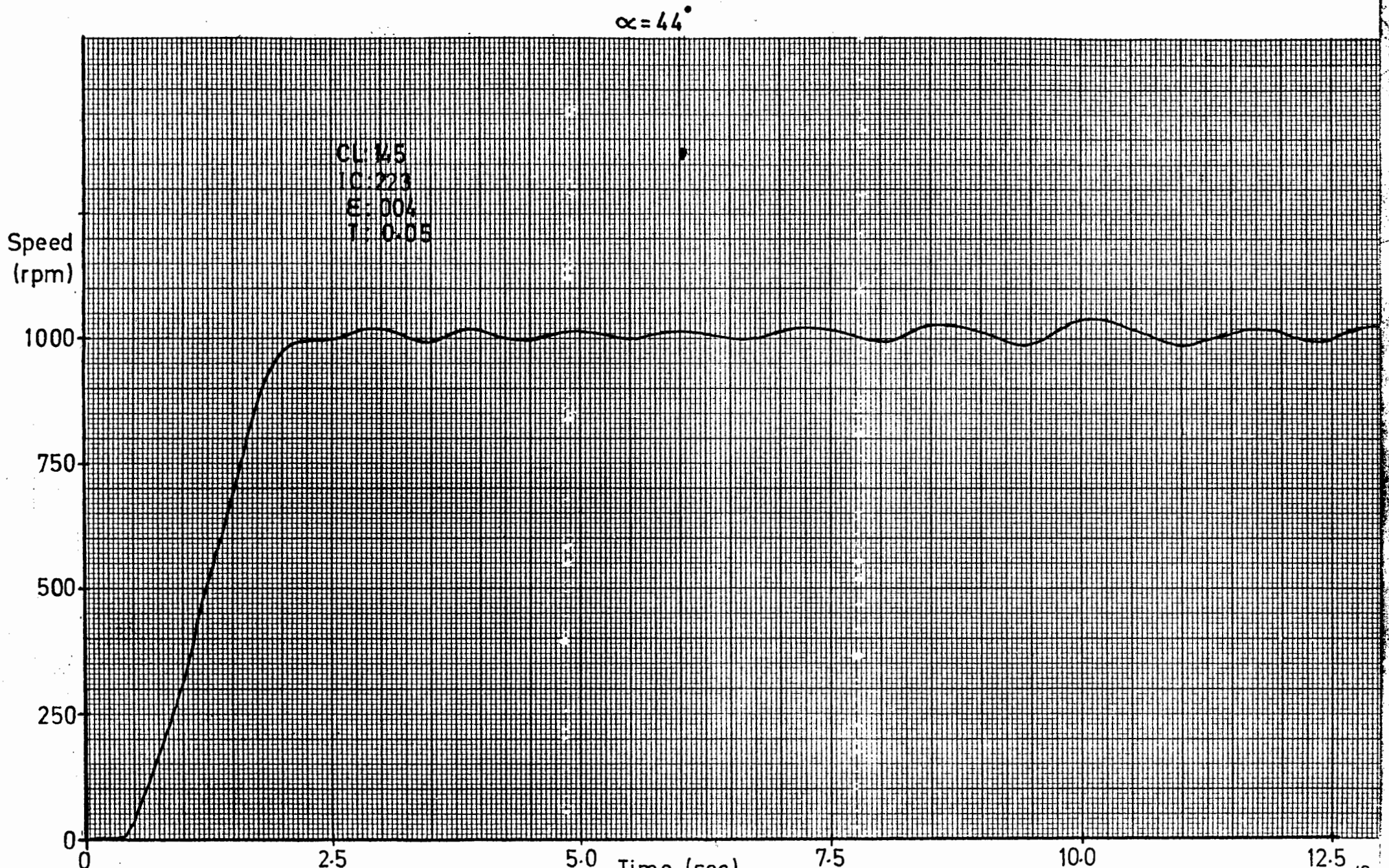
α = 44°
CL: 1.45
IC: 223
ε: 004
T: 0.05
Speed (rpm)
1000
750
500
250
0
0
2·5
5·0
7·5
10·0
12·5
Time (sec)

Figure 8.9

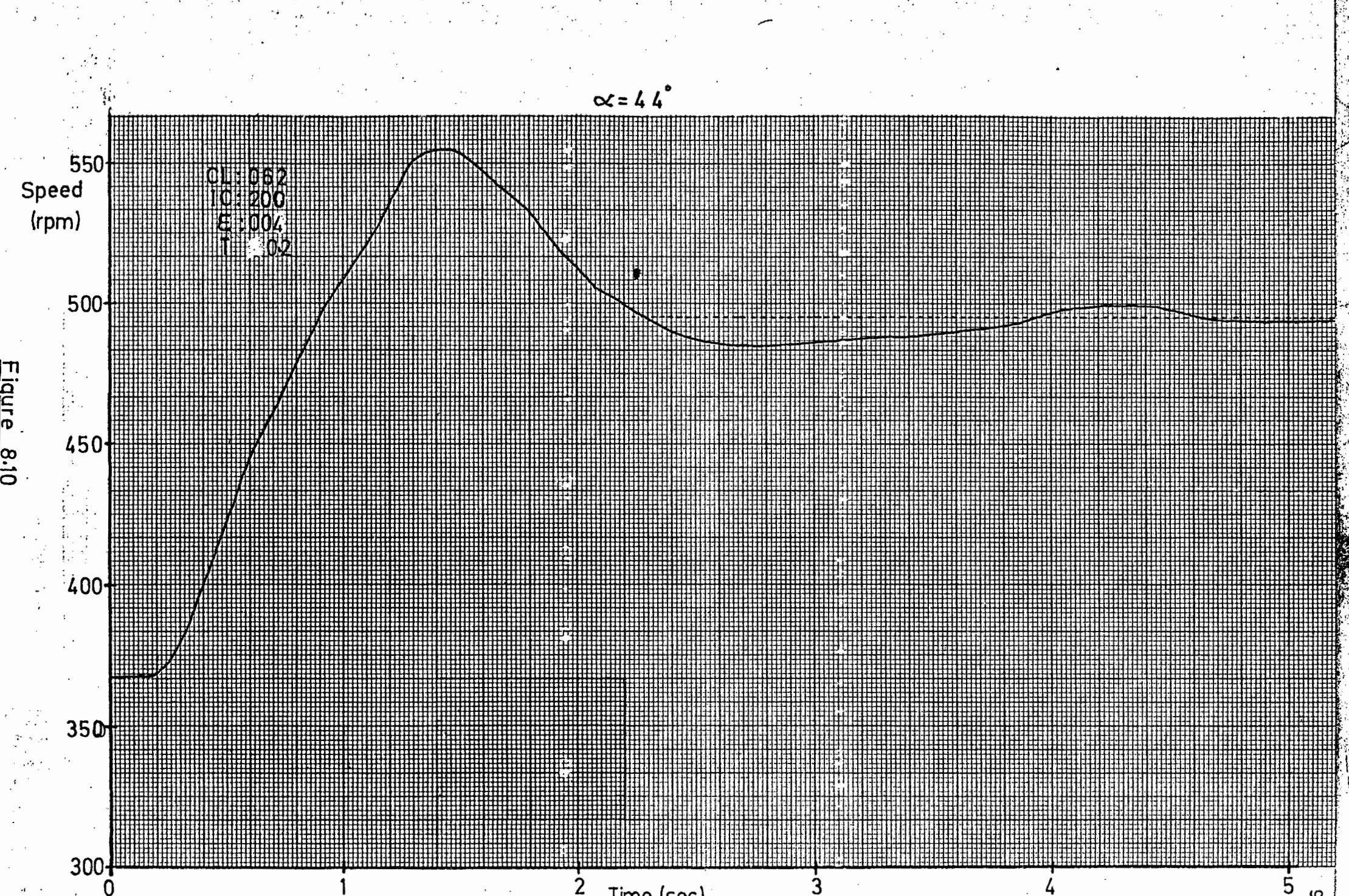
α = 44°
CL : 062
IC : 200
E : 004
T : 02
Speed (rpm)
550
500
450
400
350
300
0
1
2
3
4
5
Time (sec)

Figure 8.10

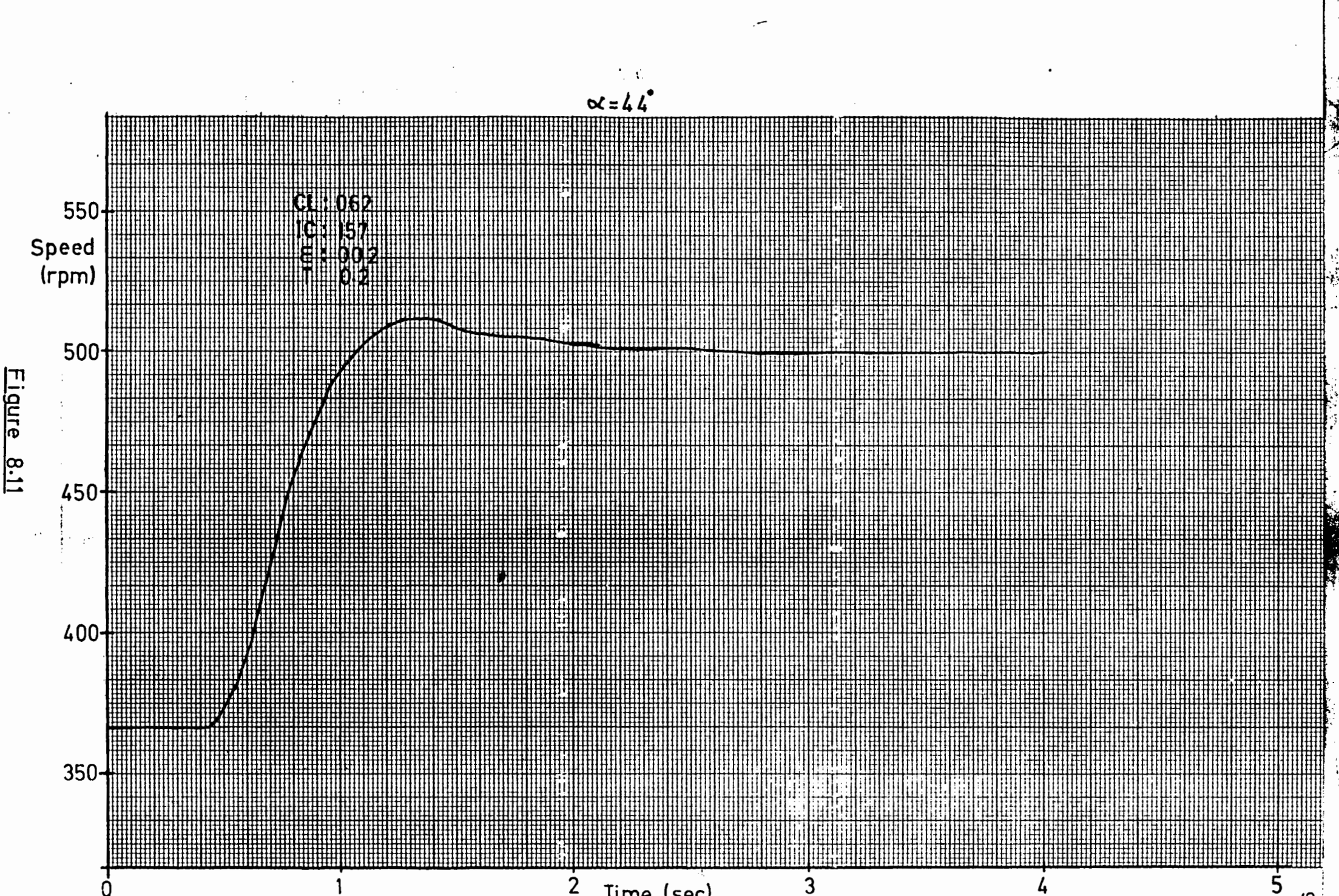
α=44°
CL : 062
IC : 157
E : 002
T 02
550
Speed
(rpm)
500
450
400
350
0
1
2
Time (sec)
3
4
5

Figure 8.11

Figs. 8.12 to 8.14 show the system response to a large step change in input. As the inverter angle of advance is only 28^{o} the current limit is necessarily low to ensure commutation (maximum line current is 8.2 A). Thus, although the power factor is high (better than 0.88), the low current produces a relatively low torque and so acceleration of the motor is small. Two different responses for closed-loop control (underdamped and overdamped) are shown together with the open-loop response.

Fig. 8.15 shows the speed error under stead state conditions. The conditions are the same as those for the response shown in Fig. 8.12. The error signal is typically of the same magnitude as the percentage change in rectifier output voltage with a one bit change of the input to the rectifier. That is, the feedback system is changing the rectifier input by $\pm$ 1 bit which is in turn causing a small change in motor speed causing the error signal shown.

Fig. 8.16 is the system response to the sudden application of a 2 kW load to the unloaded motor. Fig. 8.17 is the response when this 2 kW load is suddenly removed. The response for the case when the load is applied is faster than that when the load is removed, because for a drop in motor speed the system gives the motor full current and thus maximum torque, allowing fast recovery to the original speed. When the load is removed the system is under integral control and remains in this state until the motor speed drops below the desired speed, in addition the motor can only coast down. A more advanced drive would

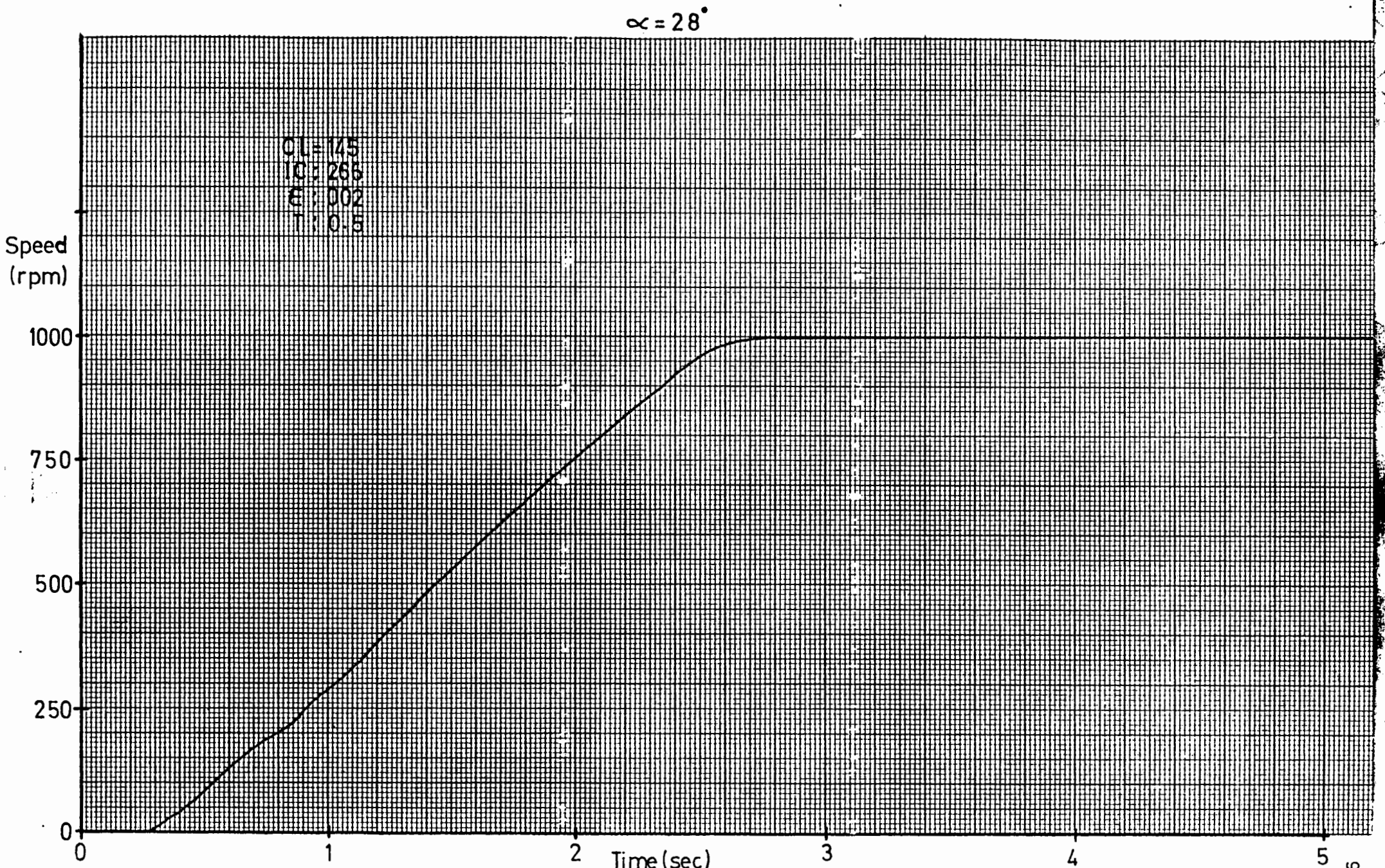
∝ = 28°
CL = 145
ID = 265
ε = 002
T = 0.5
Speed (rpm)
1000
750
500
250
0
0
1
2
Time (sec)
3
4
5

Figure 8.12

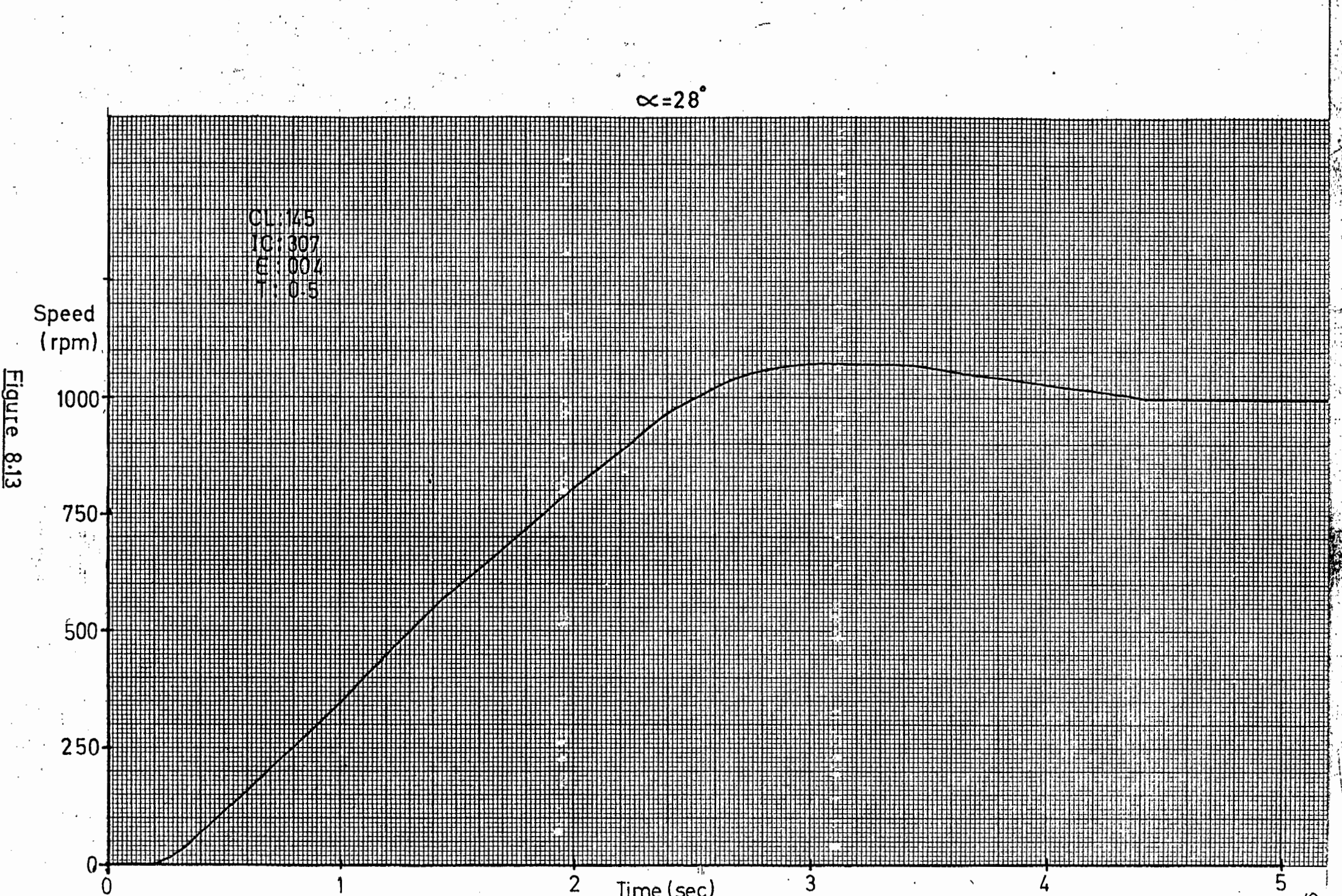
∝=28°
CL:145
IC:307
E :004
T : 0·5
Speed (rpm)
1000
750
500
250
0
0
1
2
3
4
5
Time (sec)

Figure 8.13

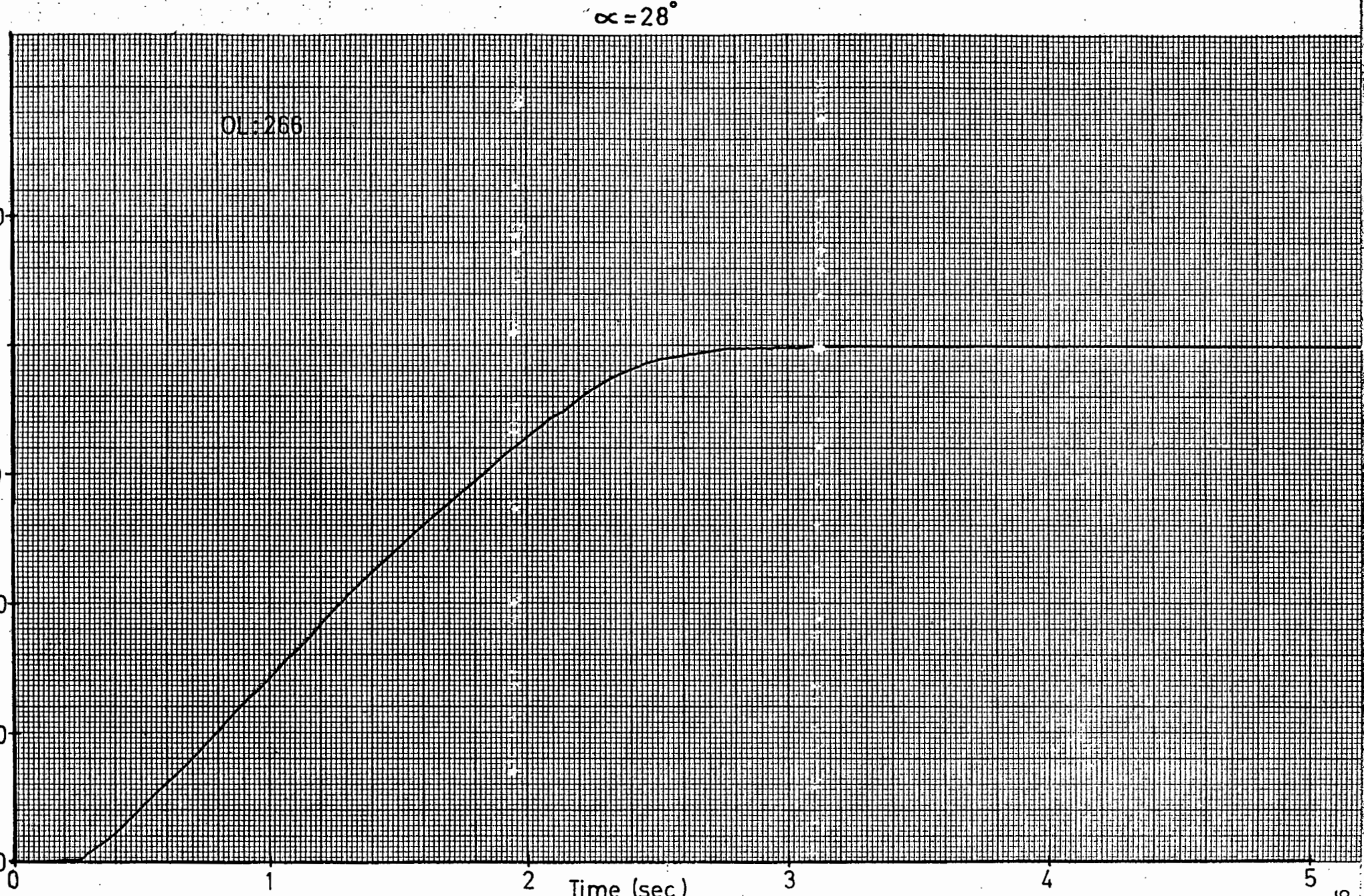

Figure 8.14

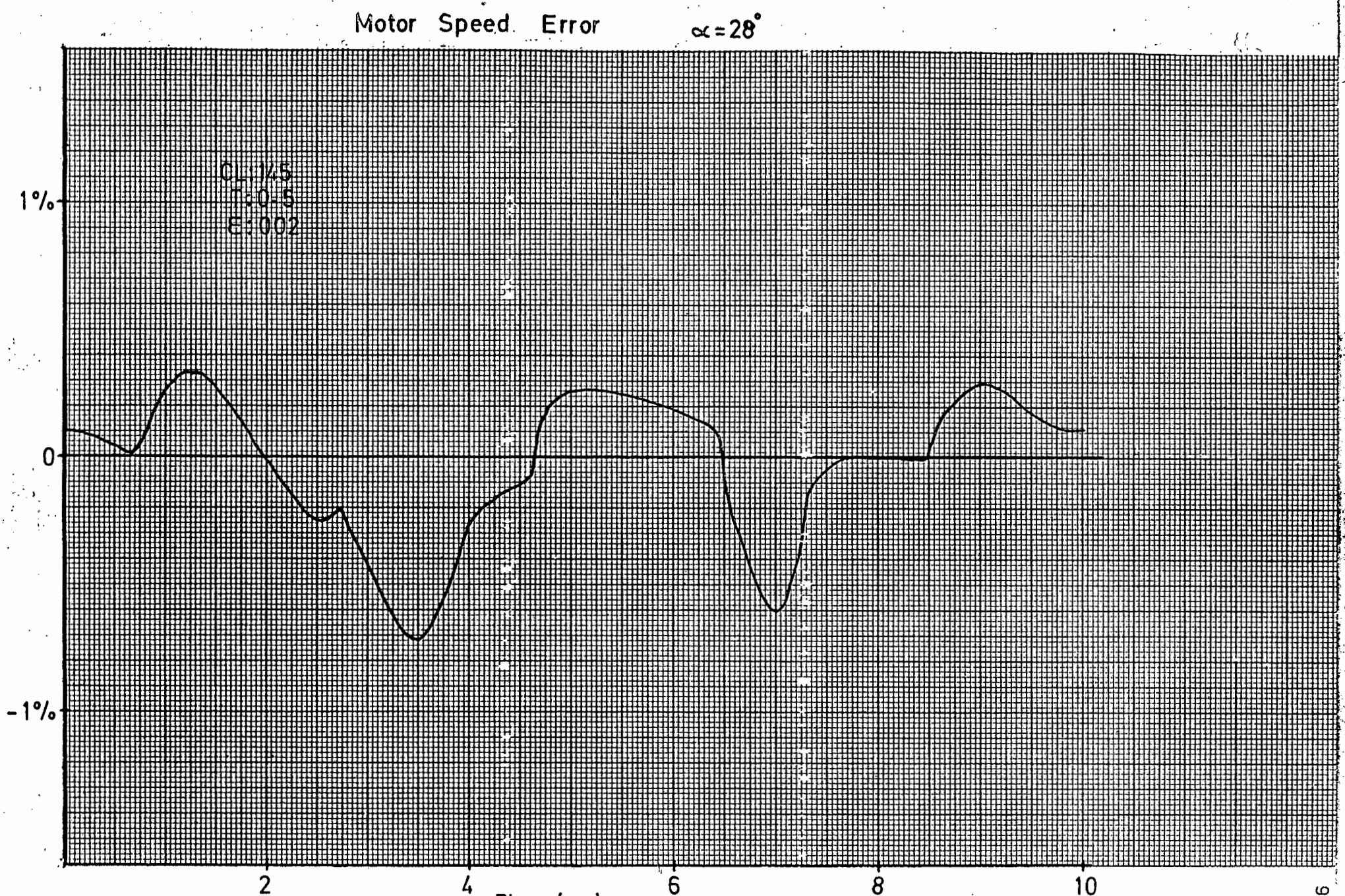
Motor Speed Error
$\alpha = 28^\circ$
C_L : 1·45
τ : 0·5
ε : 002
1%
0
-1%
2
4
6
8
10

Figure 8.15

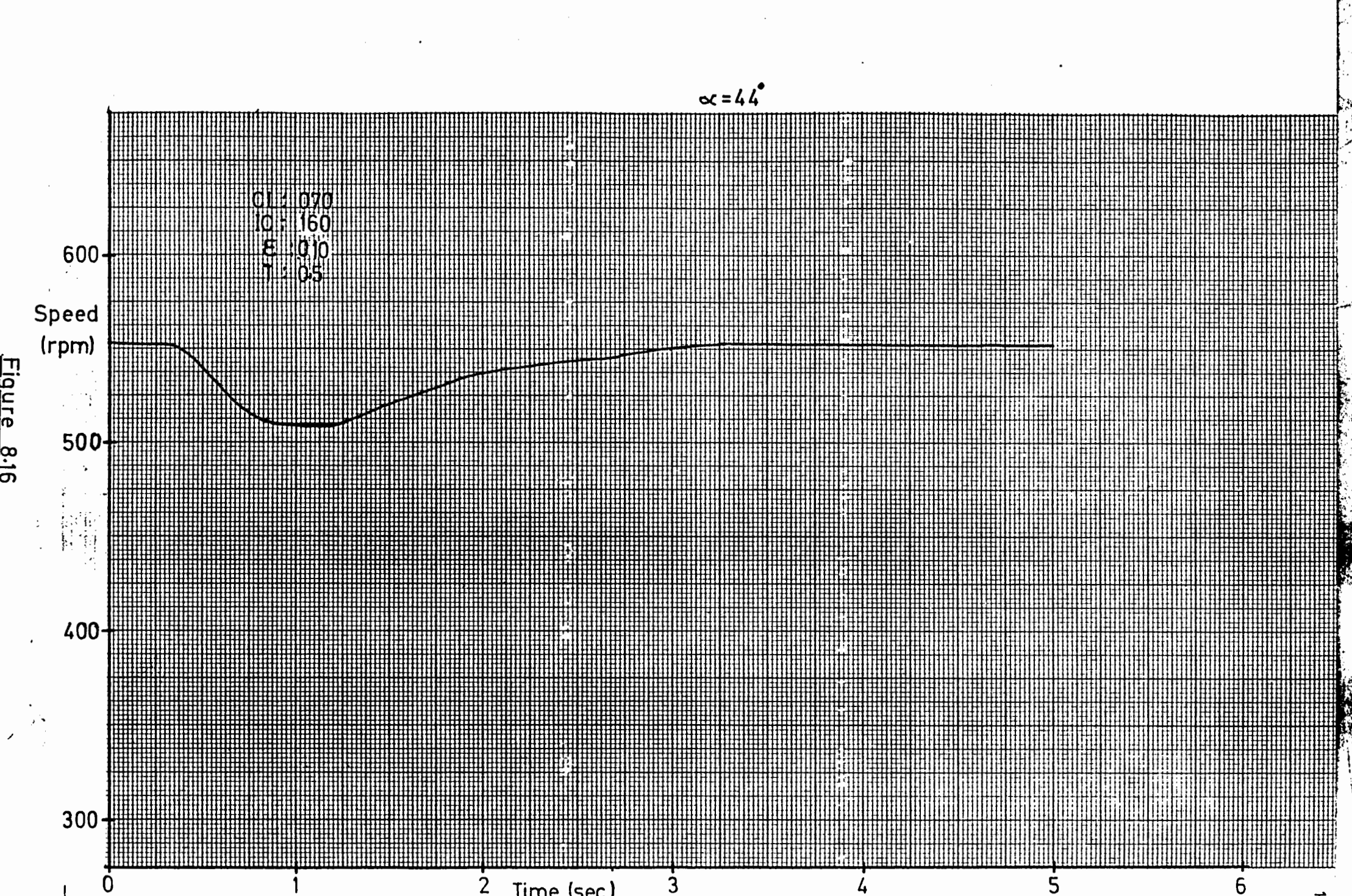
α = 44°
CL : 070
IQ : 160
ε : 010
T : 05
600
500
400
300
Speed
(rpm)
0
1
2
3
4
5
6
Time (sec)

Figure 8.16

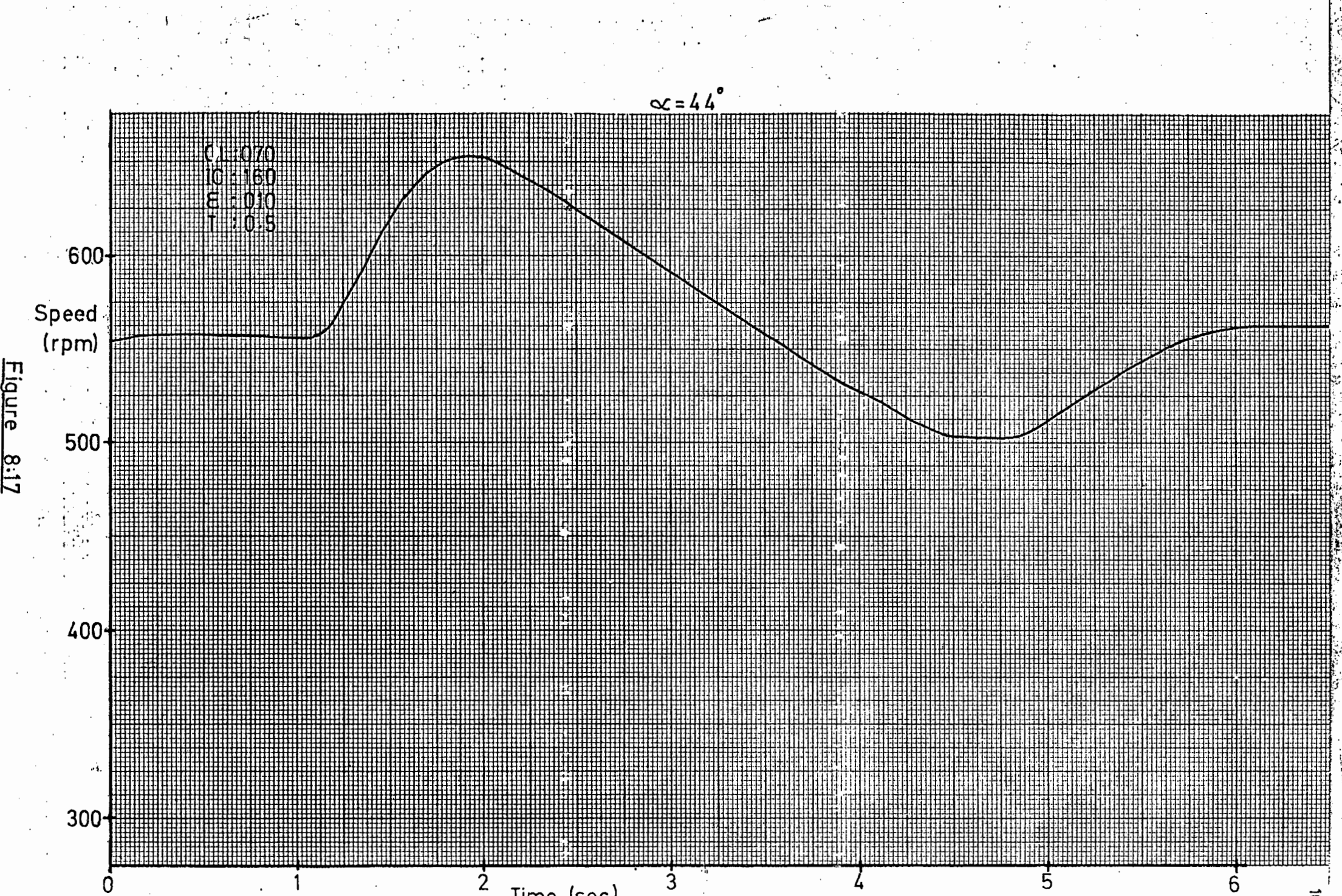
α = 44°
CL :070
IC :160
E :010
T :0.5
600
500
400
300
Speed (rpm)
0
1
2
3
4
5
6
Time (sec)

Figure 8:17

incorporate regenerative operation and thus enable much faster deceleration of the motor. The response for the removal of a load would then be similar to that shown in Fig. 8.16 for load application.

Fig. 8.18 shows the acceleration of the motor from standstill. The point at which the control logic switches from the starting routine to the normal operating routine is clearly evident by the kink in the graph. By comparison of the slopes of the two sections it can be estimated that the torque of the motor is approximately 150% of that just after the system has switched to the normal operating mode. As explained earlier, the slow-speed torque could not be measured directly with the experimental apparatus used.

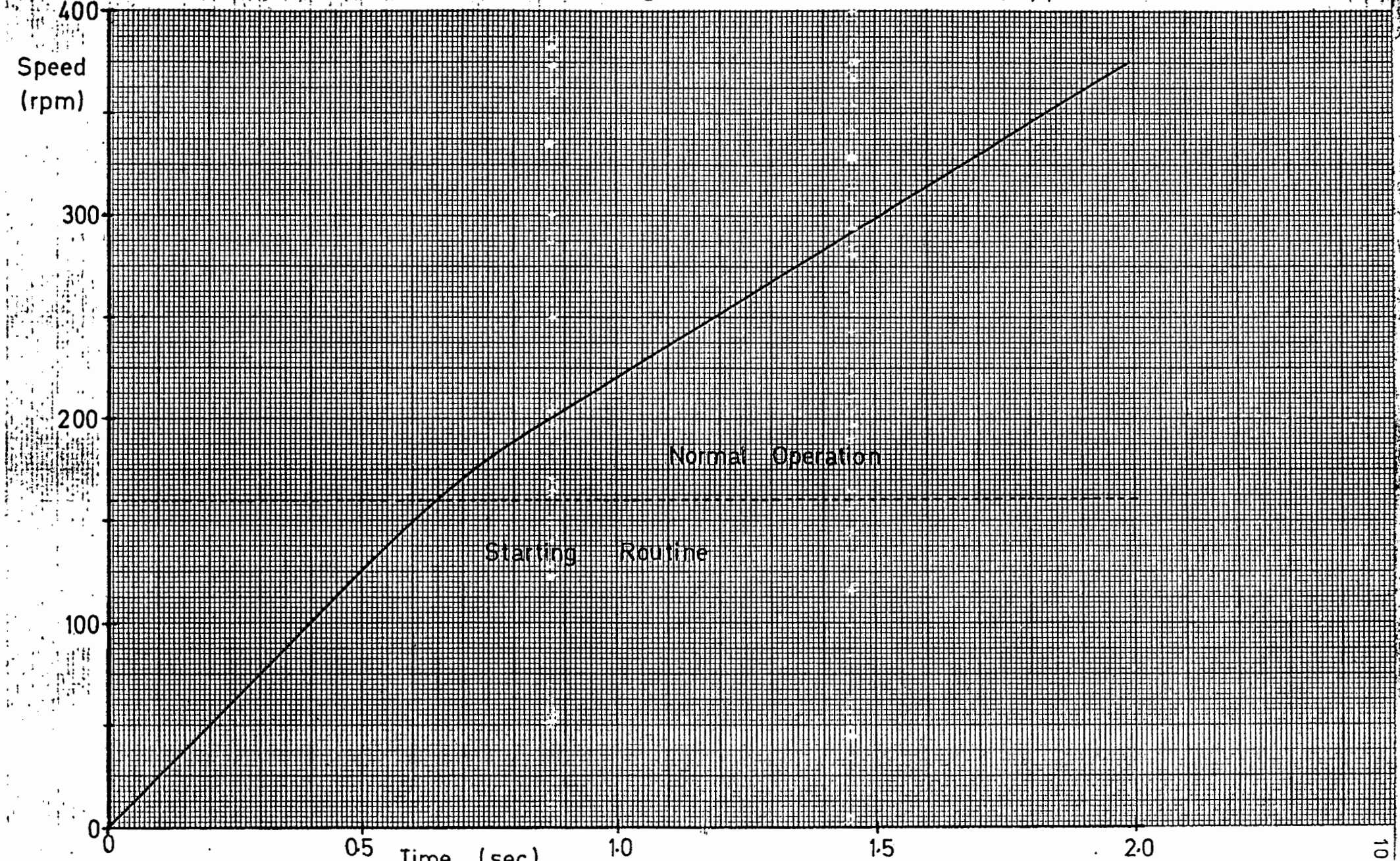
Motor Starting Acceleration
α = 44°
400
Speed
(rpm)
300
200
100
0
Normal Operation
Starting Routine
0
0·5
Time (sec)
1·0
1·5
2·0

Figure 8.18

CHAPTER 9.

CONCLUSION

The basic drive described in this thesis could be altered in a number of ways to enable improved performance to be obtained.

The present shaft encoder consists of a disc with a number of slots generating a clock pulse, there is a single slot, producing a synchronizing pulse once per motor revolution. Thus if synchronization is lost (e.g. when the power is switched off, or due to noise) it is necessary to rotate the motor at least one revolution to enable synchronization to be regained. A coded absolute position transducer would improve this shortcoming.

The limiting factor for speed precision in this thesis is the accuracy with which the rectifier can be controlled. Under normal operating conditions, rectifier delay angles of greater than 90^{o} or less than 23^{o} are not used. This corresponds to 44% of the total range of delay angles. The accuracy of rectifier control could be almost doubled if the 256 possible delay angles (8 bits) were spread over the range between 23^{o} and 90^{o} instead of between 0^{o} and 120^{o}.

To obtain the best response from the motor when under closed-loop control it is necessary for the initial condition, that is set on the integrator, to be fairly close to the output

value of the integrator when the system has reached a steady state. With the particular motor used the effects of armature reaction causes there to be a substantial difference in steady state value of the integrator output (i.e. in the D.C. voltage value) for no load and loaded conditions. Thus to obtain a particular response curve for no load and loaded conditions it is necessary to alter the integrator initial condition. The need for this could be reduced or removed if a synchronous motor that is affected to a lesser extent by armature reaction is used.

In this thesis it has been shown that the type of synchronous motor drive presented here is viable and that direct digital control of thyristor power circuits is feasible. Although the system has not been optimised for a particular task or response, it has been shown that the system is amenable to closed-loop feedback control. It is clear that inverter control is essential for an optimum system and although this would require a fairly sophisticated computing and control system, the now readily available micro-processing systems could probably be economically used for supervision of both the rectifier and inverter power circuits.

This type of drive has the advantage over frequency controlled systems in that under transcient conditions the motor cannot lose synchronization and fall out of step. It also appears that damper windings are not necessary for this type of drive although this aspect has not been investigated. Frequency controlled drives, however, do not require speed feedback as

the motor locks onto the supply frequency. The type of drive presented here has a high starting torque and this could prove advantageous in traction applications.

The major limiting factors of this drive are the effects of armature reaction, and subtranscient reactance causing long thyristor commutation times. With modern motor design techniques these effects could be reduced to acceptable levels. In a large system, the D.C. smoothing reactor could prove to be a dissadvantage but this could possibly be reduced substantially in size or removed altogether (Chino, 1975).

When the rectifier is operated at a low output voltage the input power factor is poor. This could be improved by using sector control instead of phase control of the rectifier. Alternatively, two series, sequentially fired, phase controlled rectifiers could be used. Another possibility is by using a diode rectifier supplying a D.C. chopper circuit which regulates the final D.C. voltage. This method would be applicable to battery supplied systems (e.g. a battery motor vehicle) or to D.C. traction systems (e.g. railways).

There is scope for future investigation into inverter control (possibly using the inverter advance angle as the main control variable for a variable speed but constant power drive) and harmonic effects in the motor and supply system. The regenerative and reversing aspect of this drive could also be investigated.

REFERENCES

1. DAVIS, R.M.: "Power Diode and Thyristor Circuits", University Printing House, Cambridge (1971).

2. Ramshaw, R.: "Power Electronics", Chapman and Hall, London (1973).

3. de Rubinat, J.M. and Rochet, A.: "Thyristor naturally commutated converters for variable speed drives with high power A.C. motors", I.E.E. Conference Publication Number 123. Power Electronics - Power Semiconductors and their Applications. Colmore Press, London (1974).

4. McLeod, B.D., Renfrew, A. and Shepherd, J.: "An Inverter drive suitable for traction". I.E.E. Conference Publication Number 123, Power Electronics - Power Semiconductors and their Applications. Colmore Press, London (1974).

5. Alston, I.A. and Hayden, J.T.; "Wide speed range synchronous motor drive". I.E.E. Conference Publication Number 93, Electrical Variable Speed Drives. Baldwin, Kent (1972).

6. Murphy, J.M.D.: "Thyristor control of A.C. motors". Pergamon Press, Oxford (1973).

7. Chalmers, B.J., Magureanu, R.: "New inverter-fed brushless synchronous motor". I.E.E. Conference Publication Number 93. Electrical Variable Speed Drives. Baldwin, Kent (1972).

8. Slemon, G.R., Forsythe, J.B. and Dewan, S.B.: "Controlled-Power-Angle Synchronous Motor Inverter Drive System". I.E.E.E. Transactions on Industry Applications. Volume 1A-9, Number 2, (March/April, 1973).

9. Putz, U.: "The Converter-fed Brushless Synchronous Motor", I.E.E. Conference Publication Number 123. Power Electronics - Power Semiconductors and their Applications. Colmore Press, London (1974).

10. Bowler, P. and Chan, T.Y.K.: "An efficient high frequency inverter for A.C. drives". I.E.E. Conference Publication Number 123. Power Electronics - Power Semiconductors and their Applications. Colmore Press, London (1974).

11. Gaede, H.: "A new brushless D.C. drive". I.E.E Conference Publication Number 93. Electrical Variable Speed Drives. Baldwin, Kent (1972).

12. Chino, T.: "Effects of Smoothing Reactor on the Characteristics of the Commutatorless Motor". Electrical Engineering in Japan, Volume 95, Number 2 (1975).

13. Say, M.G.: "Performance and Design of A.C. machines". Third Edition, Pitman, Great Britain (1958).

14. Say, M.G.: "A.C. Machines". 4th Edition, Pitman, London (1976).

15. Fitzgerald, A.E., Kingsley, C. and Kusko, A.: "Electric Machinary". Third Edition, McGraw-Hill, Japan (1961).

16. General Electric Company: "SCR Manual". Fifth Edition, (1972).

17. Gupta, S.C., Hansdorff, L.: "Fundamentals of Automatic Control". John Wiley and Sons, New York (1970).

18. Shinners, S.M.: "Modern Control System Theory and Application". Addison-Wesley, (1972).

19. Raven, F.H.: "Automatic Control Engineering", McGraw-Hill, Kogakusha, (1968).

20. National Semiconductor. "Linear Applications". Application Note AN-72. (September, 1972).

21. Weehuizen, H.F.: "Direct Digital Control of a D.C. Machine." M.Sc. Thesis, University of Cape Town (1972).

APPENDIX A.

RECTIFIER AND INVERTER EQUATIONS.

At any one instant the D.C. side of the bridge is connected via two conducting thyristors to two phases of the A.C. supply. The D.C. voltage is therefore connected tothe line voltage. Due to the fact that a thyristor is fired every 60^{o}, the D.C. waveform is periodic with a period of 1/6 that of the A.C. supply. The average D.C. voltage can be averaged over this 1/6 A.C. period. Reference to Fig. 3.1 and 4.1 also show that the inverter and the rectifier have the same basic equation, with the inverter delay angle shifted by 180^{o} with respect to the rectifier delay angle. This gives the opposite sign for the output voltage for the inverter. For the rectifier:

$$V_{dc} = \frac{3}{\pi} \cdot \int_{\gamma + \frac{\pi}{3}}^{\gamma + \frac{2\pi}{3}} \sqrt{6} \cdot V_{ac} \cdot \sin(wt) \cdot d(wt)$$

$$= \frac{3\sqrt{6}\, V_{ac}}{\pi} \left(\cos\left(\gamma + \frac{\pi}{3}\right) - \cos\left(\gamma + \frac{2\pi}{3}\right) \right)$$

$$= \frac{3\sqrt{6}}{\pi} \cdot V_{ac} \cdot \cos(\gamma) \qquad \text{..... A.1}$$

For the inverter:

$$V_{dc} = -\frac{3\sqrt{6}}{\pi} \cdot V_{ac} \cdot \cos(\beta) = -\frac{3\sqrt{6}}{\pi} \cdot V_{ac} \cdot \cos(180 - \alpha)$$

$$= \frac{3\sqrt{6}}{\pi} \cdot V_{ac} \cdot \cos(\alpha)$$

$$\text{i.e.} \quad V_{ac} = \frac{\pi\, V_{dc}}{3\sqrt{6}\cos(\alpha)} \qquad \text{..... A.2}$$

A more detailed analysis with the assumption that reactance is present in the A.C. circuit of the bridges is given by Davis (1971). The results of this analysis are:

Rectifier:

$$V_{dc} = \frac{3\sqrt{6}}{\pi} \cdot V_{ac} \cdot \cos(\gamma) - \frac{3}{\pi} \cdot I_{dc} \cdot X \quad \ldots\ldots\ldots A.3$$

$$I_{dc} \cdot X = \sqrt{6} \cdot V_{ac} \cdot \left(\sin^2\left(\frac{\gamma + u}{2}\right) - \sin^2\left(\frac{\gamma}{2}\right)\right) \quad \ldots\ldots\ldots A.4$$

Inverter:

$$V_{dc} = \frac{3\sqrt{6}}{\pi} \cdot E \cdot \cos(\alpha) + \frac{3}{\pi} \cdot I_{dc} \cdot X \quad \ldots\ldots\ldots A.5$$

$$I_{dc} \cdot X = \sqrt{6} \cdot E \cdot \left(\sin^2\left(\frac{\alpha + u}{2}\right) - \sin^2\left(\frac{\alpha}{2}\right)\right) \quad \ldots\ldots\ldots A.6$$

where X is the equivalent series reactance in the A.C. supply circuit. For the rectifier it includes transformer leakage inductance and supply lead inductance. In the case of the inverter it consists of the synchronous motor subtranscient reactances and the supply lead reactance.

The effects of resistance in the A.C. supply are discussed in Appendix E.

Fig. A.1 shows the expected motor terminal voltage (inverter output voltage) for steady state conditions. During thyristor overlap, the terminal voltage has a value which is the mean of the voltage of the two phase which are "shorted" together. When overlap is not present, the terminal phase voltage is

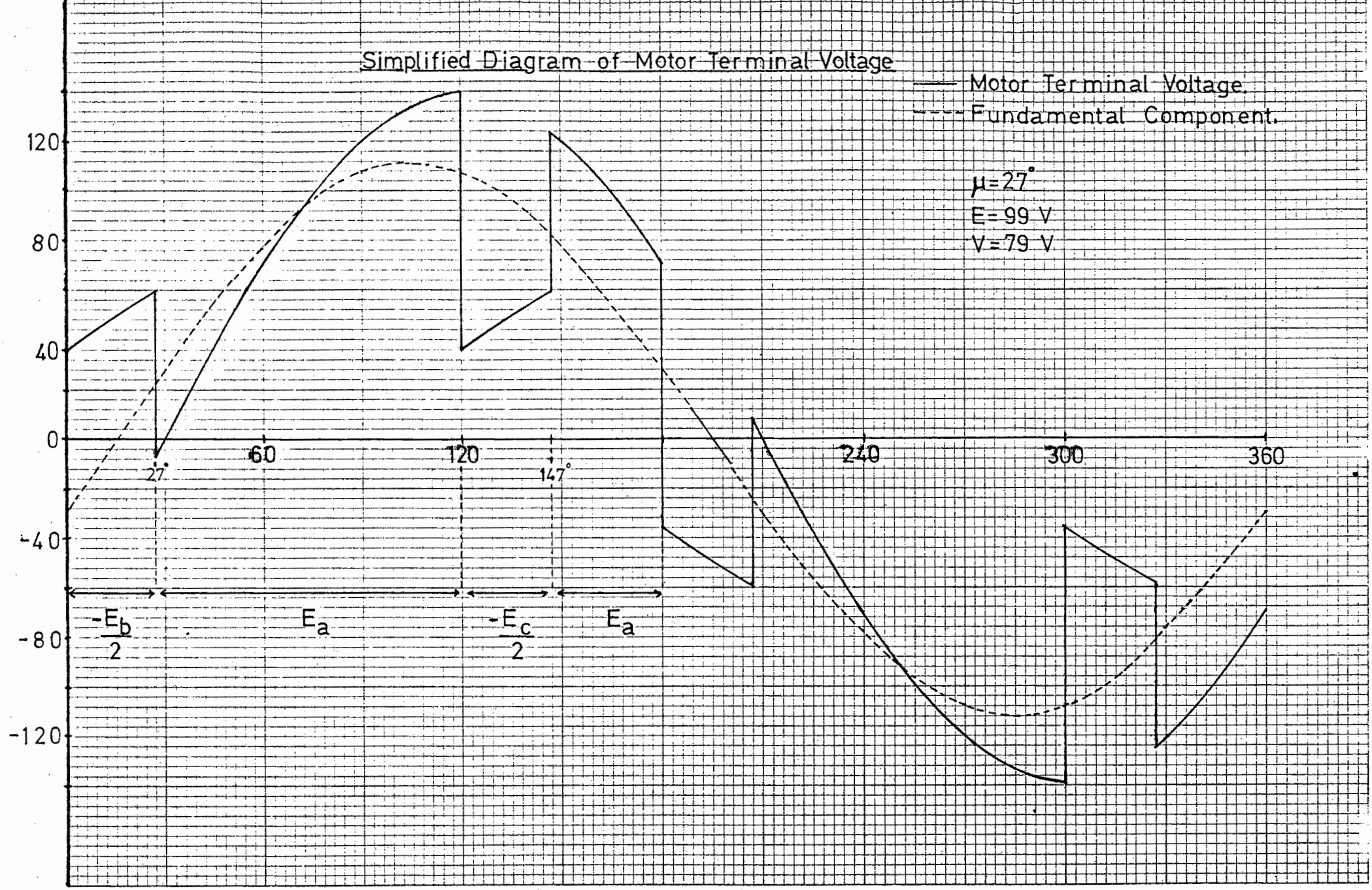
Simplified Diagram of Motor Terminal Voltage
Motor Terminal Voltage.
Fundamental Component.
μ=27°
E=99 V
V=79 V
120
80
40
0
-40
-80
-120
60
120
240
300
360
27°
147°
$\frac{-E_b}{2}$
E_a
$\frac{-E_c}{2}$
E_a

Figure A.1

equal to the motor emf. This is because the phase current is either zero or constant and there is therefore no voltage drop across the machine reactance. To enable machine calculations to be done the fundamental component of this voltage needs to be known. Fourier analysis is used to obtain this.

$$f(t) = \tfrac{1}{2} a_o + \sum_{n=1}^{\infty} (a_n.\cos(nwt) + b_n.\sin(nwt))$$

where $$a_n = \frac{2}{T} \int_o^T f(t).\cos(nwt).d(wt)$$

$$b_n = \frac{2}{T} \int_o^T f(t).\sin(n\omega t).d(\omega t)$$

$$a_1 = -\frac{\pi}{2} \int_o^{\mu} \frac{E}{2}.\sin(x - \frac{\pi}{2} - \alpha).\cos(x).dx$$

$$+ \frac{\pi}{2} \int_{\mu}^{3.\frac{\pi}{2}} E.\sin(x + \frac{\pi}{6} - \alpha).\cos(x).dx$$

$$- \frac{\pi}{2} \int_{\frac{3\pi}{2}}^{3\frac{\pi}{2}+\mu} \frac{E}{2}.\sin(x + \frac{5\pi}{6} - \alpha).\cos(x).dx$$

$$+ \frac{\pi}{2} \int_{3\frac{\pi}{2}+\mu}^{\pi} E.\sin(x + \frac{\pi}{6} - \alpha).\cos(x).dx$$

where $$E_a = E.\sin(x + \frac{\pi}{6} - \alpha)$$

$$E_b = E.\sin(x - \frac{\pi}{2} - \alpha)$$

$$E_c = E.\sin(x + \frac{5\pi}{6} - \alpha)$$

This gives:

$$a_1 = E.((\frac{3\mu}{2\pi} - 1).\sin(\alpha - \frac{\pi}{6}) + \frac{3}{2\pi}.\sin(\mu).\sin(\frac{\pi}{6} + \alpha - \mu)).$$

Similarly -

$$b_1 = E.\left(\left(1 - \frac{3\mu}{2\pi}\right).\cos\left(\alpha - \frac{\pi}{6}\right) + \frac{3}{2\pi}.\sin(\mu).\cos\left(\frac{\pi}{6} + \alpha - \mu\right)\right)$$

The r.m.s. magnitude of the fundamental component of the motor terminal voltage is then given by

$$V = \frac{1}{\sqrt{2}} \sqrt{a_1^2 + b_1^2} \qquad \text{..... A.7}$$

The phase angle is given by (for phase A)

$$\phi = \tan^{-1}\left(\frac{a_1}{b_1}\right) \qquad \text{..... A.8}$$

The phase angle between the terminal voltage and the motor emf. is then

$$\left(\frac{\pi}{6} - \alpha\right) - \phi$$

(This turns out to be approximately $\frac{\mu}{2}$).

This seems to ignore armature reaction?

APPENDIX B.

SYNCHRONOUS MOTOR SPECIFICATIONS AND TESTS

The synchronous alternator used in the final drive presented had the following specifications.

6 pole (salient poles)
3 phase
50 Hz (1000 r.p.m. rated speed)
phase voltage : 125 V
phase current : 23 A
power output : 5 kW
field current : 1 A. at 110 V.
Optional star or delta connected (star connection used).

Fig. B.1 gives the open circuit phase voltage and the short circuit phase (line) current for different field currents.

Fig. B.2 shows the open circuit voltage curve of Fig. B.1 together with the zero power factor curve and the construction of a Potier triangle from which the armature leakage reactance can be obtained.

A slip test was performed on the synchronous machine (with no field current) and from the results of this test the quadrature and direct axis synchronous reactances were obtained. This test is performed under unsaturated conditions and so does not give values that are useful for prediction. However, the

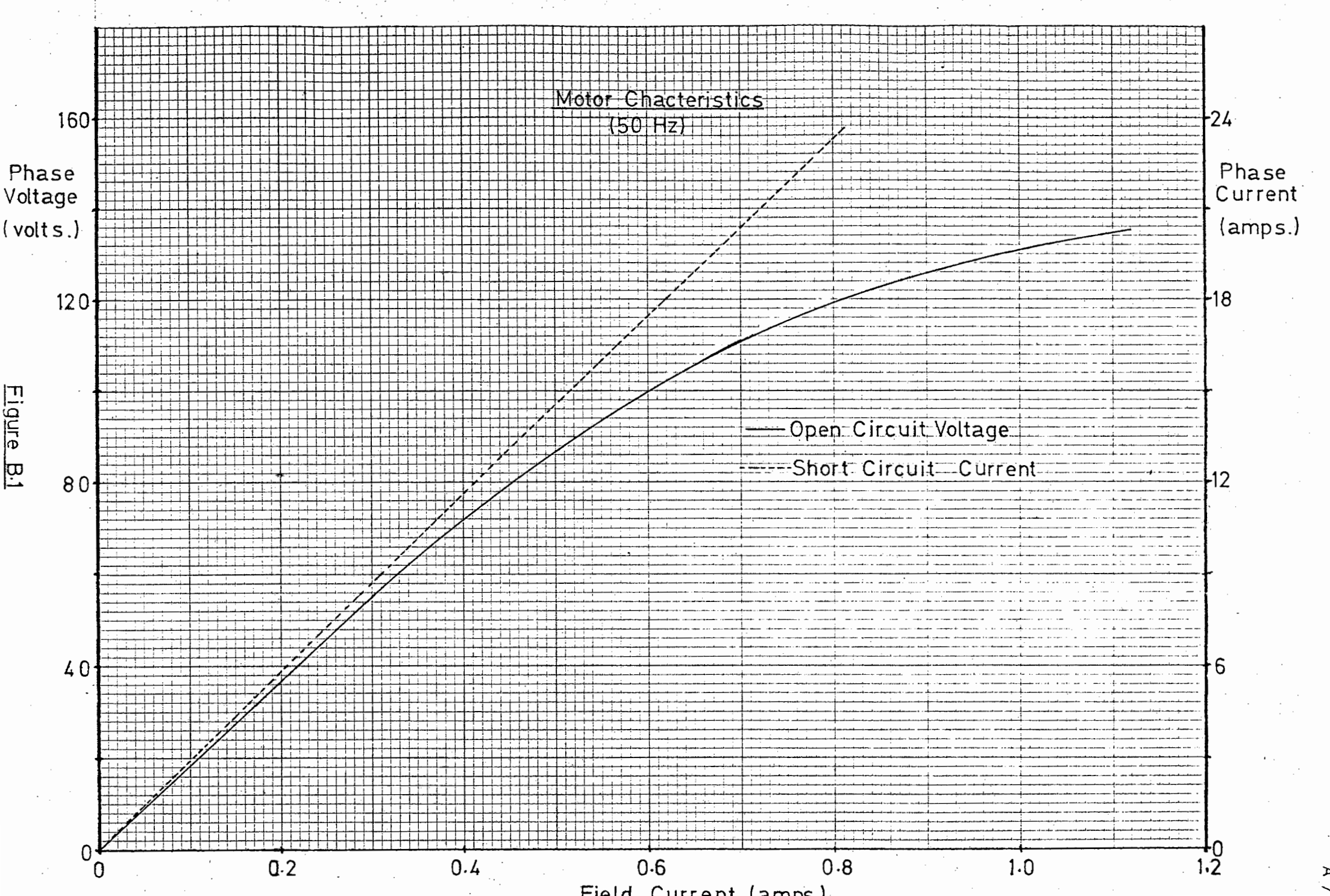
Motor Chacteristics
(50 Hz)
Phase Voltage (volts.)
Phase Current (amps.)
160
120
80
40
0
24
18
12
6
0
0
0.2
0.4
0.6
0.8
1.0
1.2
Field Current (amps.)
Open Circuit Voltage
Short Circuit Current

Figure B.1

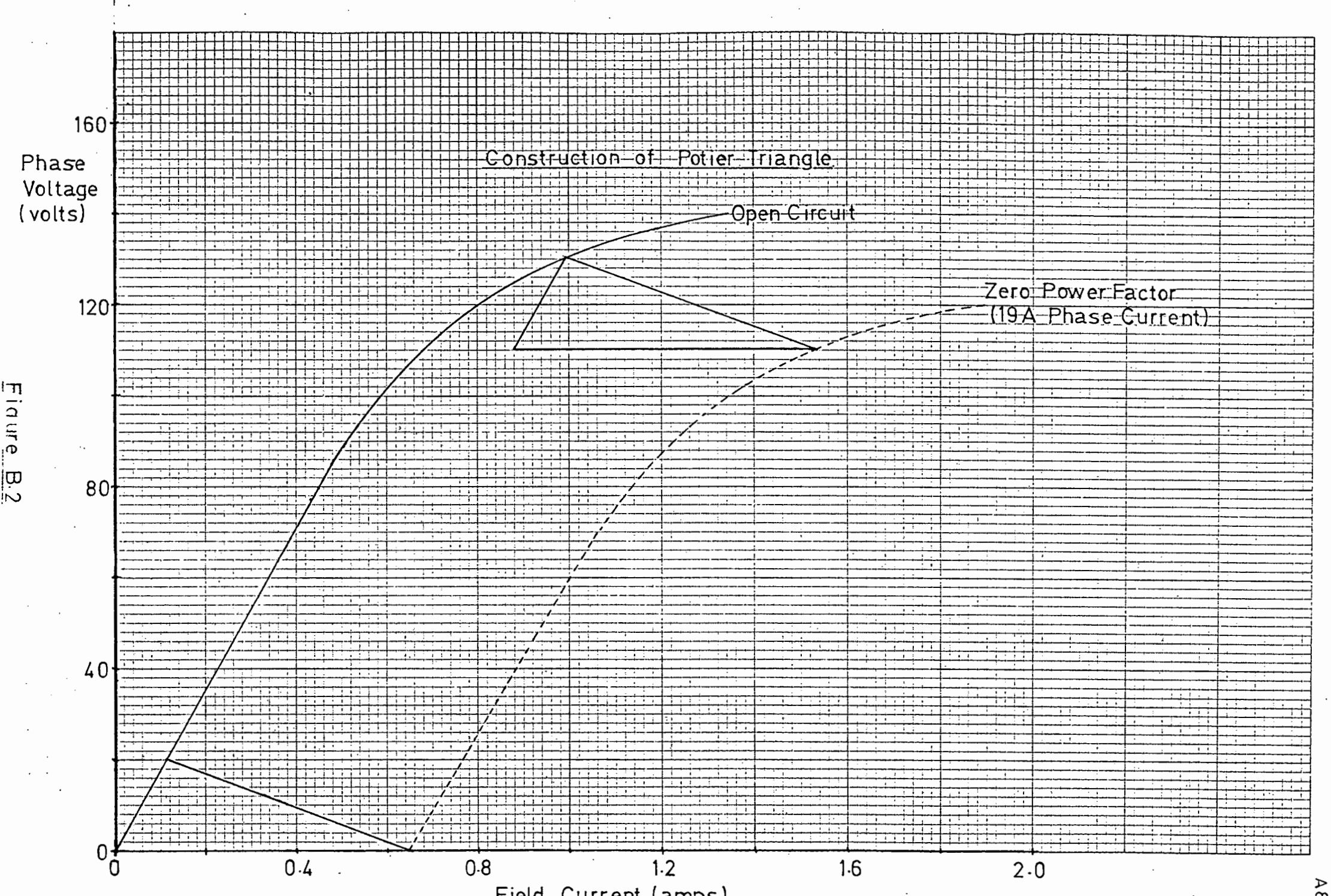
Construction of Potier Triangle
Open Circuit
Zero Power Factor
(19A Phase Current)
Phase Voltage (volts)
160
120
80
40
0
0
0.4
0.8
1.2
1.6
2.0
Field Current (amps)

Figure B.2

ratio X_{sq}/X_{sd} can be obtained. This ratio remains approximately constant because it is a function of the motor geometry (Say, 1976).

These tests enabled the reactances X_l, X_q, X_d to be approximately estimated for any load conditions (Say, 1976, p.389).

A typical set of results is -

$$\frac{X_q}{X_d} = 0.76\ \Omega$$

$$R = 0.35\ \Omega$$

$$X_l = 1.00\ \Omega \quad \text{at 50 Hz.}$$

unsaturated, direct axis, synchronous reactance: 6.12 Ω at 50 Hz.

Adjusted synchronous reactances using a graphical estimation method (Say, 1976) to account for saturation. Motor internal emf. assumed to be 136 V.

$$X_q = 0.76\ X_d$$

$$X_d = 0.39\ (6.12 - X_l) + X_l = 3.00\ \Omega$$

In per unit values these are

$$R = 0.064$$

$$X_q = 0.42$$

$$X_d = 0.55$$

$$X_l = 0.18.$$

APPENDIX C.

MOTOR EQUATIONS

Reference to the phasor diagram of Fig. 5.1 enables the motor equations to be derived.

It can be shown that

$$(E - I_d.X_d + I_q.R)^2 + (I_q.X_q + I_d.R)^2 = V^2$$

$$I_d = I.\sin(\alpha - \frac{\mu}{2})$$

$$I_q = I.\cos(\alpha - \frac{\mu}{2})$$

This can be rearranged to give:

$$I^2((R^2 + X_d^2)\sin^2(\alpha - \frac{\mu}{2} - \tan^{-1}(\frac{R}{X_d})) + (R^2 + X_q^2)\sin^2$$

$$(\alpha - \frac{\mu}{2} + \tan^{-1}(\frac{X_q}{R}))) - I(2E\sqrt{R^2 + X_d^2}\ \sin(\alpha - \frac{\mu}{2} - \tan^{-1}$$

$$(\frac{R}{X_d}))) + E^2 - V^2 = 0 \qquad \text{..... C.1}$$

where E is the motor field emf.

$$E = \frac{1}{\sqrt{2}} \cdot I_f \cdot L_{sr} \cdot \omega \qquad \text{..... C.2}$$

If I_f, N (and therefore ω), α, V_{dc} are defined, as would be the case for normal operation, then equations C.1, C.2 together with equations A.5, A.6 and A.7 provide 5 equations and thus

allow the five unknown quantities: I, μ, V, E and X to be evaluated. (X can be eliminated by substituting A.6 into A.5).

The motor torque is then given by

$$T = \frac{3}{2\sqrt{2}} \cdot L_{sr} \cdot p \cdot I_f \cdot I \cdot \cos(\alpha - \frac{\mu}{2}) \quad \ldots\ldots\ldots \text{C.3}$$

It has been assumed that the presence of thyristor overlap (angle μ) causes a shift in the fundamental component of current of $\mu/2$. Thus it has been assumed that the current decay (and rise) during commutation is a linear function of time. In reality it is exponential but closely resembles a linear function.

The relationship between the D.C. current and the fundamental component of the motor current is approximately

$$I_{a.c.\ av.} = \frac{2}{3} \cdot I_{dc}$$

$$I = 1.10\ I_{d.c.}$$

where I = r.m.s. fundamental line current.

It is clear that the solution to these equations can become very involved. For the purpose of this thesis it was decided to predict the motor torque for constant inverter D.C. voltage and various motor speeds. This was done for a few sets of conditions only to enable varification of the equations. It was considered that as only a few sets of results were to be

evaluated, development of a computer program to solve the equations would be unnecessary. A trial and error itterative process was used instead. This method was not altogether a "shot in the dark" because experimental values could be used to give starting values which proved to be fairly close to the predicted values of the various parameters.

The method is outlined below.

Let $V_{dc} = 165$ V

$\alpha = 60^{o}$

N = 730 r.p.m.

$I_f = 1.2$ A

From the open circuit curve E = 100 V

Guess: $\mu = 20^{o}$

I = 20 A (I_{dc} = 18 A)

Calculate equivalent D.C. resistance from equation E.2.

$R_{eff} = 0.64\ \Omega$

Calculate effective D.C. voltage (equation E.3)

$V_{dc(new)} = 153$ V

Use equations A.5 and A.6 to calculate μ. A.5 and A.6 give

$$V_{dc(new)} = \frac{3\sqrt{6}}{2\pi} E\ (3.\cos(\alpha) - \cos(\alpha + \mu))$$

$\therefore \mu = 18.9^{o}$ (close enough to 20^{o})

Use equations A.7 to obtain the fundamental inverter A.C. voltage (motor terminal voltage)

$$a_1 = -0.29$$

$$b_1 = 0.78$$

Thus $V = 0.832\ E = 83\ V$

Use equation C.1 to solve for I (values for X_d, X_q, R are given in Appendix B)

$$3.17\ I^2 - 257\ I + 3110 = 0$$

$$\therefore\ I = 14.8\ A \text{ (or } 66.3\ A)$$

A new estimate (of say 16 A) is used and the process repeated. Once values of I and μ sufficiently close to the estimated values are obtained the torque can be calculated using equation C.3 .

In this manner the predicted torque/speed curves shown in Fig. 5.6 were constructed.

For the purposes of the prediction given here the direct, quadrature and leakage inductances were assumed to remain constant for all speeds and currents. This is not strictly true as saturation alters these values. Estimation of saturation effects can be made by geometric methods as outlined in Say (1976) but this complicates the equations even more and so was omitted.

APPENDIX D.

THYRISTOR FIRING DELAY TIMES

Rectifier: As 8-bit counters were used to control the delay angle of the thyristor firing pulse, there are 256 possible delay angles. When the counters are loaded with 000_8 a maximum delay angle of 120^o is desired. Thus 255 counts (or clock pulses) must correspond to 120^o of a mains cycle, i.e. $\frac{20}{3}$ mS.

Therefore, clock frequency must be

$$\frac{255}{\frac{20}{3}} \text{ kHz} = 38.250 \text{ kHz}.$$

Inverter: As the shaft encoder has 270 slots for a 6-pole motor, 90 slots correspond to one electrical cycle, or 360^o.

One slot, therefore, corresponds to 4^o.

For a delay angle of 90^o the counters must be loaded with 367.4_8 (367_8 corresponds to 92^o and 370_8 to 88^o).

A delay angle of 60^o (120^o advance) : 377_8
A delay angle of 180^o (0^o advance) : 341_8.

APPENDIX E.

EFFECTIVE D.C. RESISTANCE

To enable the motor characteristics to be predicted it is necessary to be able to determine the motor terminal voltage (i.e. the output A.C. voltage of the inverter). This is a function of the overlap angle, which must therefore be determined.

It can be shown (Davis, 1971) that for a motor with no armature resistance

$$V_{dc} = \frac{3\sqrt{6}\ E}{2\pi}\ (3.\cos(\alpha) - \cos(\alpha + \mu) \qquad \ldots\ldots\ldots \text{E.1}$$

(substitution of equations A.6 into A.5)

where E is the motor emf.

To enable this equation to be used, it was decided to reduce the D.C. voltage in such a way as to compensate for the motor resistance.

Under normal conditions, 2 inverter thyristors are "on" and the D.C. current flows through 2 phases of the motor. Thus the voltage drop due to resistance is $2\ I_{dc}.R$ where R is the motor phase resistance. During commutation 3 thyristors are "on", 2 motor phases are in parallel combination and through the third phase. Thus, during thyristor overlap the resistive volt drop is $1.5\ R.I_{dc}$. Commutation occurs for a period of μ and occurs 6 times in an electrical cycle.

Thus the average effective D.C. resistance due to motor armature resistance is

$$R_{eff} = R.(2 - \frac{3\mu}{2\pi}) \quad \ldots\ldots\ldots\ldots\ldots\ldots \text{E.2}$$

Thus when equation E.1 is used the D.C. voltage is reduced to

$$V_{dc(new)} = V_{dc(old)} - I_{dc}.R.(2 - \frac{3\mu}{2\pi}) \quad \ldots\ldots\ldots \text{E.3}$$

APPENDIX F.

ORIGINAL TEST MOTOR SPECIFICATIONS

Three phase, star connected, 4 non-salient poles.

Line voltage : 400 V

Line current : 0.5 A

Power : 350 W, 0.77 power factor

Speed : 3150 r.p.m., 105 Hz.

Field current : 0.5 A at 200 V.

The synchronous impedance varied from 0.168 p.u. at zero field current to 0.086 p.u. at 0.6 A field current.

More detailed tests on the motor were not done as this motor was only used to get the system operating, after which the larger machine was used.

APPENDIX G.

OBTAINING THE MOTOR/INVERTER TRANSFER FUNCTION

As is explained in Section 5.7, the response of the inverter/motor system to a step change in inverter D.C. voltage was recorded. As no overshoot was evident it was assumed that the transfer function was of the form

$$T(S) = \frac{\omega_n^2}{S^2 + 2 \cdot \zeta \cdot \omega_n \cdot S + \omega_n^2} \qquad \text{..... G.1}$$

and that the output speed had the form:

$$f(t) = 1 + A\, e^{-at} + B\, e^{-bt}$$

Furthermore, it was assumed that one of the time constants was much smaller than the other and so died away soon after application of the input step.

Thus for large time

$$f(t) \simeq B\, e^{-bt} + 1 \qquad (A\, e^{-at} \text{ becomes small})$$

$$\ln (f(t) - 1) = \ln (B) - b.t$$

Thus $\ln (f(t) - 1)$ was plotted against t and a straight line fitted to the curve (for large t only). From this straight line, "ln(B)" and "b" were obtained.

A new function $f_2(t)$ was then constructed such that:

$$f_2(t) = f(t) - 1 - B\,e^{-bt}$$

i.e. $$f_2(t) = A\,e^{-at}$$

$$\ln\left(f_2(t)\right) = \ln(A) - a.t$$

This, when plotted, could be approximated to a straight line and so enabled "ln(A)" and "a" to be determined. In this way the step response of the system (f(t)) was mathematically defined. The calculated f(t) was graphed and found to correlate well with the actual response.

The Laplace Transform of the expression describing the output response is:

$$\mathcal{L}(f(t)) = \frac{1}{S} + \frac{A}{S + a} + \frac{B}{A + b}$$

$$= \frac{(1 + A + B)S^2 + (a + b + aB + bA)S + ab}{S(S + a)(S + b)}$$

Comparison of this with equation G.1 gives;

$$1 + A + B = 0$$

$$a + b + aB + bA = 0$$

These expressions held true for the graphically obtained values of A, B, a and b.

Also:

$$ab = \omega_n^2$$

$$a + b = 2 \cdot \zeta \cdot \omega_n$$

This second order approximation was considered to be sufficiently accurate for the simulation of the motor/inverter combination.

APPENDIX H.

Z - TRANSFORM PREDICTION OF SYSTEM RESPONSE

Initially a continuous system analysis using Laplace Transform methods was used to verify that the predicted response correlated with the simulated response for the feedback system proposed in the second part of Chapter 6, (i.e. integral control once the motor speed was within a certain error band of the desired speed.) The prediction was done with the assumption that the system had switched to integral control, as this would be where instability (if it existed) would initiate.

The system can be described mathematically as shown in Fig. H.1(a).

The predictions have been done for the inverter advance angle 44^{o}, a loop gain of 1 and an integrator time constant of 0.25 seconds.

A loop gain of 1 means that a 1 bit change in the rectifier input results in a 1 bit change in error signal (or, x% change in rectifier input produces x% change in motor speed).

Thus the transfer functions are :

Motor/inverter: $\dfrac{60.86}{S^2 + 21.3S + 60.86}$ (from equation 5.8)

Integrator (feedback controller): $\dfrac{4}{S}$

Thus the output for an input of R(S) = 1/S (step input) is

$$C(S) = \frac{1}{S} \cdot \frac{kab}{S(S + a)(s + b) + kab}$$

where $\frac{1}{k}$ = integrator time constant and a and b are parameters relating to the inverter/motor transfer function.

$$k = 4$$

$$a = 3.40$$

$$6 = 17.90$$

$$\therefore \quad C(S) = \frac{243.4}{S(S^3 + 21.3\ S^2 + 60.86\ S + 243.4)}$$

Taking the inverse Laplace Transform gives:

$$c(t) = 1 - 0.041\ e^{-18.8t} + 1.131\ e^{-1.28t} \sin(3.37t - 1.02)$$

This is plotted in Fig. 8.1.

Z-transform methods were then used to determine the effects of sampling, which a digital implementation of the proposed control system would introduce.

The mathematical model used is shown in Fig. H.1b. The system consists of an integrator that is incremented every sampling instant, followed by a zero order hold (digital latch) circuit which is "updated" at the sampling instants. From the diagram of Fig. H.1b:

$$C(S) = B(Z).G_2G_3(S)$$

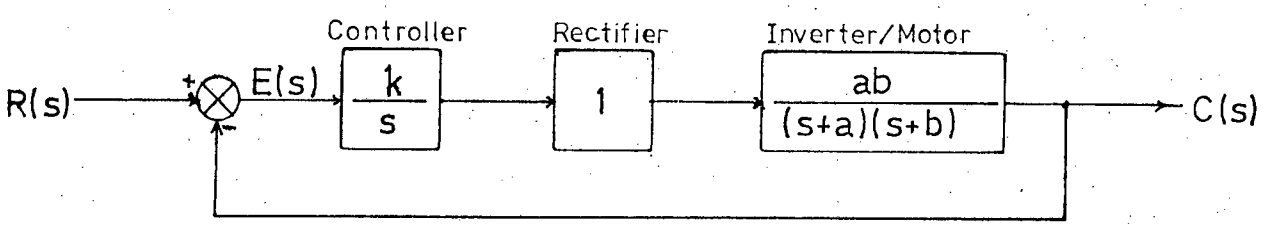

Continuous System Block Diagram.

Figure H.1a

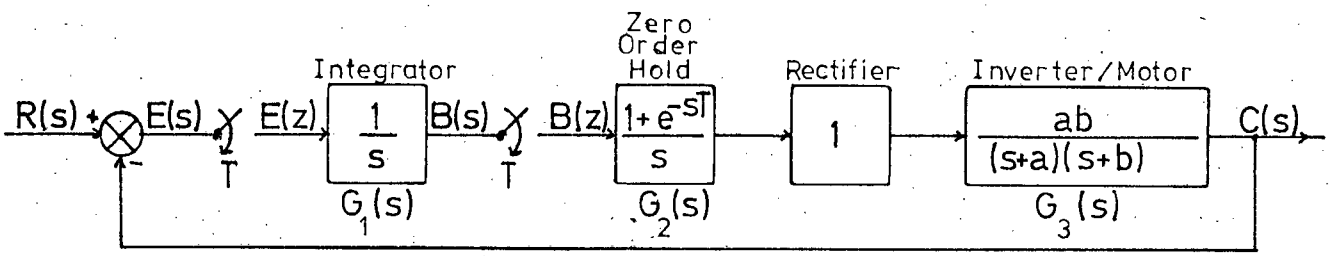

Discrete Time System Block Diagram.

Figure H.1b.

$$E(S) = R(S) - C(S)$$

$$E(Z) = R(Z) - B(Z).G_2G_3(Z)$$

$$B(S) = G_1(S).R(Z) - B(Z).G_2G_3(Z).G_1(S)$$

$$B(Z) = G_1(Z).R(Z) - B(Z).G_2G_3(Z).G_1(Z)$$

$$B(Z) = \frac{G_1(Z).R(Z)}{1 + G_2G_3(Z).G_1(Z)}$$

therefore: $$C(Z) = \frac{G_1(Z).G_2G_3(Z)}{1 + G_2G_3(Z).G_1(Z)} \cdot R(Z)$$

where:

$G_1(S)$ is the integrator, i.e. $\frac{1}{S}$

$G_2(S)$ is the zero order hold, i.e. $\frac{1 - e^{-ST}}{S}$

$G_3(S)$ is the motor/inverter system

$$G_1(Z) = \frac{Z}{Z - 1}$$

$$G_2G_3(Z) = \frac{Z - 1}{Z} \cdot Z_T \left\{ \frac{ab}{S(S + a)(S + b)} \right\}$$

$$= 1 + \frac{b}{a - b} \cdot \frac{Z - 1}{Z - e^{-aT}} - \frac{a}{a - b} \frac{Z - 1}{Z - e^{-bT}}$$

$R(S)$ is the input, i.e. $\frac{1}{S}$

$$R(Z) = \frac{Z}{Z - 1}$$

T is the sampling time and is equal to the integrator time constant of the continuous time system.

i.e. $T = 0.25$

and as before : $a = 3.40$

$b = 17.90$

C(Z) was then determined.

$$C(Z) = \frac{6.89\,Z + 1.32}{14.5\,Z^3 - 13.97\,Z^2 + 7.75\,Z - 0.071} \cdot \frac{Z^2}{Z - 1}$$

The inversion integral was then used to obtain the output of the system at the sampling instants.

C(Z) has poles at

$$Z_1 = 1$$
$$Z_2 = 0.00926$$
$$Z_3 = 0.477 + j\,0.546$$
$$Z_4 = 0.477 - j\,0.546$$

Thus

$$C(nT) = 1 - 0.000016\,(0.00926)^{n-1} + 0.727\,(0.725)^{n-1} \cdot \cos\left(-2.377 + (n-1)\,(0.853)\right)$$

for n = 0, 1, 2 ...

This can be changed into a form similar to that of the output for the continuous system analysis.

$$C(t) = 1 - 0.00173\,e^{-18.73t} + 1.003\,e^{-1.286t}\sin(3.41t - 1.66)$$

(only valid for t an integral multiple of 0.25 seconds).

A plot of C(nT) (filled in between sampling instants) is shown in Fig. 8.1.